

**The Influence of Station Keeping
Systems on Tidal Turbine Structural
Performance when Operating in
Combined-Wave Current Sea States**

A thesis submitted to the University of Strathclyde
for the degree of Doctor of Philosophy in the
Faculty of Mechanical & Aerospace Engineering

2019

Song F

Mechanical & Aerospace Engineering

Declaration of authenticity and author's rights

This thesis is the result of the author's original research. It has been composed by the author and has not been previously submitted for examination which has led to the award of a degree.

The copyright of this thesis belongs to the author under the terms of the United Kingdom Copyright Acts as qualified by University of Strathclyde Regulation 3.50. Due acknowledgment must always be made of the use of any material contained in, or derived from, this thesis.

Singed:_____

Date:_____

Contents

Nomenclature	11
1 Introduction	16
1.1 Investigating the dynamic loads on tidal stream turbines operating in the wave-current interaction	16
1.2 Models	17
1.3 Exploiting the sea states, turbines, mooring lines and models	18
1.4 Contributions	19
1.5 Thesis Organisation	19
2 Overview of tidal stream turbines – support structures, load environments and modeling techniques.	21
2.1 General description of TSTs	22
2.1.1 Theory of operation for horizontal axis TSTs	24
2.1.2 Optimum positioning in the water column and characteristic parameters	25
2.2 Station keeping system	27
2.2.1 Gravity base	29
2.2.2 Pin Pile	29
2.2.3 Mooring	31
2.3 Environment loads on tidal turbine	34
2.3.1 Wave Loading	35

2.3.2	Current Loading and Fluid Acceleration Effects	37
2.3.3	Wave and Current Interaction	38
2.4	Blade Element Momentum Theory	39
2.4.1	One Dimensional Momentum Theory	40
2.4.2	Rotational Momentum	43
2.4.3	Blade element theory	46
2.4.4	Correction factors	49
2.5	Passive control	52
2.5.1	Tuned mass damper	52
2.5.2	Tuned Liquid damper	53
2.5.3	Tuned Liquid columns damper	54
2.6	Summary	55
3	Models	56
3.1	Wave Models	56
3.1.1	Governing equations and boundary conditions	56
3.1.2	Linear wave theory model	60
3.1.3	Third order Stokes wave-current model	62
3.1.4	Fifth order Stokes wave-current model	64
3.1.5	Three step wave-current interaction model	65
3.1.6	Irregular sea-state wave model	66
3.1.7	JONSWAP power density spectrum	68
3.2	Rigid supported turbine	70
3.2.1	Numerical models for monopile support	71
3.2.2	Tuned mass damper	73
3.3	Time domain solution	76
3.3.1	Central difference (explicit) method	77

3.3.2	Runge-Kutta (explicit) method	78
3.3.3	Newmark β method	80
3.4	Added mass and damping	82
3.4.1	Infinite and viscous fluid	84
3.4.2	Infinite and inviscous fluid	84
3.4.3	Viscous and inviscous fluid with large values of α and β	85
3.4.4	Added mass and damping factors	86
3.5	Model verification	86
3.6	System parameters	87
3.7	Results	91
3.7.1	Instant impact on structure	91
3.7.2	Monopile Results Including Wave-current Interactions	93
3.7.3	Frequency Domain Analysis	95
3.8	Summary	96
4	The Dynamics of Tension Mooring Supported Tidal Turbines	98
4.1	Preliminary numerical model	99
4.1.1	Preliminary modeling of a mooring supported turbine	101
4.1.2	External forces	103
4.1.3	Modification for BEMT correction	107
4.2	Developed model with finite element method	113
4.2.1	Wave excitation on buoy	124
4.3	Solving scheme	127
4.4	Summary	128

5	Investigation of the relationships between the rotor loads and input parameters	129
5.1	Model verification	130
5.2	Investigation of waves	131
5.2.1	Initial conditions	133
5.2.2	Comparison of preliminary and developed models	135
5.2.3	Regular waves	141
5.2.4	Random waves	147
5.2.5	Blade section velocities	152
5.2.6	Buoy Effect	154
5.2.7	Morrison effects	157
5.3	Discussions in the System Parameters	158
5.3.1	Mooring line length	160
5.3.2	Smaller turbines	162
5.4	Summary	164
6	Summary and conclusion	166
6.1	Research findings and original contributions	167
6.2	Theoretical implications of the research finding	170
7	Future works	172
A	TURBINE MOTION ANIMATION	175
B	DESIGN STANDARDS FOR USE IN TIDAL ENERGY SYSTEM	179

List of Figures

2.1	Six main types of Tidal Energy Convertors, (a) horizontal axis turbine (b) vertical axis turbine (c) oscillating hydrofoil (d) archimedes screw(e) venturi (f) tidal kite [2]	23
2.2	Diagram showing the inflow velocity vectors on a blade and the generated force vectors. The figure shows the inflow coming from the left and the cross-section of one blade pointing ‘out’ of the paper [19]	24
2.3	Configurations of gravity base and mono-pile [91]	28
2.4	Schematic of mooring arrangements for a single marine renewable energy device: (from left) taut-moored systems with single and multiple lines, basic catenary system, catenary system with auxiliary surface buoy and lazy-wave system with subsea floater and sinker [45].	31
2.5	Definition of the annular stream tube control volume over the turbine and flow domain. [65]	41
2.6	The control stream tube is divided into annular sections with thickness dr [69].	44
2.7	Inflow velocity vectors on a blade section	47
2.8	Induced blade-forces on a blade section	48
2.9	Local element thrust coefficient C_{FA} for various empirical models plotted against axial induction factor with Prandtl tip-loss factor $F = 0.7$	51
2.10	(a) Schematic of a single-degree of freedom structure with a rectangular tuned liquid damper for SDOF system and (b) dimensions of the rectangular tuned liquid damper [77]	53

2.11 Schematic of a tuned liquid columns damper [16]	54
3.1 Diagram showing the definition of the flow domain as used by the wave models	57
3.2 Coordinate system transformation for each harmonic component .	68
3.3 Structural model of a flexible wind (tidal) turbine	72
3.4 Flow chart of forces input	72
3.5 Schematic of TMDx in turbine nacelle [6]	74
3.6 Time series results for monopile verification	88
3.7 Tower top displacement and TMD displacement in time series . . .	92
3.8 Tower top displacement and base bending moment in time series .	94
3.9 Mode shapes of monopile structure	96
3.10 Frequency domain results of structure	97
4.1 Schematic of tension mooring turbine in operation	100
4.2 Geometry of the flail pendulum [26]	100
4.3 The Schematic of “flail” pendulum	102
4.4 Forces on the system	104
4.5 A multi-pendulum system with a finite number of rods and masses	113
4.6 Forces on each mass node	116
4.7 System with device masses	118
4.8 “Flail” system	120
4.9 Forces on the system	125
4.10 Solving process	127
5.1 Comparison of the line’s profile in water (Fairlead at x=190m, 200m and 210m, z=310m	132

5.2	The sea site chosen by Nevalainen[19]	133
5.3	Case 1, regular waves generated from sea state 2, current speed is 2.5m/s	136
5.4	Case 1, regular waves generated from sea state 3, current speed is 2.5m/s	137
5.5	Case 1, regular waves generated from harsh winter, current speed is 2.5m/s	138
5.6	Case 2, regular waves generated from sea-state 7, current speed is 2.5m/s	139
5.7	Case 3, regular waves generated from sea-state 7, current speed is 2.5m/s	139
5.8	Case 2, turbine thrust loading in different Alpha	140
5.9	Case 3, turbine thrust loading in different Alpha	141
5.10	Thrust and torque for Case 1 in sea state 3	142
5.11	Thrust and torque for Case 1 in sea state 1	143
5.12	Thrust and torque for Case 1 in sea state 2	144
5.13	Thrust and torque for Case 1 in harsh winter	145
5.14	Thrust and torque for Case 1 in sea state 6	146
5.15	Trajectories for different sea states. (a)(b) are the turbine and buoy trajectories in sea state 3, (c)(d) are the turbine and buoy trajectories in sea state 4, (e)(f) are the turbine and buoy trajectories in harsh winter, (g)(h) are the turbine and bouy trajectories in sea state 6	149
5.16	Random waves generated from significant wave height 1.07m and mean wave period 11.07s, current speed is 2.5m/s	150
5.17	Random waves generated from significant wave height 2.665m and mean wave period 6.135s, current speed is 2.5m/s	151
5.18	Random waves generated from significant wave height 1.008m and mean wave period 4.653s, current speed is 2.5m/s	152
5.19	The inflow velocity vectors on blade sections in harsh winter	153

5.20 Case 1, regular waves generated from sea-state 3, (a) gives the buoy radius smaller than 3m, (b) gives the buoy radius larger than 3m	155
5.21 Trajectories of turbine hinge node for buoy radius 2.5m	156
5.22 Morrison effects in torque	158
5.23 Water particle paths under waves in deep water and the turbine position	159
5.24 Thrust and torque on turbines for different second mooring line length in sea state 6	160
5.25 Thrust and torque on turbines for different third mooring line length in sea state 6	161
5.26 Loading on HyTide 1000 in sea state 3 at TSR 5 for different turbine weights	164
A.1 The animation of simulation for swell waves ($H_s=1.07\text{m}$ $T_s=11.07\text{s}$)	176
A.2 The animation of simulation for seastate 3 ($H_s=2.665\text{m}$ $T_s=6.135\text{s}$)	177
A.3 The animation of simulation for harsh winter seastate ($H_s=10.12\text{m}$ $T_s=10.06\text{s}$)	178

Abstract

This thesis reports on the performance and interactions of a tidal turbine and station keeping systems based on the adoption of a tension mooring system in different sea states. The capabilities of introducing damping are being investigated to reduce the peak loads that tidal turbines experience during operational life in high energy wave-current environments and extreme sea states. A neutrally buoyant turbine is supported from a tension cable based mooring system, where tension is introduced by a buoy fully submersed in water. The loading on the turbine rotor blades and buoy are calculated using a wave and current coupled BEMT. The modeling algorithm developed is based on an inverted triple pendulum, responding to different sea state conditions to understand the system response behavior and the blade load in different sea states, including extreme conditions. The results show the tension mooring system reduces peak thrust loading on the turbine, but it was found that there are certain limitation when using this design in extreme waves conditions.

Nomenclature

Acronyms

CALM Catenary Anchor Leg Mooring

ADCP Acoustic Doppler Velocity Profiler

EIA Environmental Impact Assessment

EMEC European Marine Energy Center

FAST Fatigue, Aerodynamics, Structures and Turbulence

FPS Floating Production Storage

FPSO Floating Production Storage and Offloading

JONSWAP Joint North Sea Wave Project

PM Pierson-Moskowitz

SDOF Single Degree Of Freedom

SPAR Single Point mooring and Reservoir

TEC Tidal Energy Convertor

TLCD Tuned liquid columns damper

TLD Tuned liquid damper

TMD Tuned Mass Damper

TST Tuned Stream Turbine

TST Tuned Stream Turbine

Commonly used symbols

α Angle of attack [deg]

ϵ Wave steepness [-]

η Wave surface displacement [m]

\bar{U} Depth-averaged mean current [m/s]

C_v Hydrodynamic viscous damping matrice [Ns/m]

C Structural damping matrices [Ns/m]

$F(t)$ External forces [N]

K Structural stiffness matrices [N/m]

M Structural mass matrices [kg]

ω Wave angular frequency [rad/s]

Ω_0 Constant current vorticity [m/s]

ω_{0t} First tower modal frequency [Hz]

Ω_r Rotor angular velocity [rad/s]

ρ	Fluid density [kg/m ³]
τ	Rotor shaft torque [Nm]
θ	Blade pitch [deg]
θ_i	Angle of incidence of wave harmonic [deg]
φ	Velocity potential [-]
A	Swept rotor area [m ²]
C	Wave celerity [m/s]
c	Blade section chord length [m]
C_{FA}	Blade-Local thrust coefficient [-]
C_D	Blade drag coefficient [-]
C_L	Blade lift coefficient [-]
C_P	Turbine power coefficient [-]
C_T	Turbine thrust coefficient [-]
F	Rotor thrust [N], Tip-loss factor [-]
g	Gravitational acceleration [m/s ²]
H	Wave height [m]
h	Water depth [m]
H_s	Significant wave height [m]
k	Wave number [-]

L Wave length [m], Lagrangian of the system [J]

p Fluid pressure [Pa]

Q_i Generalized forces [N]

R Rotor radius [m]

T Kinetic energy of system [J]

T_{app} Apparent wave period [s]

T_P Peak power period [s]

U_{0i} Current component in-line with wave [m/s]

U_{∞} Rotor current upstream velocity [m/s]

U_b Bottom velocity [m/s]

U_m Eulerian mean current velocity [m/s]

U_s Surface velocity [m/s]

V Potential energy of system [J]

Acknowledgments

I would like to thank my supervisor Cameron Johnstone for his support through this project and for giving me the freedom to pursue the topics that I found interesting which is the floating tidal turbine research.

I would like to thank all my friends in the office who have helped me with my work throughout the duration of my PhD including Thomas Mikael Nevalainen for the help in BEMT code, Jose M Rivera Camacho for innumerable discussions and swell data, Stephanie Eugenia Ordonez Sanchez for all the suggestions.

I sincerely thank the funders of my research, the EPSRC through Super-Gen UKCMER, that have enabled me to work in the field of engineering that I am most interested in for the past years.

Finally, my greatest thanks go to my family and friends at home who have had to put up with my absence over the last decade. Without your support, and just being there as always, I would never have made it to where I am now.

Chapter 1

Introduction

1.1 Investigating the dynamic loads on tidal stream turbines operating in the wave-current interaction

The global resource from tidal and other marine currents may exceed 1100 TWh/y [35], tidal-stream energy may be an important contributor to global renewable energy demand and UK has an estimated 10% to 15% of the global harvestable tidal resource [36]. At the stage of writing, tidal stream turbine (TST) technology has developed to the stage where a first large scale commercial facilities are being deployed, such as the MeyGen project which has exported 17GWh to grid as of June 2019 [38], it is proving to be a reliable and economically viable renewable energy option. However, the durability is considered to be a complicated subject

due to the loading on TSTs being highly varying in the unsteady marine environment, therefore it is a challenge to achieve the requirement of a 10 - 25 years fatigue life.

This thesis investigate and aims to design a tidal turbine station keeping system based on the adoption of a tension mooring system in different sea states. The capabilities of introducing dampening are investigated to reduce the peak loads from the variations in inflow velocity cause by the surface waves and velocity profiles present in the tidal flow. These inflow variations fluctuate with a passing wave train or tidal phases over time and over the rotor plane area. A neutrally buoyant turbine which can move with the wave train and tidal phase is supported from a tension cable based mooring system, where tension is introduced by a buoy submerged in the water, and the numerical model is developed to investigate the loading on the turbine.

1.2 Models

The model for a rigid supported turbine is based on studies done for wind turbine technologies which a wind turbine with a tower-monopile supporting structure can be modeled as an inverted pendulum, and the passive control is applied to the system to reduce the structural loading. The tension mooring system is modeled as a special type of triple pendulum which is called an inverted flail. It consists of three pendula, developed into a finite element model to make it more realistic. The loading on the turbine rotor blades and buoy are calculated using a wave coupled

blade element momentum theory (BEMT). The code was developed at the University of Strathclyde to analysis the loading occurring on a turbine rotor-drive train when operating in energetic wave-current flow conditions [19].

1.3 Exploiting the sea states, turbines, mooring lines and models

The different type of turbine station keeping systems and the hydrodynamic loads on the turbines generated from the marine environment are introduced in this thesis. A brief discussion of different wave models are given and the blade element momentum theory coupled with wave interaction are indicated to calculate the load on the turbine.

A simulation code has been developed to model the monopile support structure for turbine applications and analyse their dynamics including the added mass and hydrodynamic damping effects. Moreover a passive structure control technique was employed in this methodology, which used a tuned mass damper on the structure to do a fully coupled dynamic analysis in time domain. Moreover, a parametric study varying the mass of the Tuned Mass Damper (TMD) in fore-aft direction was undertaken in order to compare the effects to the structure. The loading on the turbine rotor blades are calculated using a wave and current coupled BEMT. A coupled pendulum with external drive is expected to experience more complicated dynamics, the external drives are calculated

from the BEMT code. Simulations are taken in different sea states, turbine and mooring line parameters to give a brief understanding of their effects on the system loading and system dynamics.

1.4 Contributions

The main contribution of the work is the introduction of a method for simulating the tension mooring turbine system in different sea states. The method does not require a powerful work station with several high CPUs, it can even be run on a personal computer. Following this methodology of passive control, structural designers can determine the optimum options based on the previous studies in wind turbines. Besides, the dynamics of a turbine supported by a tension mooring system with varying input parameters can be obtained conveniently by the methodology presented in this thesis.

1.5 Thesis Organisation

The structure of the thesis is as follows:

Chapter 2 provides an augmented description of the background to tidal stream turbines and blade element momentum theory.

Chapter 3 indicates wave models and the rigid supported turbine with passive control. The results indicate the loading on the support structure and their fatigue life.

Chapter 4 outlines an algorithm that enables the turbine supported by tension mooring system to be simulated by minimization of model complexity and it is also developed to a finite element model.

Chapter 5 outlines results of simulations based on the previous model and analyses the varying input parameters.

Chapter 6 draws discussion, conclusions and contains a summary of the contributions of the work.

Chapter 7 outlines future works.

Chapter 2

Overview of tidal stream turbines – support structures, load environments and modeling techniques.

Structures deployed at sea will be subjected to a varied environment, so it is important to find the design philosophy of TSTs in ocean engineering practices in order to ensure the durability of devices. Furthermore, a successful design of a TST must be economically feasible, which means that the increase of cost in manufacture, weight, installation and retrieval should be considered.

Due to the durability of TSTs in the marine climate, the focus of the literature review presented in this chapter will be on the actual hydrodynamic

loading TSTs suffer and how these loads can be managed efficiently in turbines by a damping application. The mid part of the chapter presents an overview of the TST station keeping systems and how the fatigue performance is impacted upon by damping system in a rigid supported tower. Finally, the techniques commonly used to numerically model the loads on a TST are presented, which will be used later in this thesis to investigate the functional relationships between the unsteady sea climate and the floating TSTs; this will inform how floating TSTs interact with their environments and will further the understanding on how to reduce the marine generated load on the TST in an efficient way.

Before the discussion of hydrodynamics and loading on a TST, some basic concepts and terminologies must be introduced in the next few sections, starting with the general description and operating principles of horizontal axis TSTs.

2.1 General description of TSTs

There are six main types of Tidal Energy Convertors (TEC), which are horizontal axis turbine, vertical axis turbine, oscillating hydrofoil, enclosed tips (venturi), archimedes screw and tidal kites as shown in Figure 2.1 [2]. Moreover, horizontal axis, vertical axis and Venturi type can be classified as rotating TST design , each has its advantages and disadvantages [2]. Energy extraction of TSTs mentioned above are all based on converting the kinetic energy in the oncoming tidal flow into a rotational torque by a power capture device. Torque load is captured by the

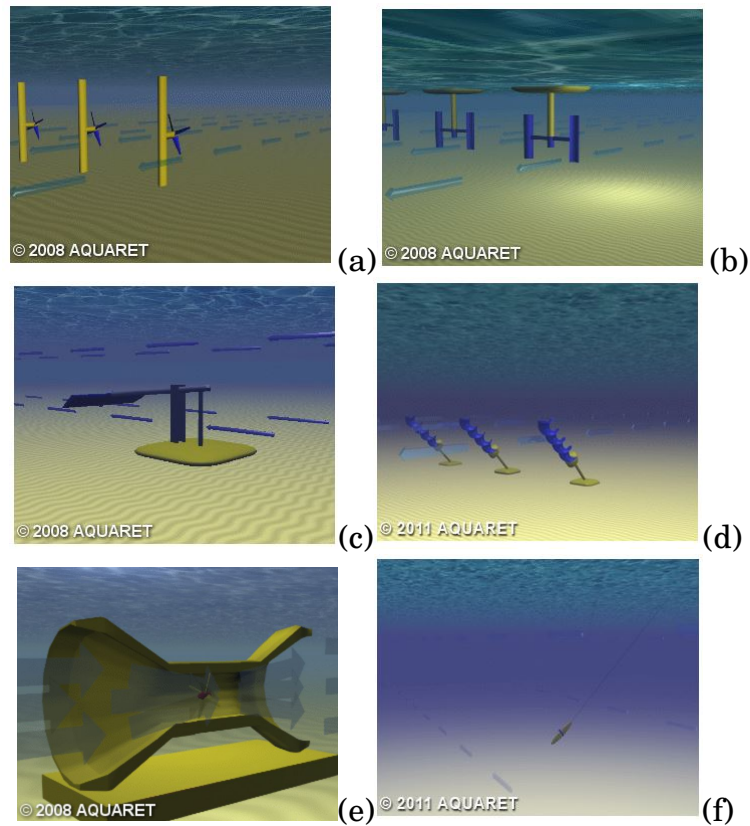


Figure 2.1: Six main types of Tidal Energy Convertors, (a) horizontal axis turbine (b) vertical axis turbine (c) oscillating hydrofoil (d) archimedes screw(e) venturi (f) tidal kite [2]

device and directly transferred to the generator after passing through the gearbox, the electricity produced is sent to the grid connection from the appropriate electrical conversion.

It is showed that out of the 95 tidal developers listed by the European Marine Energy Center (EMEC) [2], 46 were classed as horizontal axis devices. This not only means that 48 % of the total number of tested devices are horizontal axis type design but also indicates that there is currently preference for the horizontal axis type of TST device in industry. This preference is largely attributed to the fact that the loading on the drive

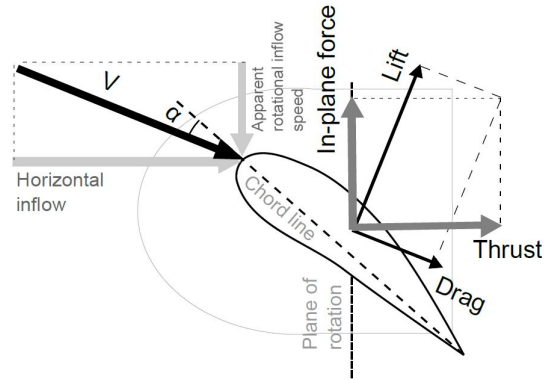


Figure 2.2: Diagram showing the inflow velocity vectors on a blade and the generated force vectors. The figure shows the inflow coming from the left and the cross-section of one blade pointing ‘out’ of the paper [19]

train of horizontal axis TSTs is smoother and more continuous since the blades do not shadow each other during operation [2]. In this thesis all the analysis and methodologies presented will be focused on horizontal axis TSTs. In addition, the station keeping system for horizontal TSTs is the other focus in this thesis and will be discussed in section 2.2.

2.1.1 Theory of operation for horizontal axis TSTs

The thrust and torque on the rotor briefly introduced in this section is influenced by the turbine station keeping from a loading perspective. The fundamental objective for TST designs is to convert the velocity momentum in the inflow to rotational torque via lifting surfaces. The blade profiles of TST is an airfoil section, so the function is same as the aircraft wing. The typical lift and drag forces on the airfoil section is shown as Figure 2.2.

The lift and drag forces are depend on the magnitude of the relative in-

flow velocity vector V , the angle of attack (AoA), α , between the inflow vector and the chord-line, the Reynolds number of the fluid flow and the geometrical shape and performance of the airfoil. The relative velocity vector has two components, one is horizontal inflow component caused by the tidal flow, the other one is apparent flow generated by the rotational speed of the blade. Furthermore, the apparent rotational inflow speed varies with radial distance from the rotational center of the turbine, because tangential velocity of the elements located closer to the hub moves slower and the angle of attack will increase towards the root. To counteract this effect, the blades of horizontal TSTs are designed to be twisted along the length of the blade in order to maintain an optimum angle of attack over the length of the blade [39]. Similarly, the chord length of the blade section closer to the turbine hub increases in order to maximize the lift generated from the lower inflow speeds.

2.1.2 Optimum positioning in the water column and characteristic parameters

The inflow current velocities have varying profile shapes depended on time and sites, this is based on the research of vertical velocity distributions in tidal stream currents using Acoustic Doppler Current Profilers (ADCP) by Sutherland [40] and Colucci [41]. The friction caused by the roughness of the seabed and bathymetry makes the vertical velocity profile vary from nearly uniform to linear to non-linear power-law distributions. Moreover, surface winds may cause a velocity shearing effect that

propagates down the water column [42], because the wind flow transfers its kinetic energy to the water surface at their interface.

Assumptions:

The highest flow velocities in the water column is close to the water surface according to the vertical velocity profile, it may seem that the turbine will have a maximum power capture at a shallow penetration depth. However this option is less than ideal due to the possibly of harmful surface wave, wind current shear and naval traffic. It is found that placing the turbine above the bottom shear friction layer and below the most energetic wave induced velocities, which will typically be in the upper half of the water column, has been considered a good trade-off for horizontal axis TSTs [43]. In order to fix the turbine in a suitable depth, the station keeping system is the main topic discussed in Section 2.2.

Since turbines operate in different conditions and have variable parameters, some characteristic non-dimensional parameters are defined to compare the performance of different turbines in a convenient way. The tip-speed ratio is commonly used to describe a turbine's operating state as

$$\text{TSR} = \frac{\Omega_r R}{U_\infty} \quad (2.1)$$

where Ω_r is the angular velocity of the rotor, R is the turbine radius and U_∞ is the inflow velocity.

The turbine's general power capture performance is defined as the power coefficient C_P , which indicates the ratio of the mechanical power in the

shaft captured by the turbine from the incoming flow over the swept area of the rotor. It is defined as

$$C_P = \frac{\Omega_r \tau}{0.5 \rho U_\infty^3 A} \quad (2.2)$$

where τ is the shaft torque, ρ is the fluid density and A is the swept rotor area.

The rotor thrust can be expressed as a non-dimensional parameter, which is thrust coefficient. It is a ratio of the force on the rotor to the dynamic force in the flow. It is defined as

$$C_T = \frac{F}{0.5 \rho U_\infty^2 A} \quad (2.3)$$

where F is the thrust force on the rotor shaft.

2.2 Station keeping system

In order to fix the turbine in a suitable depth in the tidal stream, in the prototype devices listed by EMEC, there are various methods to fix the horizontal TST to the seabed:

a, x, y|z Gravity base is a physical way to fix the TST to seabed by means of a massive weight[44].

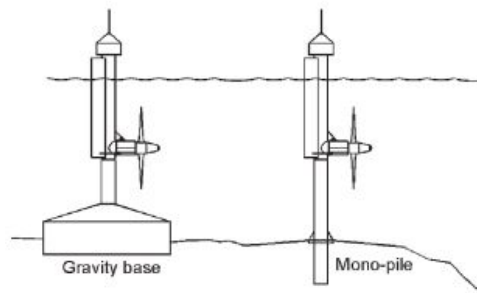


Figure 2.3: Configurations of gravity base and mono-pile [91]

2. Pile mounted is a principle that is used to mount most large wind turbines, whereby the TST is attached to a pole penetrating the ocean floor. Horizontal axis devices are able to yaw about this structure[44]. In some design the pile also allows the turbine to be raised above the water level for maintenance.
3. Flexible mooring is a structure that the TST is tethered via a cable or chain to the seabed[45]. The device is allowed to move freely and swing as the tidal current direction changes with the tide.
4. Rigid mooring is a structure that the TST is secured into position by a fixed mooring system[45]. This makes the device have minimal leeway.
5. Floating structure allows several turbines mounted to a single platform moving in relation to changes in sea level[45].

Figure 2.3 gives configurations of the gravity base and pile support systems. In this thesis a pile mounted TST will be discussed firstly and passive structure control will be applied to the system. Then a flexible

mooring system will be investigated with a buoy providing the tension and working as a damper.

2.2.1 Gravity base

Gravity bases are utilized in various forms and need or need not be fixed to the seabed. In its simplest form, the gravity base anchor or foundation will be lowered to the seabed and its weight will be sufficient to hold the structure in its location. Piles, grouting or suction techniques are used to fix the base to the sea bed in other instances[44].

Gravity base anchors are used where vertical lift components are required[44]. They are used in oil and gas industry mooring applications particularly in shallow water or surface bed rock usually for the mooring of support vessels. Moreover they are increasingly used in installing wave energy devices.

Gravity base anchors can be installed as a whole or made up of components in order to reduce lifting requirements. Besides, gravity base anchors are typically reinforced concrete designs but may have skirts, spikes or other attachments to increase horizontal friction with the seabed.

2.2.2 Pin Pile

Pin piles are widely used in the offshore industry and can be driven, drilled or sucked into position depending on the ground conditions. The

use of piles are dependent on their configurations, typically high strength grout is used to keep the structure in place and mooring applications can use fittings like ball and roller inserts. 'Bell footing' is used to increase the holding power in sand, it is a technology that the bottom of the drilled hole is expanded out and filled with cement. In softer sands an epoxy can be used to stabilize the sands around the hole.

Due to the nature of the seabed it is more likely that pin-piles will be drilled for tidal applications. Drilling of the sockets can be conducted from the surface through a conductor or using subsea drilling rigs, technology from deep water oilfield developments is enhancing the ability to develop installation methods for drilling and securing pin piles using subsea drilling rigs operated automatically from the surface [44].

Pin piles are commonly used for permanent moorings, but the cost of installation is higher. Piles can be either drilled, driven or use suction to be installed in place. Drilling is used in the conditions with harder bottom, piling and suction techniques are used in the softer sediments. The advantage of suction techniques compared with piling is that with piling the life of the pile will be reduced if too much energy is expended in the piling operation [44]. Once a pile has been placed, a mooring structure will be inserted and be cemented in place or use ball and roller type fittings to keep place.

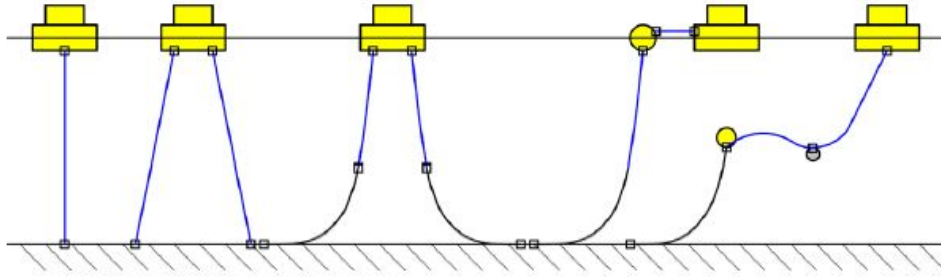


Figure 2.4: Schematic of mooring arrangements for a single marine renewable energy device: (from left) taut-moored systems with single and multiple lines, basic catenary system, catenary system with auxiliary surface buoy and lazy-wave system with subsea floater and sinker [45].

2.2.3 Mooring

Marine renewable energy mooring systems can be divided into three categories: passive, active and reactive. To provide station-keeping is the main function of a passive mooring system. These systems tend to be used for large floating platforms which have multiple marine renewable energy devices attached. The response of active mooring systems is affected significantly by the dynamic response of the moored device with both responses being coupled and affecting the power output of the device. In the case of a reactive system the mooring is an integral part of the system. Figure 2.4 shows mooring systems tended to be used for large floating platforms which support multiple marine renewable energy devices.

In the offshore industry both catenary and taut moored systems are widely used, particularly for Floating Production Storage and Offloading (FPSO), Floating Production Storage (FPS) facilities as well as Single Point mooring and Reservoir (SPAR) and Catenary Anchor Leg Mooring (CALM)

structures [45]. In order to keep a device on station, catenary mooring systems comprise single or multiple lines with a catenary geometry to provide the necessary horizontal and vertical restoring forces. The catenary mooring allows for changes in the water depth due to tidal variations and motions in several degrees-of-freedom for power generation. ‘Lazy-wave’ system which includes float and sinker components attached to the line is a developed system to increase the horizontal compliance of the catenary mooring.

Alternative materials could be used for the mid or upper sections of the line instead of using steel components for the entire line to reduce the cost and weight of mooring system and provide compliance. ‘Rider’ or ‘ground’ chains are used for the lower sections to provide tension to the line, they transferred loads horizontally to the anchor or foundation as well. A much stiffer connection provided by Taut-mooring system is between the device and seabed, the compliance is only provided by the axial properties of the mooring components such as synthetic ropes. Platforms located in deep water locations are successfully secured with ropes constructed from polyester [46]. Foundations and anchors must be specified to operate under horizontal and vertical directions due to restoring forces in both directions are provided by this type of mooring system. Unless a large mooring footprint is specified, the limited compliance of a taut-moored system may mean that the device becomes submerged during large amplitude waves or in locations with high tidal ranges [48]. Full or partial submersion of the device is not an issue for some designs and may be a way of limiting device displacements in large amplitude waves [47]. For mooring sup-

ported TSTs, the buoy will be full or partial submerged but the turbine keeps being full submerged. In the last two decades the offshore industry has successfully utilized ropes constructed from synthetic materials such as polyester, aramid, nylon and high-modulus poly-ethylene for vessel mooring, towing and equipment station-keeping. Compared to steel components, fibre ropes have particular advantages such as low cost and mass (per unit length) and load extension properties to reduce peak loading, parallel stranded polyester is one of the most common rope types. It is feasible that utilization of these materials could reduce the cost of mooring systems for marine renewable energy. Unlike steel components, synthetic materials have non-linear load-extension properties that are time dependent [49]. The fatigue, durability and stiffness of polyester is well understood through research over the last two decades. Nylon ropes which are 2-3 times more compliant than polyester, could be suitable for MRE mooring systems [50].

A basic survey of the use of elastic mooring tendons for the mooring of tidal current turbines is presented by Bowie [34]. Where it was shown that the reduction of cost and time involved in installation are reported significant reductions using flexible moorings instead of pile structure foundations, moreover the structural costs of the device and its mounting can be reduced. The utilization of orientating the device to current flow naturally reduces the cost of control systems, furthermore not only are maintenance costs reduced by allowing removal of device for onshore maintenance, but also downtime is reduced. However, the calculations undertaken by Bowie [34] did not include the thrust, torque and more

dynamic characteristics of a tension mooring turbine.

A tidal turbine with a single line (taut) mooring system will be introduced in this thesis. The advantages of this system is that it has few components and can provide a direct link between the floating part and the turbine. However, no redundancy is provided by this system in the case of line failure and anchors or foundation that can be loaded vertically are required. Another disadvantage of a normal taut mooring system is the applicability in large tidal ranges, so the floating part will be submerged in this thesis in order to make the system operate in sites with a large tide range.

2.3 Environment loads on tidal turbine

The following section will review the hydrodynamic loads on a turbine generated from the marine environment, this has been described by previous researchers. This section covers the effects of the tidal current flow, wave motions and their interactions with the currents and some other effects, this is followed by the techniques used to model the hydrodynamics, as presented in the next section.

The currents, waves and turbulence affects the fluid particle motions under the sea-surface in a highly complicated relationships, this is so complex that the topic is still an active research field to this day. Nevertheless, it is possible to simplify this chaotic environment by treating the currents, waves and turbulence as separate phenomena and to study

their individual effects on the turbine loads before attempting to resolve their interactions with each other.

First, the wave loading on a tidal turbine will be investigated. The second part of this section will describe the inflow current loading on a tidal turbine and the secondary loading on a submerged rotor generated from the resulting fluid acceleration.

2.3.1 Wave Loading

Since the 1970's wave loading on structures in marine environment has been extensively investigated via researches in the oil and gas industries. However, for tidal stream turbine the effects of surface waves has only been investigated recently. Most of the experiments of wave interaction studies on TSTs are in the form of tow-tank or flume tests on scale models, full scale TSTs experiments in oceans has been implemented only in recent years such as ATLANTIS AR1000 and AR1500 [51, 38].

A scale turbine of 350 mm diameter towed through incident waves is presented by Barltrop et al. [54], the variations of the blade root bending moments were as large as 50% of the mean load for the out-of-plane moment and 100% of the mean load for the in-plane moment. The experimental results showed that the main load oscillation occurred at the encountered wave frequency and that the in-plane-bending moment load signal for a single blade had a superimposed self-weight component resulting from the gravity load of the blade.

Whilst tow-tank testing provides a controlled environment to study the effects of different inflow parameters on a turbine, the towing through still water generates a turbulence free environment which is not representative of a real tidal flow-site. Furthermore, since the waves propagate over still water, no wave-current interactions are in effect using this method. On the other hand, testing small-scale devices in recirculating flumes can provide a more realistic inflow condition in terms of turbulence intensities and wave-current interactions.

Gaurier et al. [52] performed such a study that a three bladed turbine with 400 mm long blades was subjected to various wave and current inflow conditions and there were in plane and out of plane strain gauges assembled on the blades. The results of the blade loading showed that the standard deviation of the blade strains increased with an order of 2 - 3 times in wave conditions compared to the current only case, which is in alignment with Barltrop et al. [28]. Also, it was observed that the mean value of the blade strain was the same for the wave and pure current cases, which Galloway et al. [53] attribute to the use of sinusoidal waves with an average net velocity of zero, a result that is likely to change if steeper waves with greater peak-trough asymmetry are used. It is again reported that the fatigue performance of a turbine will be dominated by the wave contribution and that this will be a significant driver of turbine durability and cost [52].

2.3.2 Current Loading and Fluid Acceleration Effects

The thrust forces and the useful shaft torque generated from the tidal stream inflow currents are the main static forces on a turbine's rotor. The early small-scale experimental tests on TSTs were performed by Batten et al. [55] in 2007 showed that tidal turbines which are subjected to uniform inflow conditions produce performance curves (C_P and C_T plotted as functions of the TSR) that are similar to those of wind turbines with peak values of C_P and C_T at 0.45 and 0.80 respectively. The blade root pitch setting was a significant influence for both the performance parameters and the optimal TSR position. Both Baen et al. [55] and Barltrop et al. [54] successfully managed to replicate the experimental performance curves of TSTs using BEMT codes, which generally perform well close to the optimum TSR but become less accurate at the higher TSR regions of high induction operation (Section 3.2.2). A similar performance-drop is also present in the high TSR region where the rotor enters the turbulent wake state [56]. It is also noted that in the higher and lower bounds of the studied TSRs by Milne et al. [57], causes the values of C_P and C_T to exhibit a comparatively large degree of scatter.

All submerged objects in an oscillating flow field experience drag forces due to pressure gradients and skin friction, and inertia forces due to the acceleration of the fluid. Tidal turbines operate in a medium with 800 times greater density than air so it is suspected that inertial effects, also termed added mass effects, will be appreciable in the tidal environment. The most widely used method of calculating wave-induced inertial forces on submerged objects is the Morison equation [58] which Buckland [59]

presented and it is based on the original description of Chapman [31], the Morrison effect is a significant impact for the mooring supported turbine and will be discussed in Chapter 5.

2.3.3 Wave and Current Interaction

The basic calculation method of wave loading on offshore structures has been successfully developed and utilized by the offshore industry, but it has been a standard practice in ocean engineering disciplines for a long time to consider the current and surface wave particle velocities as separate entities [60]. In most engineering cases where current and wave loads are to be determined, the velocity fields from the currents and waves are calculated individually and then added in a process called linear superposition [61].

The interactions can be treated as a simple Doppler shift of the wave frequency [62]. On the other hand, waves propagating over a current with a linear shear-profile (constant vorticity), where the rotational flow is still maintained for the wave motion, effects arise in form of a modification to the dispersion relationship between the wave period and wave length (Section 3.1) [63]. During the presence of more complex non-linear shear velocity flow distributions, the near-surface vorticity leads to an important modification of the dispersion relationship which affects the water-particle velocities throughout the water column [63] whilst also changing the surface elevation profile. Consequently, as wave-current interactions tend to modify the shape of the surface elevation and underlying flow-

fields, they also affect the hydrodynamic forces on submerged structures. The wave-current interaction models will be discussed in detail in Chapter 3.

2.4 Blade Element Momentum Theory

According to an international design standard for marine energy converters, Design requirements for marine energy systems (IEC 62600-2) [42], a simulation time domain should not be less than 3 hours for each sea-state to ensure that the load output is statistically stationary when wave load on the structures are analyzed. It is obvious that this standard gives a strict requirement on the convergence speed of the models used for load investigations of TSTs with the required time-step size.

This section introduces the theory behind the hydrodynamic rotor-load model used in this thesis and the alterations made to it to enable the capture of the marine loading phenomena. The model was based on an unsteady BEMT formulation due to its superior computational efficiency and was implemented in the Matlab R2017b[98] which could easily be run on a laptop.

Several assumptions have been made in BEMT model to simplify the complex interactions between rotating machinery and the fluid. A major one of these is that the turbine operates in a non-turbulent, steady-state environment in order to allow the force equations of the blade and the fluid to be equated [64].

The CFD simulations for tidal turbines operating in wave-current may take weeks to get results, the BEMT models only spends hours to run a simulation. However, there are theoretical limits on BEMT due to its simplified and low computational cost. One of these limitations is that the axial induction factor a can exceed its upper theoretical limit of 0.5 at high TSRs, this makes the downstream wake of the rotor reverse. However, in reality, at these TSR regions the downstream flow becomes turbulent which is known as the turbulent wake state [65].

2.4.1 One Dimensional Momentum Theory

This section describes the fundamental governing equations of the BEMT method. These equations are the momentum theory equations adopted for an actuator disc and the blade element equations, which are combined within the BEMT method in order to close the mathematical problem and solved for the loading forces.

A turbine generates power by extracting energy from the working fluid passing through the rotor area. If it is assumed that the fluid affected by the rotor disc does not interact with the ambient fluid, a control volume can be defined in the form of a stream tube enclosing the rotor and the passing flow as shown in Figure 2.5.

The turbine's rotor can be assumed to be an actuator disc, it changes the shape of the stream tube from smaller than the rotor area to larger than it downstream because of the mass conservation across the stream tube.

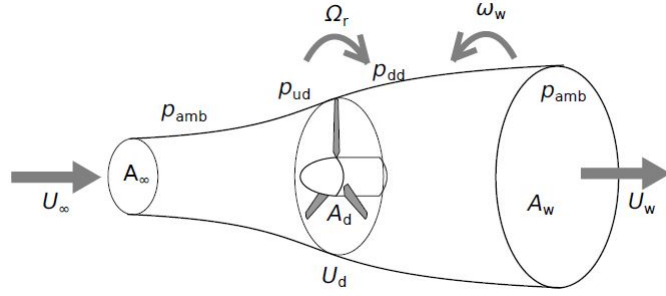


Figure 2.5: Definition of the annular stream tube control volume over the turbine and flow domain. [65]

The relationship between the areas, velocities and fluid density in the upstream, downstream and at the actuator disc region [66] is given by:

$$\dot{m} = U_{\infty} A_{\infty} \rho = U_d A_d \rho = U_w A_w \rho \quad (2.4)$$

where \dot{m} is the mass flow rate, U is the fluid speed, A is the area, ρ is the fluid density and the corresponding subscripts stand for conditions in the far upstream (∞), at the actuator disc (d) and in the wake (w) as illustrated in Figure 2.5.

The in flow velocity at the actuator disc can be described with the axial induction factor a which is the fractional reduction in flow speed between the free stream and the actuator disc, this is:

$$U_d = U_{\infty}(1 - a) \quad (2.5)$$

The rate of change of fluid momentum is caused by the total velocity

change and it is given as

$$\text{Rate of change of momentum} = (U_\infty - U_w)\rho A_d U_d \quad (2.6)$$

The left hand side in Equation 2.6 can be substituted by the force on the disc caused by the pressure differential across it and the velocity at the disc U_d can be substituted by Equation 2.5, giving:

$$(p_{ud} - p_{dd})A_d = (U_\infty - U_w)\rho A_d U_\infty(1 - a) \quad (2.7)$$

The Bernoulli equation can be applied along the stream tube to find the pressure differential of the upstream and downstream regions. Assuming that the flow is incompressible and horizontal, this gives:

$$\frac{1}{2}\rho U_\infty^2 + p_{amb} = \frac{1}{2}\rho U_d^2 + p_{ud} \quad (2.8)$$

$$\frac{1}{2}\rho U_d^2 + p_{dd} = \frac{1}{2}\rho U_w^2 + p_{amb} \quad (2.9)$$

where p_{amb} is pressure far up and down stream from the rotor, which is assumed to be an ambient pressure. Subtracting the above equations gives the pressure gradient as:

$$A_d(p_{ud} - p_{dd}) = \frac{1}{2}\rho(U_\infty^2 - U_w^2) \quad (2.10)$$

then insertion into Equation 2.7 gives:

$$\frac{1}{2}\rho(U_\infty^2 - U_w^2) = (U_\infty - U_w)\rho A_d U_\infty(1 - a) \quad (2.11)$$

and it is shown that:

$$U_w = (1 - 2a)U_\infty \quad (2.12)$$

and the force can be obtained from the combination of Equation 2.7 with Equation 2.12, to give:

$$F = A_d(p_{ud} - p_{dd}) = 2\rho A_d U_\infty^2 a(1 - a) \quad (2.13)$$

2.4.2 Rotational Momentum

The analysis in the previous section can be extended to the case where the rotor imparts angular momentum to the flow as presented by Masters & Orme [67] in order to derive an expression for turbine torque.

Since the torque generated by the fluid on the rotor is dependent on the local turbine radius, r , the analysis is based on the method of dividing up the stream tube into several annular sections with thickness dr with a cross sectional area of $2\pi r dr$ as illustrated in Figure 2.6.

If it is assumed that the angular velocity ω_w imparted on the flow is small compared to the turbine angular velocity Ω_r , it can be assumed that the

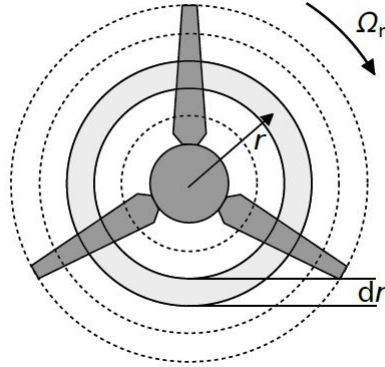


Figure 2.6: The control stream tube is divided into annular sections with thickness dr [69].

pressure in the far wake is the same as the pressure in the free stream [69].

The analysis of wake rotation is based on an annular control volume rotating with the turbine's angular velocity Ω_r . This allows the Bernoulli energy equation to be used in the sections before and after the actuator disc to calculate the pressure difference across it by assuming the axial flow across the disc is constant [68] giving:

$$p_{ud} - p_{dd} = \rho(\Omega_r + \frac{1}{2}\omega_w)r^2\omega_w \quad (2.14)$$

The resulting thrust across an annular element is the pressure difference multiplied by the annular area giving:

$$dF_{A1} = (\rho(\Omega_r + \frac{1}{2}\omega_w)r^2\omega_w)2\pi r dr \quad (2.15)$$

and the angular induction is defined as:

$$b = \frac{\omega_w}{2\Omega_r} \quad (2.16)$$

rewriting the annular thrust with the angular induction factor gives:

$$dF_{A1} = (4b(1-b)\frac{1}{2}\rho\Omega_r^2 r^2)2\pi r dr \quad (2.17)$$

an expression for the torque on an annular stream tube section can be written as:

$$dT = dm(\omega_w r)r = \rho U_d 2\pi r dr (\omega_w r)r \quad (2.18)$$

substituting Equation 2.5 and Equation 2.16 into Equation 2.18 gives an expression for annular torque as:

$$dT_1 = 4\pi\rho b(1-a)U_\infty\Omega_r r^2 r dr \quad (2.19)$$

the kinetic energy in the wake is increased because of the turbine generates an angular velocity component to the flow [66], this increase in wake energy is equivalent to the loss of static pressure in the wake and is defined as:

$$\Delta p = 0.5\rho(2\Omega_r br)^2 \quad (2.20)$$

Equation 2.13 can be rewritten by the annular area of $2\pi r dr$ to give:

$$dF_A = 4\pi\rho U_\infty^2 a(1-a)rdr \quad (2.21)$$

the induced force of this pressure drop can be obtained by Multiplying Equation 2.20 with the annular area of $2\pi r dr$, then adding to Equation 2.21, the final expression for the thrust on the fluid is given as:

$$dF_{A1} = 4\pi\rho(U_\infty^2 a(1-a) + (b\Omega_r r)^2)rdr \quad (2.22)$$

Although momentum theory gives the expressions for the thrust and torque, the axial and angular induction factors, a and b are still not known. Thus, momentum theory must be combined with blade element theory in order to close the set of equations.

2.4.3 Blade element theory

Blade element theory is based on a principle of dividing the rotor's blades into several equally sized elements that intersect with the stream tubes defined in Figure 2.6. The lift and drag forces on the blade elements are solved by treating the elements as independent two-dimensional airfoil sections. Look-up tables are used to check the 2-D airfoil data and the geometric turbine parameters such as twist and chord distributions at the blade radius for each section.

Figure 2.7 shows the relative inflow velocity vectors on a blade sections. The resultant flow vector V is the resultant vector composed of the in-

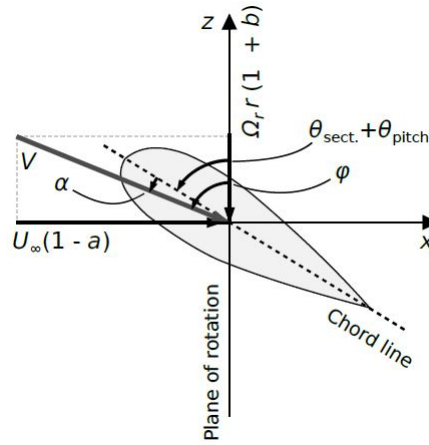


Figure 2.7: Inflow velocity vectors on a blade section

duced axial in flow velocity $U_\infty(1-a)$ and the induced angular inflow velocity $\Omega_r r(1+b)$. The angle of attack α is the angle between V and the chord line of the blade element, it is determined by the resultant velocity's angle of incidence φ , the blade root pitch θ_{pitch} and the local blade twist at particular blade section θ_{sect} . This is given as:

$$\alpha = \varphi - (\theta_{sect} + \theta_{pitch}) \quad (2.23)$$

The magnitude of the lift and drag forces are determined by the angle of attack, Figure 2.8 shows the elemental lift dL , drag forces dD , elemental axial forces and elemental radial forces.

The elemental axial and radial forces can be calculated from:

$$dF_{A2} = dL \cos \varphi + dD \sin \varphi \quad (2.24)$$

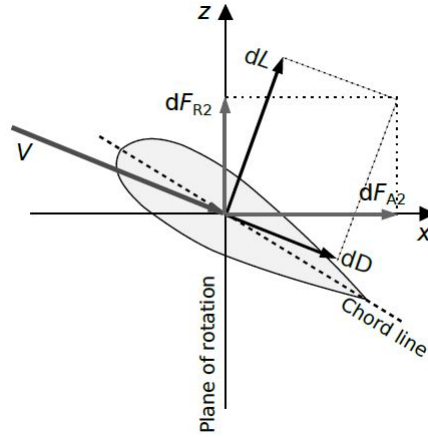


Figure 2.8: Induced blade-forces on a blade section

$$dF_{R2} = dL \sin \varphi - dD \cos \varphi \quad (2.25)$$

where φ is determined through the Pythagorean theorem from Figure 2.6 as

$$\varphi = \tan^{-1} \left(\frac{U_{\infty}(1-a)}{\Omega_r r(1+b)} \right) \quad (2.26)$$

and the resultant flow vector becomes

$$V = \sqrt{((U_{\infty}(1-A))^2 + (\Omega_r r(1+b))^2)} \quad (2.27)$$

The elemental thrust and torque contributions to rotor loads can be defined as

$$dF_{A2} = N \frac{1}{2} \rho V^2 c (C_L \cos \varphi + C_D \sin \varphi) dr \quad (2.28)$$

$$dT_2 = N \frac{1}{2} \rho V^2 c (C_L \sin \varphi - C_D \cos \varphi) r dr \quad (2.29)$$

where C_L and C_D are the lift and drag coefficients for the airfoil sections for the specific α at the blade section, N is the number of blades of the turbine and c is the blade section chord length.

The method used to solve the set of equations derived from momentum theory and blade element theory is to make the two thrust Equations 2.17 and 2.28 equal and make the two torque Equations 2.18 and 2.29 equal. After the iteration reaches the convergence criterion, the solution of a and b will be found. Then the elemental forces of each blade are added to obtain the total thrust and torque acting on the the rotor.

The solution method used in this thesis is presented by Nevalainen [32] with the error minimization through an optimization routine as presented by Masters & Orme [67] and Chapman [31].

2.4.4 Correction factors

The Prandtl tip loss correction is a factor representing the turbine's efficiency loss in BEMT due to the rise in tip vortices, which decrease the performance close to blade tips. The factor tends to zero at the blade tips and to one at the root [70]. It is defined as:

$$F_{\text{tip}} = \frac{2}{\pi} \cos^{-1} \left(\exp \left[-\frac{N (1 - (r/R))}{2 (r/R) \sin \varphi} \right] \right) \quad (2.30)$$

where R is the rotor radius. A hub loss correction factor may also be added in a similar manner as suggested by Moriarty [71] as:

$$F_{\text{hub}} = \frac{2}{\pi} \cos^{-1} \left(\exp \left[-\frac{N}{2} \frac{(r - R_{\text{hub}})}{r \sin \varphi} \right] \right) \quad (2.31)$$

where R_{hub} is the radius of the turbine hub. The total loss factor is then defined as:

$$F = F_{\text{tip}} F_{\text{hub}} \quad (2.32)$$

Combining the factor with the momentum equations for thrust and torque gives:

$$dT_1 = 4\pi\rho F b(1 - a)U_\infty \Omega_r r^2 r dr \quad (2.33)$$

$$dF_{A1} = 4\pi\rho F (U_\infty^2 a(1 - a) + (b\Omega_r r)^2) r dr \quad (2.34)$$

As the turbine enters its turbulent wake state during high axial induction factors at high TSRs, the original BEMT theory will under predict the thrust on the rotor. This can be corrected by using an empirical formulation of the axial induction factor at large a -values, which is obtained from experimental data.

A frequently used method to correct for the thrust under-prediction in the

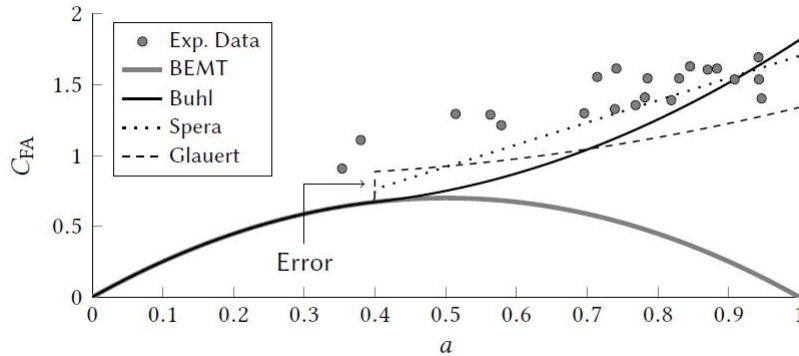


Figure 2.9: Local element thrust coefficient C_{FA} for various empirical models plotted against axial induction factor with Prandtl tip-loss factor $F = 0.7$

turbulent wake state is the Spera high induction correction as discussed in Shen et al. [70].

Another widely used empirical method of high induction correction that has been included as an option for the presented BEMT model is the high induction correction factor by Glauert [68].

Finally, Buhl [72] addressed the issue that the Spera and Glauert high induction corrections fail to incorporate the Prandtl loss factor by fitting a parabolic curve to the highly loaded experimental turbine data shown in Figure 2.9.

The blades on fixed-pitch rotors will operate in the full range of boundary layer regimes for the airfoils which are classified as the ‘attached’, the ‘high lift’ and the ‘stall’ regions of the lift and drag curves. So it is important to know the details of the lift and drag behaviour of the airfoils in the high lift and stall regime. An empirical model modifies the experimental or numerical 2-D airfoil lift and drag data in the high lift/post-stall

boundary layer regimes to more accurately capture the airfoil behaviour observed for stalling turbines, which is developed by Viterna & Corrigan and discussed in Spera [73].

2.5 Passive control

In the wind industry, one of the main problems and governing failure modes is the wind turbine tower fatigue, due to turbulent wind loading and dynamic loading from rotation of the turbine. The cost of the entire wind turbine tower may be reduced if the dynamic response of the turbine tower is suppressed. The dynamic loading in tidal turbine towers is more complicated, so that it becomes necessary to reduce the dynamic response of the turbine tower.

2.5.1 Tuned mass damper

The TMD concept was first applied by Frahm in 1909 [74] to reduce the rolling motion of ship and ship hull vibrations. Ormondroyd and Den Hartog [75] presented a theory for TMD later, followed by a detailed discussion of optimal tuning and damping parameters in Den Hartog's book [76]. The theory was firstly applicable for an undamped Single Degree Of Freedom (SDOF) system with a sinusoidal force excitation. This theory for damped SDOF systems has been investigated by numerous researchers.

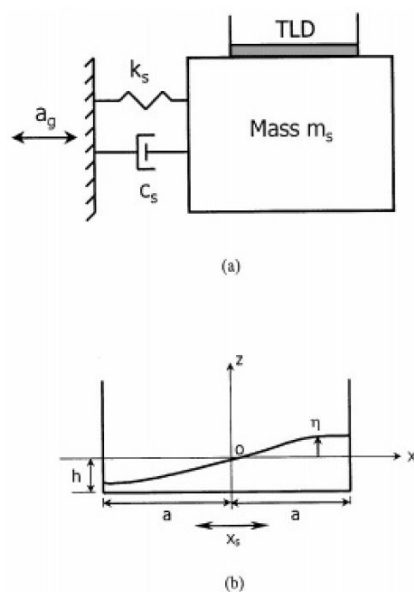


Figure 2.10: (a) Schematic of a single-degree of freedom structure with a rectangular tuned liquid damper for SDOF system and (b) dimensions of the rectangular tuned liquid damper [77]

The principle of a TMD is adding an extra structural damping to the structure, where leads to a significant reduction of the fatigue load. This is the passive control method utilised in this thesis, details will be given in Chapter 3.

2.5.2 Tuned Liquid damper

A tuned liquid damper (TLD) is placed on a structure and its frequency is tuned to the natural frequency of structure, it generally consists of a rigid tank with shallow water in it, as shown in Figure 2.10.

The TLD creates dynamic forces which absorbs excitation when the liquid in it moves. Tanmura et. al. [78] presented a study of Nagasaki

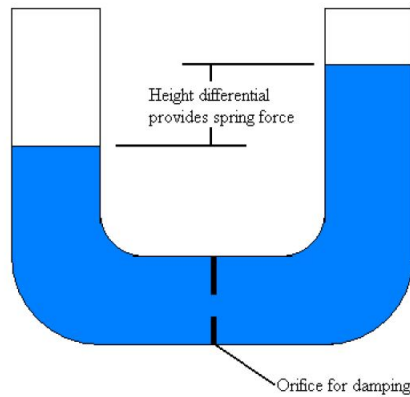


Figure 2.11: Schematic of a tuned liquid columns damper [16]

Airport Tower equipped with a TLD system. The results showed that the damping ratio of the tower increased by 4.5 times the original value.

It is simple to manufacture and install a TLD. Moreover, It is considered to be cost-effective due to the infrequent maintenance required[77].

2.5.3 Tuned Liquid columns damper

The principle of a tuned liquid column damper is similar to a tuned liquid damper except that the tuned liquid column damper has two vertical columns. The height difference in these columns plays the role of a spring. Likewise, the fluid passing through the orifice separating these two columns provides a damping force [16]. Figure 2.11 shows schematic of a tuned liquid columns damper.

A TLCD consists of a rigid piping system which is integrated in a structure and partially filled with liquid, preferably water. Its dynamics can be derived using the extended instationary Bernoulli's equation for moving

reference systems. Extending the passive TLCD by an actively controlled air-spring setup, and applying a suitable control strategy results in a novel hybrid active damper which combines both, the advantages of active control devices, and the salient features of TLCD, e.g., cheap and easy implementation into civil engineering structures, simple modification of the natural frequency and damping properties, little maintenance costs, a performance comparable to TMD as well as little additional weight if the TLCD is used as water reservoir for fire fighting [99].

2.6 Summary

In this chapter, the basic types of station keeping systems for TSTs are introduced, the mono-pile and mooring are the support systems modeled in this thesis. Basic theories of BEMT is explained to give an understand of the further application in the next chapters. The loading calculations on TSTs for the mono-pile and mooring supported are basis on the BEMT code. Then three kinds of structural passive controls are listed and briefly discussed to show which method is taken in this thesis for load reduction.

Chapter 3

Models

3.1 Wave Models

This following section discusses the mathematical challenge for modeling surface wave motions expressed as a potential flow problem. Figure 3.1 shows the definition of the flow domain in all wave models used here, where the origin is at the mean water level (MWL), C is wave celerity (wave speed), H is wave height, a is wave amplitude, L is wave length and h is water depth.

3.1.1 Governing equations and boundary conditions

Due to the fluid flow is considered to be two dimensional, irrotational and incompressible in all potential flow wave models, a potential flow field may be assumed throughout the domain and thus the Laplace equation

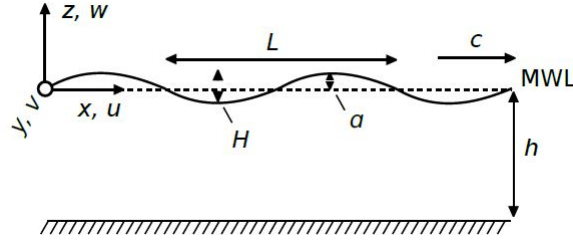


Figure 3.1: Diagram showing the definition of the flow domain as used by the wave models

[79] shown below must be satisfied along the horizontal x and vertical z coordinates as:

$$\frac{\partial^2 \varphi}{\partial x^2} + \frac{\partial^2 \varphi}{\partial z^2} = 0 \quad (3.1)$$

where φ is the velocity potential and from potential flow theory the horizontal and vertical velocity components are given as:

$$u = \frac{\partial \varphi}{\partial x}, \quad w = \frac{\partial \varphi}{\partial z} \quad (3.2)$$

Navier-Stokes equations can be used to represent the equations of motion for a fluid parcel in the flow, which gives the relationship between forces acting upon the parcel and its mass and acceleration according to Newton's second law. If considering the fluid is inviscid, this relationship can be simplified to the Euler equation [80] due to the viscous forces, which can be neglected and written as:

$$\rho \frac{\partial \bar{v}}{\partial t} = -\nabla p + \rho \bar{g} \quad (3.3)$$

where ρ is the fluid density, \bar{v} is the fluid velocity vector, ∇p is the pres-

sure gradient over the fluid parcel and \bar{g} is the gravitational acceleration. As the flow is assumed to be irrotational, the Euler equation can be integrated over a streamline and transformed to a generalized Bernoulli equation as:

$$gz + \frac{p}{\rho} + \frac{1}{2} \left(\left(\frac{\partial \varphi}{\partial x} \right)^2 + \left(\frac{\partial \varphi}{\partial z} \right)^2 \right) + \frac{\partial \varphi}{\partial t} = C(t) \quad (3.4)$$

The boundary conditions for the problem can be separated into free surface boundary conditions, bottom boundary conditions and periodicity boundary conditions. because there is no flow going through the seabed, the bottom boundary condition is set to be zero vertical velocity as:

$$w = 0 \rightarrow \frac{\partial \varphi}{\partial z} = 0 \text{ for } z = -h \quad (3.5)$$

The fluid is allowed to slip along the seabed, which means that there is no constraint for the horizontal velocity component. The kinematic boundary condition and dynamic free surface condition are set at the surface. The kinematic boundary condition relates the surface water-particles' vertical velocity component to the surface vertical velocity component and is expressed as:

$$\frac{\partial \varphi}{\partial z} = \frac{\partial \eta}{\partial t} + \frac{\partial \eta}{\partial x} \frac{\partial \varphi}{\partial x} \text{ for } z = \eta \quad (3.6)$$

where η is the free surface displacement around the mean water level. For a dynamic free surface boundary condition, the pressure at the sur-

face must be equal to the atmospheric pressure which is assumed as a constant p_0 . The pressure at the free surface can be expressed by using Equation 3.4 as:

$$gz + \frac{p}{\rho} + \frac{1}{2}(u^2 + w^2) + \frac{\partial\varphi}{\partial t} = \frac{p_0}{\rho} \quad (3.7)$$

when setting $z = \eta$ as the surface displacement and $p = p_0$ at the surface, the equation above may be expressed as:

$$g\eta + \frac{1}{2}\left(\left(\frac{\partial\varphi}{\partial x}\right)^2 + \left(\frac{\partial\varphi}{\partial z}\right)^2\right) + \frac{\partial\varphi}{\partial t} = 0 \text{ for } z = \eta \quad (3.8)$$

The final boundary condition states that the periodicity of the waves must be upheld, which is expressed as:

$$\eta(x, t) = \eta(x + nL, t) = \eta(x, t + nT) \quad (3.9)$$

where n is all positive integers.

The free-surface kinematic boundary condition in Equation 3.5 and dynamic boundary condition in Equation 3.8 are both non-linear; this makes an analytical solution impossible, combining with governing Equation 3.1 for this mathematical problem. So suitable approximations for the governing equations are needed which will allow for the creation of useful wave models.

3.1.2 Linear wave theory model

The linear approach is based on Dean & Dalrymple [80] to solve the governing equations of motion. The wave-steepness, H/L , is assumed to be so small that the unknown surface elevation, η , can be eliminated from the governing equations, so as the surface boundary conditions is evaluated at $z = 0$ instead of $z = \eta$.

The neglect of non-linear term in Equation 3.6 only generates a small error by assuming that $H/L \ll 1$ [80]. The final form of the linearised kinematic free-surface boundary condition by using Taylor expansions around $z = 0$ becomes:

$$\frac{\partial \varphi}{\partial z} = \frac{\partial \eta}{\partial t} \text{ for } z = 0 \quad (3.10)$$

The dynamic boundary condition is linearised in the same method and becomes:

$$g\eta + \frac{\partial \varphi}{\partial t} = 0 \text{ for } z = 0 \quad (3.11)$$

Equations 3.10 and 3.11 can be combined to form a single free surface boundary condition, which is given by:

$$\frac{\partial \varphi}{\partial z} + \frac{1}{g} \frac{\partial^2 \varphi}{\partial t^2} = 0 \text{ for } z = 0 \quad (3.12)$$

The exact solution of the Laplace equation can be obtained by using the linearised free surface boundary condition in Equation 3.12, the bottom boundary condition in Equation 3.1 and the periodicity condition can be expressed by the method of separation of variables and Laplace equation separately. The final expression of the linear velocity potential then becomes:

$$\varphi = \frac{ag}{\omega} \frac{\cosh k(z+h)}{\cosh kh} \sin(\omega t - kx) \quad (3.13)$$

where ω is the wave angular frequency defined as $\omega = 2\pi/T$ and k is the wave number defined as $k = 2\pi/L$.

The dispersion relationship of a linear wave is defined as:

$$\omega^2 = gk \tanh(kh) \quad (3.14)$$

The simplest form of wave current interactions can be found when observing waves propagating on a current which is uniform with depth and flow direction. The velocity potential can be obtained by using the methodology described by Dean & Dalrymple [80], and given as:

$$\varphi = U_{\infty}x + \frac{ga}{\omega(1 - U_{\infty}k/\omega)} \cosh k(h+z) \cos(kx - \omega t) \quad (3.15)$$

The analytical expressions for the horizontal and particle velocities can be defined as:

$$u = U_\infty + \frac{gak}{\omega(1 - U_\infty k/\omega)\cosh kh} \cosh k(h+z) \sin(kx - \omega t) \quad (3.16)$$

$$w = -\frac{gak}{\omega(1 - U_\infty k/\omega)\cosh kh} \sinh k(h+z) \cos(kx - \omega t) \quad (3.17)$$

and the dispersion relationship becomes:

$$\omega^2 = \frac{gk \tanh(kh)}{1 - U_\infty k/\omega^2} \quad (3.18)$$

3.1.3 Third order Stokes wave-current model

In order to solve the governing potential flow equations with non-linear boundary conditions, Stokes wave theory is widely used. The order of the theory indicates that the number of terms kept in the perturbation expansion of the variables will be insert into the governing equations and solved for.

Kishida & Sobey [81] presented a third order Stokes theory coupled with a linear shear current profile. The mean Eulerian current U_m and constant current vorticity Ω_0 are calculated by:

$$U_m = U_s - \frac{(U_s - U_b)}{2} \quad (3.19)$$

$$\Omega_0 = \frac{(U_s - U_b)}{h} \quad (3.20)$$

where U_s is the surface velocity and U_b is the bottom velocity.

When current and wave parameters are specified, the first definition of Stokes wave speed is used as a dispersion relationship to define the celerity C which is used as the velocity of the moving reference frame [81]. The dispersion relationship for the model is defined as:

$$C = C_0(a_{11} - \epsilon^2 a_{20}) + U_m + \frac{1}{2}\omega_0 h \quad (3.21)$$

$$C_0 = [gk \tanh(kh)]^{1/2} \quad (3.22)$$

$$\omega_0 = \Omega_0/kC_0 \quad (3.23)$$

where the lengthy perturbation constants a_{11} and a_{20} are as given in Kishida & Sobey [81].

The third order solution of the stream function ψ was presented by Kishida & Sobey [81] as:

$$\begin{aligned} \psi = \frac{C_0}{k} [& a_{00}kz_l + a_{01}(kz_l)^2 + \epsilon a_{11} \frac{\sinh kz_l}{\sinh kh} \cos kx_l + \epsilon^2 (a_{20}kz_l + a_{22} \frac{\sinh 2kz_l}{\sinh 2kh} \cos 2kx_l) \\ & + \epsilon^3 (a_{31} \frac{\sinh kz_l}{\sinh kh} \cos kz_l + a_{33} \frac{\sinh 3kz_l}{\sinh 3kh} \cos 3kx_l) \end{aligned} \quad (3.24)$$

where the x_l and z_l coordinates are in the lagrangian frame of reference which are related to the global reference frame by $x_l = x - C(t)$ and $z_l = z$. ϵ is the wave steepness equals to $kH/2$, the perturbation constants can be found in Kishida & Sobey [81].

3.1.4 Fifth order Stokes wave-current model

A higher order method is needed to solve the governing potential equations for waves which are close to the breaking limit. Fenton [62] presented a model of fifth order Stokes theory for the dimensionless steepness, $\epsilon_F = H/gT$, above 0.02.

The celerity of the waves is calculated by the definition of the mean uniform current. The Eulerian time-averaged fluid velocity at any point is given by:

$$c_E = C - \bar{u} \quad (3.25)$$

where \bar{u} is the mean current speed user defined and dispersion relationship is given by Fenton [62] as:

$$\left(\frac{k}{g}\right)^{1/2} c_E - \frac{2\pi}{T(gk)^{1/2}} + C_0 + \left(\frac{kH}{2}\right)^2 C_2 + \left(\frac{kH}{2}\right)^4 C_4 = 0 \quad (3.26)$$

where C_0, C_2 and C_4 are coefficients which have functional dependence on kh .

The velocity potential in an Eulerian reference frame with the celerity and wave number solved from Equation 3.25 and 3.26 is given by:

$$\varphi = (c - \bar{u})x + C_0 \left(\frac{g}{k^3}\right)^{1/2} \sum_{i=1}^5 \epsilon^i \sum_{j=1}^i A_{ij} \cosh jkz \sin jk(x - ct) \quad (3.27)$$

where the fluid velocities are $u = \partial\varphi/\partial x$ and $w = \partial\varphi/\partial z$. The constants of A_{ij} are given by Fenton [62].

3.1.5 Three step wave-current interaction model

A fifth order wave model combined with BEMT code named 'three step' approximate wave-current interaction model has been developed by Dalrymple [82] since the original fifth order Stokes model is only applicable for waves on a uniform current. The method works by calculating the wave period that an observer moving with the depth-averaged mean current velocity would see, this period is defined as apparent period T_{app} and is given as

$$\frac{L}{T} = \frac{L}{T_{\text{app}}} + \bar{U} \quad (3.28)$$

where \bar{U} is the depth-averaged mean current. The wave length and period are related by the first-order dispersion relationship:

$$T_{\text{app}}^2 = \frac{2\pi L}{g \tanh(2\pi h/L)} \quad (3.29)$$

and the depth-mean current is approximated via linear wave theory:

$$\bar{U} = \frac{4\pi L}{\sinh(4\pi h/L)} \int_0^h U(z) \cosh\left(4\pi \frac{(z+h)}{L}\right) dz \quad (3.30)$$

where $U(z)$ is the arbitrary vertical current velocity profile.

3.1.6 Irregular sea-state wave model

A large number linear wave harmonics with random wave parameters are superimposed to represent the stochastic sea-state [85]. According to this method, the wave elevation in one dimension can be written as the sum of the displacement contributions from N number of waves from:

$$\eta(x, t) = \sum_{i=1}^N a_i \cos(k_i x - \omega_i t + \varphi_i) \quad (3.31)$$

where a_i is the wave amplitude, k_i is the wave number, ω_i is the angular frequency and φ_i is the random phase angle between 0- 2π for i -th wave component. The wave number and angular frequency are based on the dispersion relationship and wave amplitudes are obtained by Joint North Sea Wave Project (JONSWAP) [83] power spectral function which will be described in 3.1.7.

Similarly to the surface displacement, the linear equations for particle velocities can be re-written in harmonic form as:

$$u_i(x, z, t) = \frac{g a_i k_i}{\omega_i (1 - U_{0i} k_i / \omega_i) \cosh k_i h} \cosh k_i (h + z) \sin(k_i x - \omega_i t + \varphi_i) \quad (3.32)$$

$$w_i(x, z, t) = -\frac{ga_i k_i}{\omega_i(1 - U_{0i}k_i/\omega_i)\cosh k_i h} \sinh k_i(h + z) \cos(k_i x - \omega_i t + \varphi_i) \quad (3.33)$$

the term of the current velocity U_∞ will be added to the equations in later stage and U_{0i} is the current velocity component aligned with individual wave harmonic's direction of propagation.

The wave harmonic components are given a random distribution of directional spread. Each harmonic component is given a normally distributed random incidence angle θ_i between the wave orthogonal and the current flow in x direction. A coordinate system rotated to the angle of incidence is defined for each wave component. Then Equations 3.313.323.33 are evaluated by using the x'_i -coordinate from this reference frame which is transformed from the global reference frame by:

$$x'_i = \cos(\theta_i)x + \sin(\theta_i)y \quad (3.34)$$

the coordinate system is shown in Figure 3.2

The wave induced velocities for the added wave harmonics are now expressed as:

$$u(x, y, z, t) = U_\infty + \sum_{i=1}^N \cos(\theta_i)u_i(x'_i, t) \quad (3.35)$$

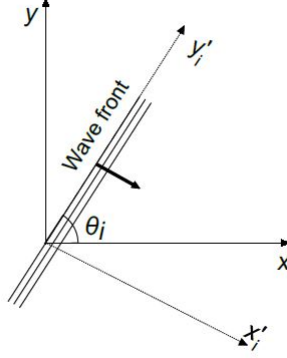


Figure 3.2: Coordinate system transformation for each harmonic component

$$v(x, y, z, t) = \sum_{i=1}^N \sin(\theta_i) u_i(x'_i, t) \quad (3.36)$$

$$w(x, y, z, t) = \sum_{i=1}^N w_i(x'_i, t) \quad (3.37)$$

3.1.7 JONSWAP power density spectrum

It will be unrealistic for the wave energy or steepness, if the values of a_i and ω_i are assigned arbitrarily. Field tests were undertaken by Pierson & Moskowitch [84] to record the irregular ocean surface elevation and to derive the spectral density for a natural sea-state from the collected signal by discrete Fourier transfer. Then the Pierson-Moskowitch (PM) spectrum $S_{PM}(\omega)$ was generated by fitting a function to the power density spectra in the frequency domain.

Based on PM spectrum, Hasselmann et al. [83] modified the spectrum to fit data from the JONSWAP which was collected from the North Sea. The

PM spectrum is defined by the DNV standard [60] as:

$$S_{\text{PM}}(\omega) = \frac{5}{16} H_s^2 \omega_p^4 \omega^{-5} \exp\left(-\frac{5}{4} \left(\frac{\omega}{\omega_p}\right)^{-4}\right) \quad (3.38)$$

where H_s is the significant wave height of the sea which is the mean of the third largest recorded wave heights, $\omega_p = 2\pi/T_p$ is the spectral peak angular frequency which is the frequency of the highest wave energy. The JONSWAP spectrum is defined as:

$$S_{\text{J}}(\omega) = A_{\gamma} S_{\text{PM}}(\omega) \gamma^{\exp(-0.5(\frac{\omega-\omega_p}{\sigma\omega_p})^2)} \quad (3.39)$$

$$A_{\gamma} = (1 - 0.287 \ln(\gamma)) \quad (3.40)$$

$$\sigma = \begin{cases} 0.07, & \omega \leq \omega_p \\ 0.09, & \omega > \omega_p \end{cases} \quad (3.41)$$

where γ is a non-dimensional peak shape parameter and σ is a spectral width parameter. For $\gamma = 1$, the JONSWAP spectrum collapses into the PM spectrum. In this thesis the value of γ is defined to 3.3 as recommended in DNV-RP-C205 [60].

According to Faltinsen [85], the relationship between the wave component amplitudes and angular frequencies can be expressed as:

$$\frac{1}{2}a_i^2 = S_J(\omega_i)\Delta\omega \quad (3.42)$$

where $\Delta\omega$ is the constant bandwidth between the N sampled frequencies from the power density spectrum used to construct the irregular sea-state.

The zero-crossing period for the JONSWAP spectrum can be empirically fitted to the peak period [60] by:

$$T_P = T_z / (0.6673 + 0.05037\gamma - 0.006230\gamma^2 + 0.0003341\gamma^3) \quad (3.43)$$

where T_z is the average zero-crossing period.

3.2 Rigid supported turbine

Considering unsteady wave-current coupled forces as excitation, the dynamic load experienced on a tidal turbine is a complicated physical problem which poses a challenge for engineers trying to design larger tidal turbine foundations and other floating support structures. Different structural damping strategies have been implemented in the wind industry such as tuned mass dampers and some control technologies like generator torque control and blade pitch control are also developed to reduce the fatigue and structural loading.

Even though structural damping control strategies have not been studied in the tidal energy field, strategies used by the offshore wind industry

can be used as a first approximation to augment the structural life of diverse components. Passive control approaches are widely adapted for wind turbines [6, 5, 3]. The use of a tuned mass damper (TMD) on a wind turbine structure, is a simple passive structural control technique to absorb energy at one of the natural frequencies of the entire structure [4]. The aim of this project is to design a tidal turbine station keeping system with a tuned mass damper in order to reduce fatigue and peak structural loading experienced by the support structures. This may result in a reduction of mass and costs associated with the structural support and station keeping system.

3.2.1 Numerical models for monopile support

A model to study the application of Tune Mass Dampers (TMD) on structures used for tidal turbines is presented in this section. This model is based on studies done for wind turbine technologies, as presented by Temple[8]. A wind turbine with a tower-monopile supporting structure can be modeled as an inverted pendulum, a general representation of the system is shown in Figure 1.

The tower-monopile dynamics can be modeled as a forced response of a non-gyroscopic damped linear system, a finite element model, established for wind turbines [12] is given by:

$$\mathbf{M}\ddot{\mathbf{x}} + \mathbf{C}\dot{\mathbf{x}} + \mathbf{K}\mathbf{x} = \mathbf{F}(t) \quad (3.44)$$

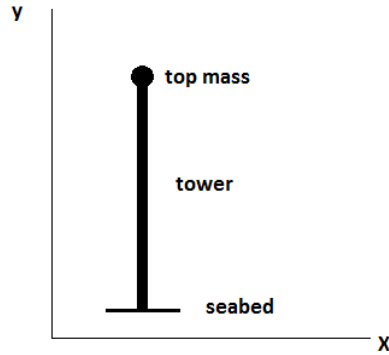


Figure 3.3: Structural model of a flexible wind (tidal) turbine

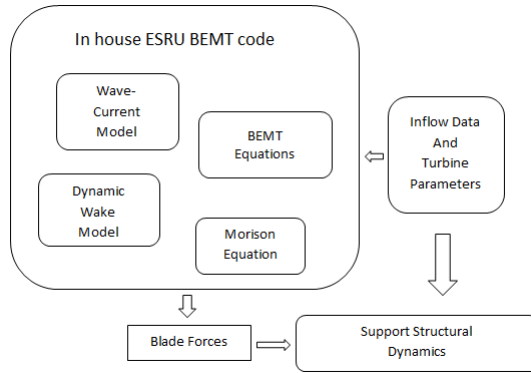


Figure 3.4: Flow chart of forces input

where M , C and K are the structural mass, damping and stiffness matrices; \ddot{x} , \dot{x} and x are structural nodal acceleration, velocity and displacement vectors in x -axis respectively ; $F(t)$ is the applied force, which in this case is predominantly the rotor thrust applied on the top node of structure and drag forces on the tower due to the tidal current. The rotor thrust is calculated by Blade Element Momentum Theory in wave-current coupled conditions, Figure 3 shows the procedure using Nevalainen's data [19, 20] in the dynamic analysis.

The structural damping is related to the first tower modal frequency ω_{0t}

as follows [14, 15]:

$$\mathbf{C} = 2\zeta_t\omega_{0t}\mathbf{M} \quad (3.45)$$

where ζ_t is structural damping ratio for steel structure which is set to 0.005 [14].

Unlike onshore and offshore wind turbines, tidal turbines are fully submerged in water, so the effect of added mass cannot be ignored, the added mass is the inertia added to a system because an accelerating or decelerating body must move (or deflect) some volume of surrounding fluid as it moves through it. It will change the natural frequencies of the structure, this will be shown in the results section. The tower is considered to be a vibrating rod in the water column in order to calculate the added mass and viscous damping [9] which will be discussed in Section 3.4. So the equation of motion can be corrected as:

$$(\mathbf{M} + \mathbf{M}_A)\ddot{\mathbf{x}} + (\mathbf{C} + \mathbf{C}_V)\dot{\mathbf{x}} + \mathbf{K}\mathbf{x} = \mathbf{F}(t) \quad (3.46)$$

where \mathbf{M}_A is the added mass matrix and \mathbf{C}_V is the hydrodynamic viscous damping matrix.

3.2.2 Tuned mass damper

The location of the Tuned Mass Damper (TMD) is in the nacelle, this model initially considers a nacelle oscillating in a horizontal fore-aft di-

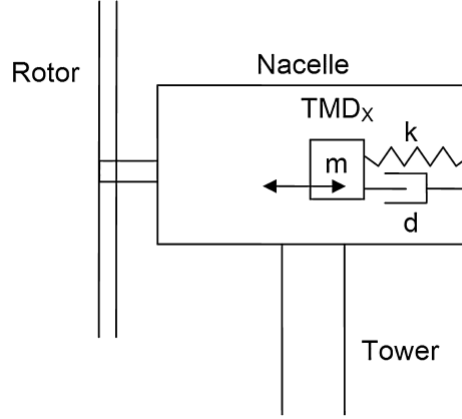


Figure 3.5: Schematic of TMDx in turbine nacelle [6]

rection which is denoted by TMDx. Figure 3.5 shows a simple schematic of the TMDx configuration.

The TMDx is considered as an additional degree of freedom in the x -axis. Once the tower-monopile's natural frequencies have been derived, the TMD properties can be calculated as Yilmaz[11]:

$$\omega_{\text{TMD}} = \sqrt{\frac{k_{\text{TMD}}}{m_{\text{TMD}}}} \quad (3.47)$$

$$\zeta_{\text{TMD}} = \frac{c_{\text{TMD}}}{2\sqrt{m_{\text{TMD}}k_{\text{TMD}}}} \quad (3.48)$$

where ω_{TMD} is the TMD natural frequency, k_{TMD} is the TMD spring stiffness, m_{TMD} is the TMD mass, c_{TMD} is the TMD damping constant and ζ_{TMD} is the damping ratio. As suggested by Stewart[16], the optimal TMD natural frequency is approximately 93% of the tower natural frequency. Then the damping ratio ζ_{TMD} can be estimated according to the study [17].

The TMD properties are applied to obtain the mass matrix of TMDx, \mathbf{M}_{TMD} , the damping matrix, \mathbf{C}_{TMD} , and the stiffness matrix, \mathbf{K}_{TMD} . The discrete equation of motion defined with TMDx can be written as:

$$\begin{aligned}
 & \begin{bmatrix} \mathbf{M} + \mathbf{M}_A & 0 \\ 0 & \mathbf{M}_{\text{TMD}} \end{bmatrix} \begin{Bmatrix} \ddot{\mathbf{x}} \\ \ddot{\mathbf{x}}_{\text{TMD}} \end{Bmatrix} + \\
 & \begin{bmatrix} \mathbf{C} + \mathbf{C}_V + \mathbf{C}_{\text{TMD}} & -\mathbf{C}_{\text{TMD}} \\ \mathbf{C}_{\text{TMD}} & \mathbf{C}_{\text{TMD}} \end{bmatrix} \begin{Bmatrix} \dot{\mathbf{x}} \\ \dot{\mathbf{x}}_{\text{TMD}} \end{Bmatrix} \\
 & + \begin{bmatrix} \mathbf{K} + \mathbf{K}_{\text{TMD}} & -\mathbf{K}_{\text{TMD}} \\ -\mathbf{K}_{\text{TMD}} & \mathbf{K}_{\text{TMD}} \end{bmatrix} \begin{Bmatrix} \mathbf{x} \\ \mathbf{x}_{\text{TMD}} \end{Bmatrix} \\
 & = \begin{Bmatrix} \mathbf{F}(t) \\ 0 \end{Bmatrix} \tag{3.49}
 \end{aligned}$$

set

$$\begin{aligned}
 \mathbf{K}_T &= \begin{bmatrix} \mathbf{K} + \mathbf{K}_{\text{TMD}} & -\mathbf{K}_{\text{TMD}} \\ -\mathbf{K}_{\text{TMD}} & \mathbf{K}_{\text{TMD}} \end{bmatrix}, \\
 \mathbf{C}_T &= \begin{bmatrix} \mathbf{C} + \mathbf{C}_V + \mathbf{C}_{\text{TMD}} & -\mathbf{C}_{\text{TMD}} \\ \mathbf{C}_{\text{TMD}} & \mathbf{C}_{\text{TMD}} \end{bmatrix}, \\
 \mathbf{M}_T &= \begin{bmatrix} \mathbf{M} + \mathbf{M}_A & 0 \\ 0 & \mathbf{M}_{\text{TMD}} \end{bmatrix},
 \end{aligned}$$

$$\ddot{\mathbf{X}} = \begin{Bmatrix} \ddot{\mathbf{x}} \\ \ddot{\mathbf{x}}_{\text{TMD}} \end{Bmatrix}, \dot{\mathbf{X}} = \begin{Bmatrix} \dot{\mathbf{x}} \\ \dot{\mathbf{x}}_{\text{TMD}} \end{Bmatrix},$$

$$\mathbf{X} = \begin{Bmatrix} \mathbf{x} \\ \mathbf{x}_{\text{TMD}} \end{Bmatrix} \text{ and } \mathbf{P}(t) = \begin{Bmatrix} \mathbf{F}(t) \\ 0 \end{Bmatrix}.$$

then the equation of motion for the whole structure is as follow:

$$\mathbf{M}_T \ddot{\mathbf{X}} + \mathbf{C}_T \dot{\mathbf{X}} + \mathbf{K}_T \mathbf{X} = \mathbf{P}(t) \quad (3.50)$$

3.3 Time domain solution

Most numerical solution methods are step-by-step methods because the equation is solved at a succession of values of $t, t + \Delta t, t + 2\Delta t$. The accuracy of the solution depends on the length of the step interval Δt . It must be short enough for the load time history, the response time history and in many cases the shortest natural periods should be well defined. There are two categories for numerical solution, explicit and implicit.

A value at $t + \Delta t$ is obtained by considering equilibrium at time t in explicit methods. This is good for highly non-linear systems, but require short time steps. For implicit methods, a value at $t + \Delta t$ is obtained by considering equilibrium at time $t + \Delta t$. This system can be calculated with long time steps for linear systems. Some explicit and implicit methods are compared in Table 3.1.

	Examples	Method	Stability
Explicit	Central difference	Obtain value at $t + \Delta t$ by considering equilibrium at time t	Conditional (depends on time step length), but reasonably accurate solution if stable
	Runge-Kutta		
Implicit	Newmark β	Obtain value at $t + \Delta t$ by considering equilibrium at time $t + \Delta t$	Can be made unconditionally stable (but solution is no necessarily accurate)
	Newmark-Wilson		

Table 3.1: Summary of numerical solution methods

In order to solve the equations of motion, three methods are discussed in this section.

3.3.1 Central difference (explicit) method

It is required to step through time t calculating x at each step in Equation 3.50 as

$$\mathbf{M}_T \ddot{\mathbf{X}}_t + \mathbf{C}_T \dot{\mathbf{X}}_t + \mathbf{K}_T \mathbf{X}_t = \mathbf{P}(t) \quad (3.51)$$

the finite difference relationships are used:

$$\dot{\mathbf{X}}_t = \frac{1}{2\Delta t} [\mathbf{X}_{t+\Delta t} - \mathbf{X}_{t-\Delta t}] \quad (3.52)$$

$$\ddot{\mathbf{X}}_t = \frac{1}{\Delta t} (\dot{\mathbf{X}}_{t+\Delta t/2} - \dot{\mathbf{X}}_{t-\Delta t/2}) = \frac{1}{\Delta t^2} [\mathbf{X}_{t+\Delta t} - 2\mathbf{X}_t + \mathbf{X}_{t-\Delta t}] \quad (3.53)$$

Equations 3.52 and 3.53 can be substituted into equation 3.51 to form an equation for $\mathbf{X}_{t+\Delta t}$ as

$$\mathbf{X}_{t+\Delta t} = \left[\frac{\mathbf{M}_T}{\Delta t^2} + \frac{\mathbf{C}_T}{2\Delta t} \right]^{-1} \left\{ \mathbf{P}(t) - \mathbf{K}_T \mathbf{X}_t - \frac{\mathbf{M}_T}{\Delta t^2} (\mathbf{X}_{t+\Delta t} - 2\mathbf{X}_t) + \frac{\mathbf{C}_T}{2\Delta t} \mathbf{X}_{t-\Delta t} \right\} \quad (3.54)$$

This equation can be used for SDOF and MDOF of progress with the time history. Initial condition $\mathbf{X}_{t-\Delta t}$ and \mathbf{X}_t are required, then $\mathbf{X}_{t+\Delta t}$ will be obtained by this equation. Time is progressed by Δt now so that $\mathbf{X}_{t-\Delta t}$ becomes \mathbf{X}_t and \mathbf{X}_t becomes $\mathbf{X}_{t+\Delta t}$ to calculate the next value of $\mathbf{X}_{t+\Delta t}$. The procedure is repeated until the required length of time history has been reached.

3.3.2 Runge-Kutta (explicit) method

German mathematicians Carl Runge and Wilhelm Kutta developed a method to solve the ordinary differential equations in 1900 [86, 87], named as Runge-kutta method. It has two stages to calculate each time step as shown in Table 3.2.

The first stage is the use of the relationships below:

$$\ddot{\mathbf{X}}_t = \mathbf{M}_T^{-1} (\mathbf{P}(t) - \mathbf{K}_T \mathbf{X}_t - \mathbf{C}_T \dot{\mathbf{X}}_t) \quad (3.55)$$

$$\dot{\mathbf{X}}_{t+\Delta t} = \dot{\mathbf{X}}_t + \ddot{\mathbf{X}}_t \Delta t, \quad \mathbf{X}_{t+\Delta t} = \mathbf{X}_t + \dot{\mathbf{X}}_t \Delta t \quad (3.56)$$

then evaluates these equations at the beginning, middle and end of each overall time step. For the middle of the time step the equations are eval-

Stage 1 estimate of \mathbf{X} , $\dot{\mathbf{X}}$ and $\ddot{\mathbf{X}}$ at the beginning, middle and end of the time step.					
T	t	$\ddot{\mathbf{X}}$	\mathbf{X}	$\ddot{\mathbf{X}}$	Estimate based on equilibrium at
1	t	$\dot{\mathbf{X}}_t$	\mathbf{X}_t	$M_T^{-1} \left\{ \mathbf{P}(t) - \mathbf{K}_T \mathbf{X}_t - \mathbf{C}_T \dot{\mathbf{X}}_t \right\}$	
$2a$	$t + \frac{\Delta t}{2}$	$\ddot{\mathbf{X}}_{2a} = \ddot{\mathbf{X}}_t + \ddot{\mathbf{X}}_t \frac{\Delta t}{2}$	$\mathbf{X}_{2a} = \mathbf{X}_t + \dot{\mathbf{X}}_t \frac{\Delta t}{2}$	$M_T^{-1} \left\{ \mathbf{P}(t + \Delta t/2) - \mathbf{K}_T \mathbf{X}_{2a} - \mathbf{C}_T \dot{\mathbf{X}}_{2a} \right\}$	t
$2b$	$t + \frac{\Delta t}{2}$	$\ddot{\mathbf{X}}_{2b} = \dot{\mathbf{X}}_t + \ddot{\mathbf{X}}_{2a} \frac{\Delta t}{2}$	$\mathbf{X}_{2b} = \mathbf{X}_t + \dot{\mathbf{X}}_{2a} \frac{\Delta t}{2}$	$M_T^{-1} \left\{ \mathbf{P}(t + \Delta t/2) - \mathbf{K}_T \mathbf{X}_{2a} - \mathbf{C}_T \dot{\mathbf{X}}_{2b} \right\}$	$t + \Delta t/2$
3	$t + \Delta t$	$\dot{\mathbf{X}}_3 = \dot{\mathbf{X}}_t + \ddot{\mathbf{X}}_{2b} \frac{\Delta t}{2}$	$\mathbf{X}_3 = \mathbf{X}_t + \dot{\mathbf{X}}_{2b} \frac{\Delta t}{2}$	$M_T^{-1} \left\{ \mathbf{P}(t + \Delta t/2) - \mathbf{K}_T \mathbf{X}_3 - \mathbf{C}_T \dot{\mathbf{X}}_3 \right\}$	$t + \Delta t/2$
Stage 2 estimate of \mathbf{X} and $\dot{\mathbf{X}}$ at the end of the time step based on the result of stage 1.					
	$\mathbf{X}_{t+\Delta t} = \mathbf{X}_t + \frac{\Delta t}{6}(\ddot{\mathbf{X}}_t + 2\ddot{\mathbf{X}}_{2a} + 2\ddot{\mathbf{X}}_{2b} + \ddot{\mathbf{X}}_3)$			$\dot{\mathbf{X}}_{t+\Delta t} = \dot{\mathbf{X}}_t + \frac{\Delta t}{6}(\ddot{\mathbf{X}}_t + 2\ddot{\mathbf{X}}_{2a} + 2\ddot{\mathbf{X}}_{2b} + \ddot{\mathbf{X}}_3)$	

Table 3.2: Runge-Kutta method [88]

uated by the forces acting at the beginning of the time step and the forces calculated to be acting at the middle of the time step.

The four values of \ddot{X} in stage 1 are then used with a Simpson's rule formula to obtain a better estimate the change of \dot{X} for the overall time step in stage 2. Then the four values of \dot{X} are used to obtain a better estimate of the change X .

The Runge-Kutta method gives a more accurate result for each time step than the central difference method. Runge-Kutta method may require less computing resources than a smaller step length central difference method to get the same accuracy in SODF system.

The Runge-Kutta method may not be better than the central difference method for a realistic MDOF system, due to the time step not being determined by accuracy of the solution but by the shortest structural period for solution stability. The best type of solutions for MDOF structural system is the implicit type.

3.3.3 Newmark β method

Newmark β method is selected for wind turbines with finite element model [12]. This method is widely used in numerical evaluation of the dynamic response of structures and solids such as in finite element analysis to model dynamic systems. Equation 3.51 discretized in the time domain by this algorithm is presented below:

$$\mathbf{X}_{t+\Delta t} = \mathbf{X}_t + \Delta t \dot{\mathbf{X}} + \Delta t^2 \left[\left(\frac{1}{2} - \beta \right) \ddot{\mathbf{X}}_t + \beta \ddot{\mathbf{X}}_{t+\Delta t} \right] \quad (3.57)$$

$$\dot{\mathbf{X}}_{t+\Delta t} = \dot{\mathbf{X}}_t + \Delta t [(1 - \gamma) \mathbf{X}_t + \gamma \mathbf{X}_{t+\Delta t}] \quad (3.58)$$

Theoretical analysis of the method shows that the approximation will be stable with $\beta > 0.25$ and the equations will be linear.

Substituting Eqn 3.57 3.58 into Equation 3.51 and rearranging to obtain the final form of the equation so that $\mathbf{X}_{t+\Delta t}$ can be solved, gives:

$$\begin{aligned} & [\mathbf{K}_T + \frac{\gamma}{\beta \Delta t} \mathbf{C}_T + \frac{1}{\beta (\Delta t)^2} \mathbf{M}_T] \mathbf{X}_{t+\Delta t} = \mathbf{P}(t + \Delta t) \\ & + \mathbf{C}_T \left\{ \frac{\gamma}{\beta \Delta t} \mathbf{X}_t + \left(\frac{\gamma}{\beta} - 1 \right) \dot{\mathbf{X}}_t + \Delta t \left(\frac{\gamma}{2\beta} - 1 \right) \ddot{\mathbf{X}}_t \right\} \\ & - \mathbf{M}_T \left\{ \frac{1}{\beta (\Delta t)^2} \mathbf{X}_t + \frac{\gamma}{\beta \Delta t} \dot{\mathbf{X}}_t + \left(\frac{\gamma}{2\beta} - 1 \right) \ddot{\mathbf{X}}_t \right\} \end{aligned} \quad (3.59)$$

β and γ are set to 0.25 and 0.5 respectively in order to make the method implicit and unconditionally stable[13]. Moreover, the formula reverts to central difference method when β is set to 0.

This method is selected to solve the Equation 3.50. The equation of motion can be solved by 3.59 once the step interval Δt has been determined.

The method is also good for non-linear systems with a shorter time step in order to avoid instability. For linear systems the method may be applied separately to each normal mode or in matrix form to the coupled

Cartesian equations. For non-linear systems the matrix form is the most convenient.

3.4 Added mass and damping

When a structural component vibrates in a viscous fluid, the presence of the fluid gives rise to a fluid reaction force which is known as added mass and a damping contribution to the dynamic response of a component. Added mass and damping are dependent on fluid properties as well as being a functions of component geometry and adjacent boundaries. M.W.Wambsganss et.al.[9] presented an appropriate form of the Navier-Stokes equation to solve and give the radial and tangential velocity components of the viscous flow in the fluid annulus formed by a vibrating rod and rigid containment shell.

The resultant force per unit length of a cylinder is given as:

$$F = -iMU\omega H e^{i\omega t} \quad (3.60)$$

where M is the mass of fluid per unit length displaced by the cylinder which equals to $\rho\pi d^2$ and d is the radius of the cylinder, U is the velocity of the fluid at the cylinder surface, ω is oscillating frequency of the cylinder and H is given as:

$$\begin{aligned}
H = & \{2\alpha^2[I_0(\alpha)K_0(\beta) - I_0(\beta)K_0(\alpha)] - 4\alpha[I_1(\alpha)K_0(\beta) + I_0(\beta)K_1(\alpha)] \\
& + 4\alpha\gamma[I_0(\alpha)K_1(\beta) + I_1(\beta)K_0(\alpha)] - 8\gamma[I_1(\alpha)K_1(\beta) - I_1(\beta)K_1(\alpha)]\} \\
& / \{ \alpha^2(1 - \gamma^2)[I_0(\alpha)K_0(\beta) - I_0(\beta)K_0(\alpha)] + 2\alpha\gamma[I_0(\alpha)K_1(\beta) \\
& - I_1(\beta)K_0(\beta) + I_1(\beta)K_0(\alpha) - I_0(\beta)K_1(\beta)] + 2\alpha\gamma^2[I_0(\beta)K_1(\beta) \\
& - I_0(\alpha)K_1(\alpha) + I_1(\alpha)K_0(\beta) - I_1(\alpha)K_0(\beta)] \} - 1 \tag{3.61}
\end{aligned}$$

where α, β, γ are defined as

$$\begin{aligned}
\alpha &= kd \\
\beta &= kD \\
\gamma &= d/D \tag{3.62}
\end{aligned}$$

and D is the radius of the boundary, $k = \sqrt{i\frac{\omega}{\nu}}$ where ν is the kinematic viscosity of fluid.

The real part of Equation 3.60 gives

$$F = MU\omega[\text{Re}(H)\sin\omega t + \text{Im}(H)\cos\omega t] \tag{3.63}$$

This equation shows that two forces are required. The first one is $-MU\omega\text{Re}(H)\sin\omega t$ where $M\text{Re}(H)$ is the added mass of the cylinder. The second one is $-MU\omega\text{Re}(H)\cos\omega t$ which is related to the damping mechanism.

According to Equation 3.61, H depends on α , β and γ in a very complicated way. However in some special cases, the equation can be simplified.

3.4.1 Infinite and viscous fluid

In this case, the value of H can be obtained by taking the limits of Bessel's functions. Here $D \sim \infty$, $\gamma \sim \infty$ and $\beta \sim \infty$. Then $I_0(\beta) \sim \infty$, $I_1(\beta) \sim \infty$, $K_0(\beta) \sim 0$ and $K_1(\beta) \sim 0$. Finally the Equation 3.61 reduces to:

$$H = 1 + \frac{4K_1(\alpha)}{\alpha K_0(\alpha)} \quad (3.64)$$

This case can be applied to the monopile structure in the ocean where the boundary can be considered as infinite.

3.4.2 Infinite and inviscid fluid

If the fluid is inviscid, this means $\alpha \sim \infty$, then Equation 3.64 becomes:

$$H = 1 \quad (3.65)$$

This result is consistent with the classical result that the added mass of a cylinder vibration in an infinite fluid is equal to the mass of the fluid displaced by the cylinder [9].

3.4.3 Viscous and inviscid fluid with large values of α and β

For cases have large values of α and β , the results can be greatly simplified with the asymptotic formulae:

$$\begin{aligned}
 I_0(z) &\sim \frac{e^z}{\sqrt{2\pi z}} \\
 I_1(z) &\sim \frac{e^z}{\sqrt{2\pi z}} \\
 K_0(z) &\sim \sqrt{\frac{\pi}{2z}} e^{-z} \\
 K_1(z) &\sim \sqrt{\frac{\pi}{2z}} e^{-z}
 \end{aligned} \tag{3.66}$$

then H becomes:

$$\begin{aligned}
 H = & \{[\alpha^2(1 + \gamma^2) - 8\gamma] \sinh(\beta - \alpha) + 2\alpha(2 - \gamma + \gamma^2) \cosh(\beta - \alpha) \\
 & - 2\gamma^2 \sqrt{\alpha\beta} - 2\alpha \sqrt{\frac{\alpha}{\beta}}\} / [\alpha^2(1 - \gamma^2) \sinh(\beta - \alpha) \\
 & - 2\alpha\gamma(1 + \gamma) \cosh(\beta - \alpha) + 2\gamma^2 \sqrt{\alpha\beta} + 2\alpha \sqrt{\frac{\alpha}{\beta}}]
 \end{aligned} \tag{3.67}$$

If the fluid is considered to be inviscid, Equation 3.67 reduces to:

$$H = \frac{1 + \gamma^2}{1 - \gamma^2} \tag{3.68}$$

Table 3.3: Monopile verification parameters

TMD	Mass {kg}	k {N/m}	d {N/(m/s)}	ω_n {rad/s}	ω_d {rad/s}	ζ (%)
Optimal	20000	64000	10000	1.79	1.77	14

3.4.4 Added mass and damping factors

The added mass correction factor C_M is defined as a constant, added mass can be obtained by multiplying the factor to the mass of displaced fluid. From Equation 3.63 it can be defined as:

$$C_M = \text{Re}(H) \quad (3.69)$$

Similarly, from Equation 3.63 the damping coefficient can be written as:

$$C_V = M\omega \text{Im}(H) \quad (3.70)$$

3.5 Model verification

A parametric study for the monopile offshore 5MW wind turbine, 126 m rotor diameter and a 90 m hub height, with TMDx has been investigated by M.A. Lackner [89] using FAST (Fatigue, Aerodynamics, Structures and Turbulence). In this thesis, the present rigid support model is simulated in the same case as M.A. Lackner's study to do verification. The parameters are given in Table 3.3.

Note that the TMD mass is approximately 8% of the nacelle mass and 6% of the tower top mass. The baseline case is established by providing an

initial perturbation of 1 m to the tower top fore-aft displacement, TTD_{FA} . Only the first tower fore-aft DOF is turned on. The comparison of two models in time series of TTD_{FA} for the baseline case is shown in Figure 3.6, the average difference of the amplitudes for two models is 9.2%, at beginning the difference of the first amplitude is 1.1% then it rise to 17.7% at last. Next, the TMDx DOF is turned on, a time series of TTD_{FA} and the TMDx displacement is shown in Figure 3.6 as well. For TTD_{FA} displacement, the average difference of the amplitudes for the two models for the first 50 seconds is 13.1%, at first the difference is 0.1% then it rise to 27.9%, , and the motion is tend to close 0 after 50 seconds. For the TMDx displacement, the average difference of the amplitudes for the two models from 4s to 12s is around 4.6% and the it is totally 22.1% for the first 50 seconds. It is satisfied that the results of the present model are approach to the FAST simulation in vibration frequencies according to Figure 3.6, and the amplitudes of two models at the beginning of simulation matches appropriately, but the difference will increase with time.

3.6 System parameters

In the previous chapter, generative models of monopile supported turbines with a tuned mass damper was described. Construction of such models is the factor that defines the sea states to generate the external forces on these systems and the parameters of the tuned mass dampers in the nacelles. The design of the turbine support structure investigated is based on Torr Head Tidal Energy Array project proposed by Tidal ven-

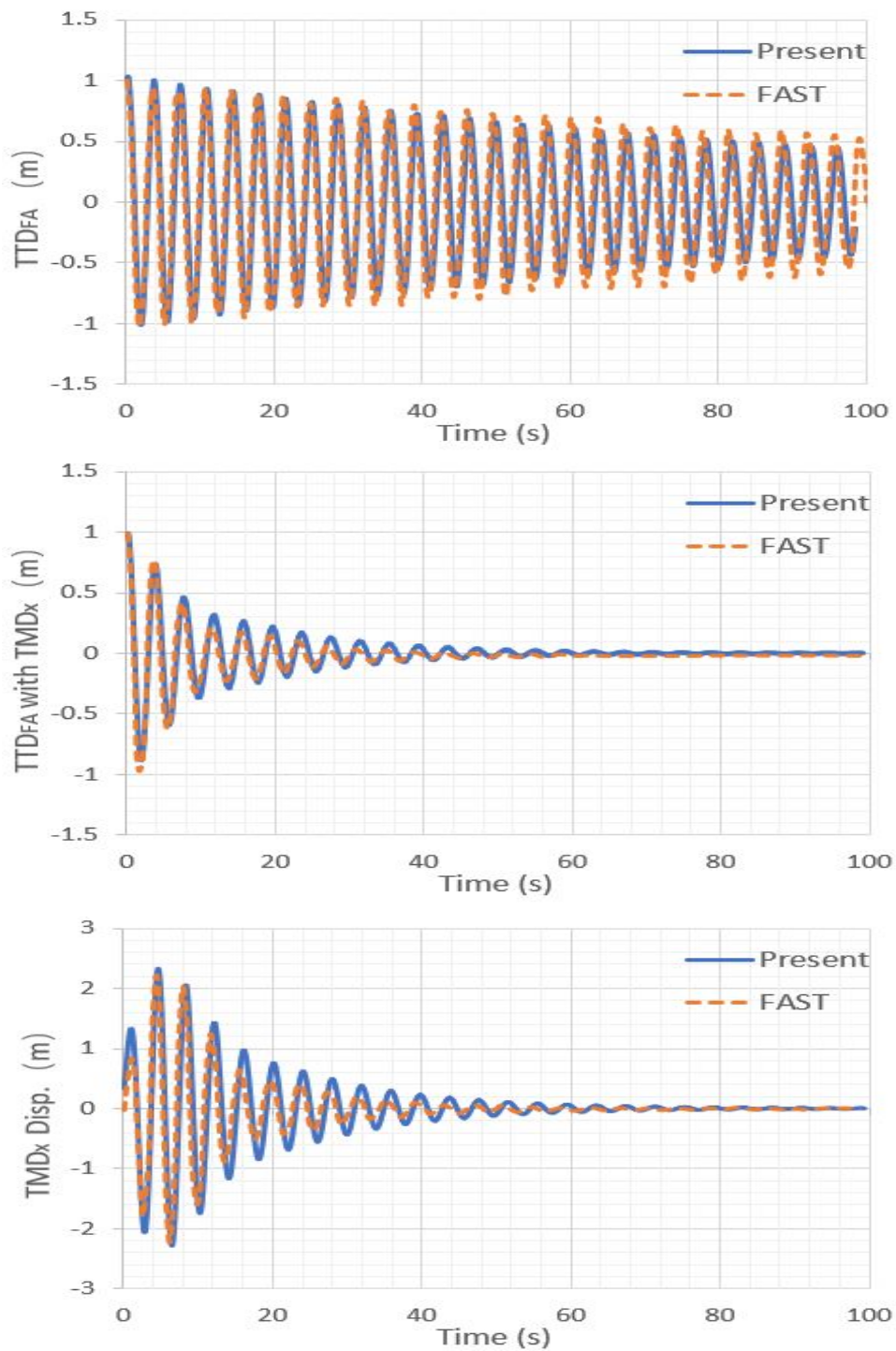


Figure 3.6: Time series results for monopile verification

Table 3.4: tower-monopile support parameters.

Materials	Steel
Height of nacelle center	25m
Pile diameter	2.5m
Structure weight	Dry weight of 120 tonnes
Thickness	0.073m
Top mass	150 tonnes

tures. This project is located in the north coast of County Antrim in Northern Ireland with a maximum capacity is 100MW from 50 to 100 turbines each with a rated power output of at least 1MW. This project started its feasibility and site research in 2013 and had planed to be operational in 2020, now it is at Consent and Environmental Statement (ES) Submission stage. The Environmental Impact Assessment (EIA) report lists three types of turbine support structures relevant to the project [7], which are gravity base structures including sub-sea bases, drilled monopiles and drilled pin pile tripods.

For this investigation, a drilled monopile structure for a 1MW turbine is selected and the relevant parameters are given in Table 3.4. Most of the parameters are from the EIA report, but there is no information of the pile wall thickness and the top mass (rotor and nacelle weight). The thickness here is estimated from the pile diameter, material density, weight and length. Moreover, the top mass is from Alstom's 1MW tidal turbine [22]. Some parameters can be changed in order to simulate different conditions and sensitivity.

The calculation for the first natural frequency of the structure is the first step to determine the optimum TMD parameter. In this study only the

Table 3.5: TMD parameters

mass percentage	mass (kg)	k (N/m)	c (N*s/m)	ζ (-)
1%	1200	85359	1233.4	0.0609
2%	2400	170720	3471.4	0.0858
3%	3600	256080	6346.4	0.1045
4%	4800	341440	9723.8	0.1201

fore-aft TMD system, TMDx, is under consideration, so the first tower bending mode is the most important [6]. According to the model, the first natural frequency for the structure is 9.069 rads/s (1.443Hz) for the structure support case study. This is a high value compared to a 5MW offshore wind turbine with monopile support which usually has a first nature frequency of 1.71 rads/s (0.272Hz) [11]. Based on an investigation [6], the mass of the TMD is suggested as 2% of the total mass of the monopile. This results in a final mass of 2400kg in this case study. In order to understand the effects of the TMD mass on the structure, a parametric study using four different masses is performed.

In this thesis, 1200kg, 2400kg, 3600kg and 4800kg TMDx mass values are chosen which are related to 1%, 2%, 3% and 4% of the monopile mass respectively. Table 3.5 summarized the TMD parameters obtained.

This study uses the unsteady wave-current coupled loads data generated from an improved Blade Element Momentum Theory [10]. The tidal current speed is 2.5m/s, significant wave height is 5.979m, average zero crossing period is 7.616s for a sea-state generated by an estimated wind speed of 25.628m/s. These data were taken from the British Oceanographic Data Center [23], provided by the UK Offshore Operators Associ-

ation and funded by the Institute of Oceanographic Sciences. The water depth is assumed to be 50m.

3.7 Results

3.7.1 Instant impact on structure

The tower top fore-aft deflection with and without TMDx are simulated over 120s, an instant load of 450kN which is considered as the value of the thrust load on the turbine is applied on the structure at the time step 0.4s then removed at 0.5s, Figure 3.7 shows the results.

The results shows that TMDx has a clear effect on the structural response when an instant load is applied on the structure such as from a impact of an extreme wave-current coupled force on turbine or a large marine mammal impact. The TMD shows a better performance in deflection reduction with a higher mass ratio. However the results for the TMDs with a mass ratio higher than 2% does not show a significant improvement in the deflection reduction. Furthermore, all the TMDx with the mass percentages of 2%, 3% and 4% will make the system stop vibrating in 45s and the TMD displacement is also within the range of 0.2m, which is small relative to the Alstom's 1MW tidal turbine nacelle which is 22m in length. Besides, the TMD mass (mass ratio 2%) is only 1.6% of the top mass. This means that using a TMD on tidal energy applications is valuable in terms of their space requirement and ease of installation hence it can be installed in the nacelle or in the tower.

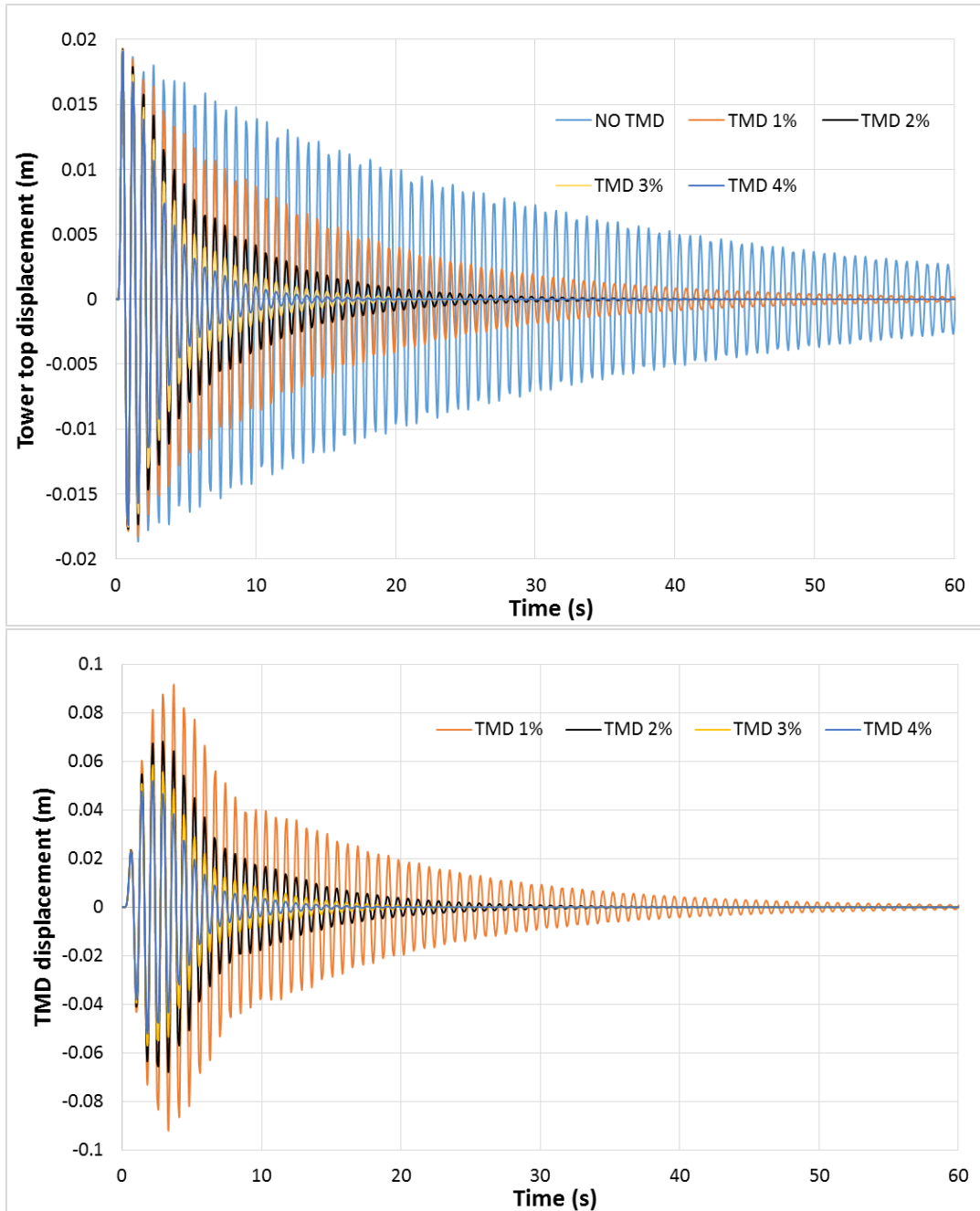


Figure 3.7: Tower top displacement and TMD displacement in time series

3.7.2 Monopile Results Including Wave-current Interactions

This study uses the unsteady wave-current coupled load data generated from an improved Blade Element Momentum Theory [10]. The tidal current speed is 2.5m/s, significant wave height is 5.979m, average zero crossing period is 7.616s for a sea-state generated by an estimated wind speed of 25.628m/s. Again, these data was taken from the British Oceanographic Data Center [23], provided UK Offshore Operators Association and funded by the Institute of Oceanographic Sciences. The water depth is assumed to be 50m. A 5 minutes simulation is applied under this load condition and figure 3.8 shows a result of tower top displacement and fore-aft bending moment at tower base in a time window of 14s .

It is obvious that for a longer term run the TMD effect can be almost ignored because the reduction of displacements and loads is small as the figure shows. When the structure becomes stable, a rainflow-counting algorithm [18] is applied here to do a primary fatigue evaluation for the maximum stress at tower base from 200s to 300s of the simulation. Table 3.6 and 3.7 shows the results of the the fatigue analysis done for a monopile when not using and using TMD.

From these tables, the two factors cyclic stress ranges and the number of cycles in this range, which are more important than the mean peak stress [92], are almost same in these two conditions (less than 5% difference). By the use of S-N curves, it can be demonstrated that the smaller amplitude stress fluctuations in the case using TMD will yield a longer fatigue

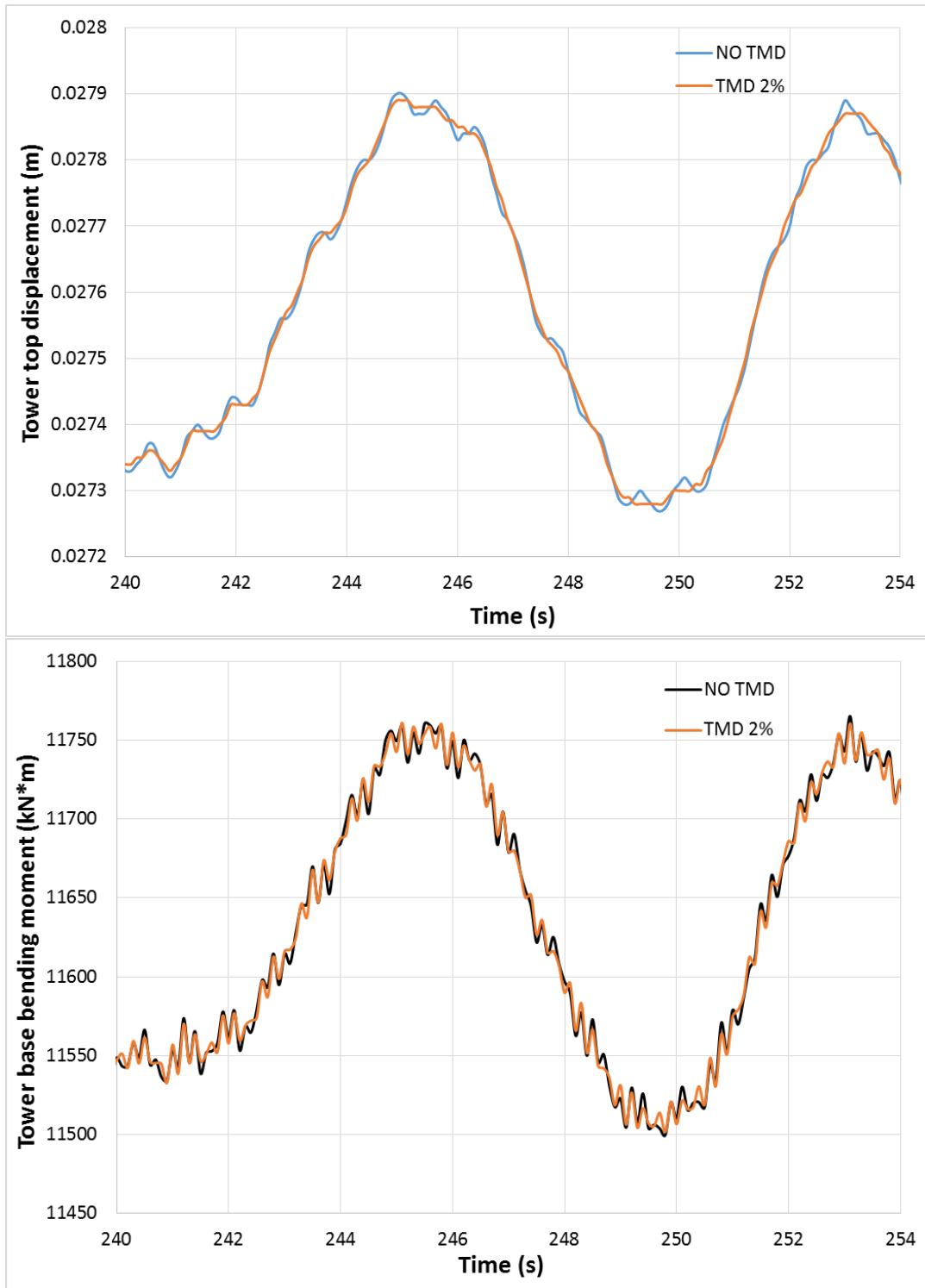


Figure 3.8: Tower top displacement and base bending moment in time series

Table 3.6: number of cycles at various stress range and mean stress combination for structure without TMD

Stress Range (MPa)	Mean Stress (MPa)				
	216	218	220	222	224
0.97	27	110	85	120	26
2.90	N/A	N/A	N/A	N/A	N/A
4.83	N/A	N/A	9	N/A	N/A
6.77	N/A	N/A	1	N/A	N/A
8.70	N/A	N/A	3	N/A	N/A

Table 3.7: number of cycles at various stress range and mean stress combination for structure with TMD

Stress Range (MPa)	Mean Stress (MPa)				
	216	217	218	219	220
0.95	26	105	86	118	27
2.86	N/A	N/A	N/A	N/A	N/A
4.76	N/A	N/A	9	N/A	N/A
6.67	N/A	N/A	1	N/A	N/A
8.57	N/A	N/A	3	N/A	N/A

life (number of cycles to failure) [21]. However, it can also be seen that the effect of the TMD on the fatigue load reduction is negligible for long term operations of the system.

3.7.3 Frequency Domain Analysis

A frequency domain analysis is presented in this section to investigate the influence of added mass and TMD to the structure. Figure 3.9 shows the first 4 mode shapes of the structure. Figure 3.10 shows a plot of the tower base fore-aft bending moment in frequency domain with three different conditions. The first figure presents the results where no added mass effect and no TMD is considered, second one has added mass effect but no TMD, the last one has both added mass and TMD.

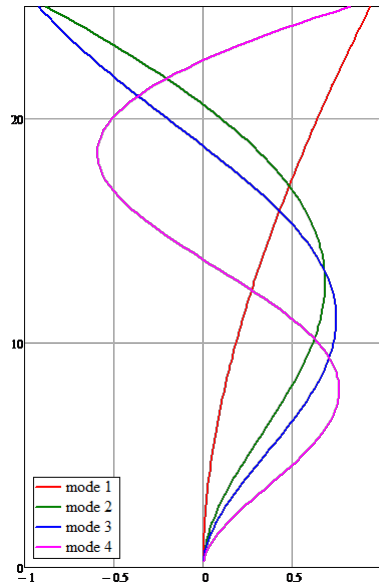


Figure 3.9: Mode shapes of monopile structure

As Figure 3.10 shows, there is a peak at the first natural frequency of the structure which is mode 1, the natural frequency will reduce slightly from 1.533Hz to 1.443Hz when considering the added mass effect. Moreover, the amplitude of resonance in fore-aft direction decreases significantly when TMDx is applied on the structure. Generally, the passive structural control such as tuned mass damper is an effective method to reduce the loads due to the vibration of structural modes.

3.8 Summary

This chapter has presented some major wave models as well as a method to model the passive structural control technology for tidal stream turbines combined with wave-current interactions. A simple and fast simulation method has been developed to model the monopile support struc-

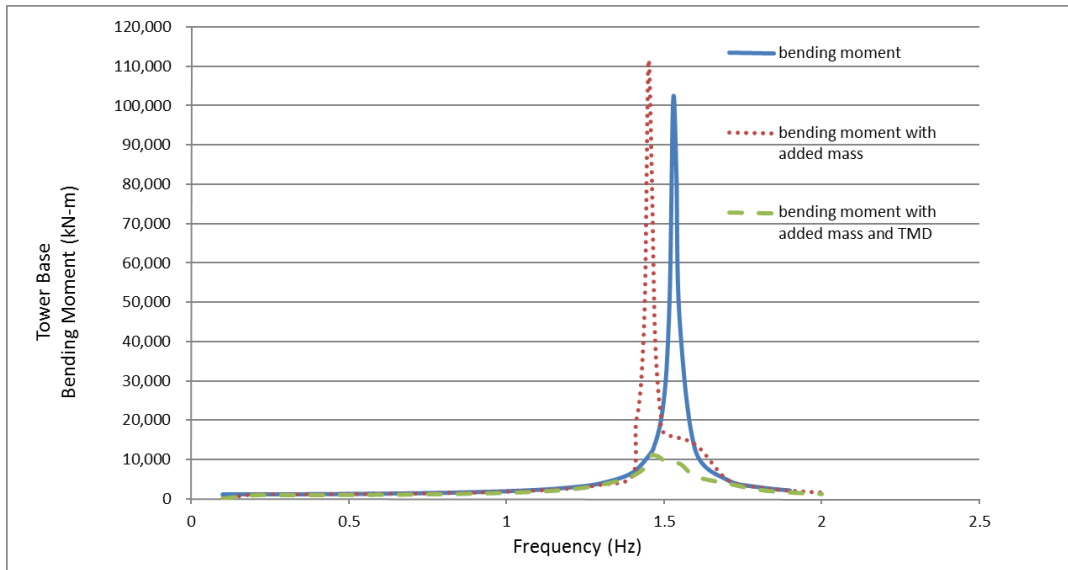


Figure 3.10: Frequency domain results of structure

tures for turbine applications and analyze their dynamics including the added mass and hydrodynamic damping effects. A passive structure control technique was employed in this methodology, which used a TMD on the structure to do a fully coupled dynamic analysis in time domain using a Newmark β method. The forces on the turbine are calculated by the BEMT model for each time step. It is shown that the tuned mass damper had significant effects on the resonance reduction and fore-aft fatigue load-reduction under instant impacts. However, compared to the instant fluctuating impact, TMD had an insignificant effect when modest unsteady wave-current coupled forces were applied on the structure for long operating periods. By changing the shape of tower-monopile supporting structure, this will make a better performance in fatigue analysis.

Chapter 4

The Dynamics of Tension Mooring Supported Tidal Turbines

This chapter reports the design of a tidal turbine station keeping system based on the adoption of a tension mooring system and investigates the potential introduction of into the system and the capabilities to reduce the peak loads tidal turbines experience during operations in high energy wave-current environments. This is investigated using a model of a neutrally buoyant turbine supported from a tension cable based mooring system, where tension is introduced by a submersed buoy in water. The loading on the turbine rotor blades and buoy are calculated using a wave and current coupled BEMT. A basic survey of the use of elasticated mooring lines for the mooring of tidal current turbines is presented by Bowie[34]. It reports that the reduction of cost and time involved

in installation are significant by using flexible moorings instead of pile structure foundations, moreover the structural costs of the device and its mounting are reduced. The utilization of orientating the device to current flow naturally reduces the cost of control systems, furthermore maintenance costs and the downtime can be reduced by easier removal of device for onshore maintenance.

4.1 Preliminary numerical model

The focus of this section is to present a methodology which assesses the behavior of a neutrally buoyant turbine supported from a tension cable based mooring system, where tension is introduced by a buoy acting as a damper and fully submersed in water, the schematic of the system in operation is shown as Figure 4.1.

The tension mooring system is modeled as a special type of triple pendulum which is called an inverted flail. It consists of three pendula, the first one is attached to a fixed point which is considered to be an anchor, and to its end mass the other two pendulum are joined. An original flail system without external drive in the absence of a gravity field is shown in Figure 4.2 and it was analyzed in Przybylska[26].

Unlike the original flail system, the tension mooring supported turbine is driven by external forces, the loading on the turbine rotor blades and buoy are calculated using the same BEMT code as the last Chapter. In addition, due to the turbine being able to move and respond to the moving

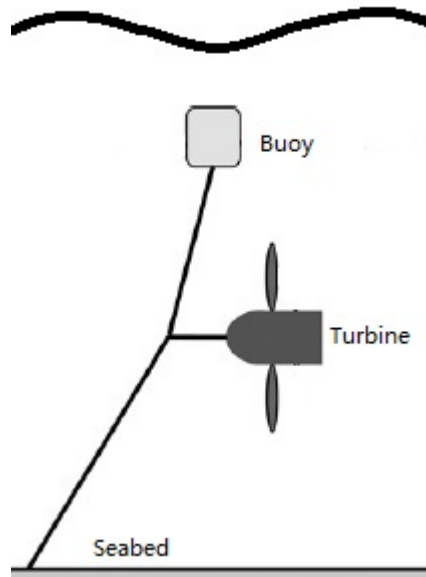


Figure 4.1: Schematic of tension mooring turbine in operation

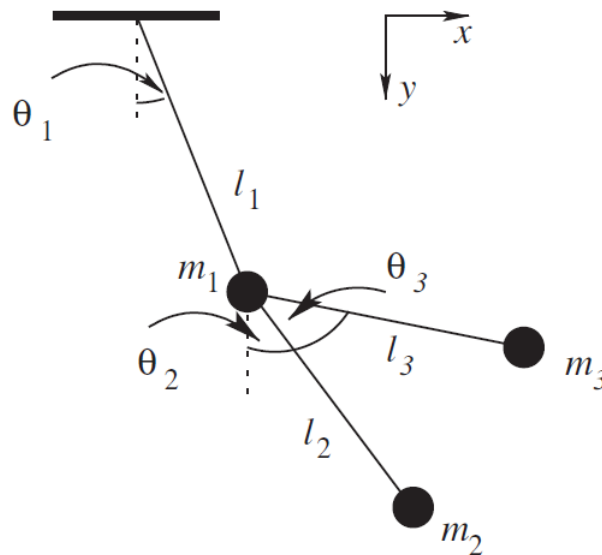


Figure 4.2: Geometry of the flail pendulum [26]

flow field, the resulting motions due to flow field interactions should be taken into consideration.

4.1.1 Preliminary modeling of a mooring supported turbine

The mooring lines are assumed to continuously be in tension during operation. Therefore this system can be modeled as an inverted flail pendulum in order to calculate its dynamics, Figure 4.3 provides the model for the three elements in flail pendulum. Equations of motion of the pendulum system can be derived using the following Lagrange's equation:

$$\frac{d}{dt} \left(\frac{\partial L}{\partial \dot{\theta}_i} \right) - \frac{\partial L}{\partial \theta_i} = Q_i \quad (4.1)$$

where $L = T - V$ is defined as the Lagrangian of the system, T is the kinetic energy and V the potential energy of system.

When an external force function Q_i is not considered, the Lagrangian of the system can be written as:

$$\begin{aligned} L = & \frac{1}{2}(m_1 + m_2 + m_3)l_1^2\dot{\theta}_1^2 + \frac{1}{2}m_2l_2^2\dot{\theta}_2^2 + \frac{1}{2}m_3l_3^2\dot{\theta}_3^2 \\ & + m_2l_1l_2\dot{\theta}_1\dot{\theta}_2\cos(\theta_1 - \theta_2) + m_3l_1l_3\dot{\theta}_1\dot{\theta}_3\cos(\theta_1 - \theta_3) \\ & + (m_1 + m_2 + m_3)gl_1\cos\theta_1 + m_2gl_2\cos\theta_2 + m_3gl_3\cos\theta_3 \end{aligned} \quad (4.2)$$

where m_1 is the lumped mass of three mooring lines at the connection

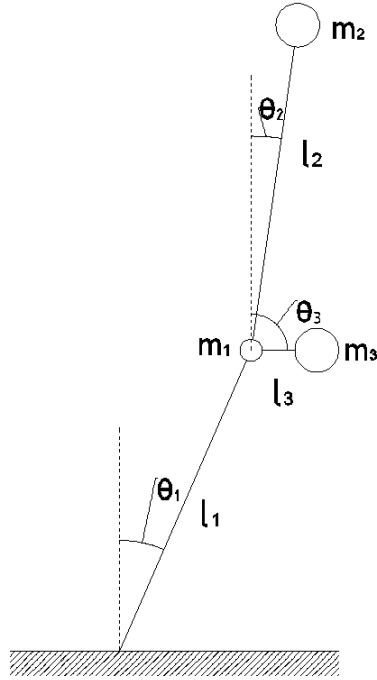


Figure 4.3: The Schematic of “flail” pendulum

node, m_2 represents the mass of buoy, m_3 represents the mass of the turbine. l_1 , l_2 and l_3 are the length of each segment. θ_1 , θ_2 and θ_3 are generalized coordinates as shown in Figure 4.3.

It is assumed that the turbine and the buoy are neutrally buoyant, so the potential energy terms in Equation 4.2 can be eliminated. The new Lagrangian of the system becomes:

$$\begin{aligned}
 L = & \frac{1}{2}(m_1 + m_2 + m_3)l_1^2\dot{\theta}_1^2 + \frac{1}{2}m_2l_2^2\dot{\theta}_2^2 + m_2l_1l_2\dot{\theta}_1\dot{\theta}_2\cos(\theta_1 - \theta_2) \\
 & + \frac{1}{2}m_3l_3^2\dot{\theta}_3^2 + m_3l_1l_3\dot{\theta}_1\dot{\theta}_3\cos(\theta_1 - \theta_3)
 \end{aligned} \tag{4.3}$$

Substituting Equation 4.3 into Equation 4.1 yields the Euler-Lagrange

differential equations of the system:

$$\begin{aligned}
(m_1 + m_2 + m_3)l_1^2\ddot{\theta}_1 + m_2l_1l_2\ddot{\theta}_2\cos(\theta_1 - \theta_2) + m_2l_1l_2\dot{\theta}_2^2\sin(\theta_1 - \theta_2) \\
+ m_3l_1l_3\ddot{\theta}_3\cos(\theta_1 - \theta_3) + m_3l_1l_3\dot{\theta}_3^2\sin(\theta_1 - \theta_3) \\
= Q_1 \quad (4.4)
\end{aligned}$$

$$\begin{aligned}
m_2l_2^2\ddot{\theta}_2 + m_2l_1l_2\ddot{\theta}_1\cos(\theta_1 - \theta_2) - m_2l_1l_2\dot{\theta}_1^2\sin(\theta_1 - \theta_2) \\
= Q_2 \quad (4.5)
\end{aligned}$$

$$\begin{aligned}
m_3l_3^2\ddot{\theta}_3 + m_3l_1l_3\ddot{\theta}_1\cos(\theta_1 - \theta_3) - m_3l_1l_3\dot{\theta}_1^2\sin(\theta_1 - \theta_3) \\
= Q_3 \quad (4.6)
\end{aligned}$$

where Q_1 , Q_2 and Q_3 are the generalized forces. In this case Q_3 equates to the momentum thrust develop by a turbine loading where this is operating under combined wave and currents conditions. Q_2 relates to the buoyant forces occurring on the floater, which are considered in the form of buoyancy and wave excitation forces. Q_1 will be obtained from the relationship between Q_2 and Q_3 .

4.1.2 External forces

Figure 4.4 shows the forces in the system, thrust F_3 can be obtained from the ESRU in house BEMT code [10]. Modifications have been made in the

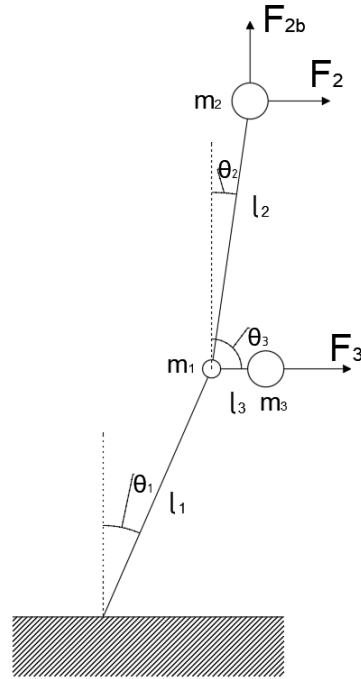


Figure 4.4: Forces on the system

original code due to the relative velocity between the turbine and inflows:

$$\mathbf{U} = \mathbf{u} - \mathbf{U}_T \quad (4.7)$$

where \mathbf{u} is the inflow velocity which is calculated from the wave-current model in Section 3.1, \mathbf{U}_T is the inertia velocity of the turbine itself, which can be calculated in vertical and horizontal directions as:

$$U_{T,x} = \dot{\theta}_1 l_1 \cos\theta_1 + \dot{\theta}_3 l_3 \cos\theta_3 \quad (4.8)$$

$$U_{T,y} = \dot{\theta}_1 l_1 \sin\theta_1 + \dot{\theta}_3 l_3 \sin\theta_3 \quad (4.9)$$

The buoy is assumed to be a sphere, F_{2b} , and represents the net buoyancy, the drag force F_3 is also calculated from the BEMT code, the relative velocity between buoy and in flows is now considered as:

$$\mathbf{V} = \mathbf{u} - \mathbf{U}_B \quad (4.10)$$

the inflow velocity u can be calculated by wave-current model with the coordinates of the buoy. \mathbf{U}_B is the inertia velocity of buoy, given by:

$$U_{B,x} = \dot{\theta}_2 l_2 \cos\theta_2 + \dot{\theta}_1 l_1 \cos\theta_1 \quad (4.11)$$

$$U_{B,y} = \dot{\theta}_2 l_2 \sin\theta_2 + \dot{\theta}_1 l_1 \sin\theta_1 \quad (4.12)$$

According to Anli and Ohlhoff[24, 27], the generalized force can be obtained as:

$$Q_k = \sum_{i=1}^n F_i \frac{\partial r_i}{\partial q_k} \quad (4.13)$$

where Q_k is the Generalized force associated with the k^{th} Euler-Lagrange differential equation, F_i is the external force, r_i is the position of the point of application and q_k is the generalized coordinate.

Thus, the generalize forces for this system are given as:

$$Q_1 = F_3 l_1 \cos \theta_1 - F_{2b} l_1 \sin \theta_1 + F_2 l_1 \cos \theta_1 \quad (4.14)$$

$$Q_2 = F_2 l_2 \cos \theta_2 - F_{2b} l_2 \sin \theta_2 \quad (4.15)$$

$$Q_3 = F_3 l_3 \cos \theta_3 \quad (4.16)$$

When the generalized forces are obtained, the Euler-Lagrange differential equations of the system can be solved with given initial conditions.

Substituting Equations 4.14 4.15 4.16 into Equations 4.4 4.5 4.6 then divide by l_1 , l_2 and l_3 yields:

$$\begin{aligned} (m_1 + m_2 + m_3) l_1 \ddot{\theta}_1 + m_2 l_2 \ddot{\theta}_2 \cos(\theta_1 - \theta_2) + m_2 l_2 \dot{\theta}_2^2 \sin(\theta_1 - \theta_2) \\ + m_3 l_3 \ddot{\theta}_3 \cos(\theta_1 - \theta_3) + m_3 l_3 \dot{\theta}_3^2 \sin(\theta_1 - \theta_3) \\ = F_3 \cos \theta_1 - F_{2b} \sin \theta_1 + F_2 \cos \theta_1 \end{aligned} \quad (4.17)$$

$$\begin{aligned} m_2 l_2 \ddot{\theta}_2 + m_2 l_1 \ddot{\theta}_1 \cos(\theta_1 - \theta_2) - m_2 l_1 \dot{\theta}_1^2 \sin(\theta_1 - \theta_2) \\ = F_2 \cos \theta_2 - F_{2b} \sin \theta_2 \end{aligned} \quad (4.18)$$

$$\begin{aligned}
m_3 l_3 \ddot{\theta}_3 + m_3 l_1 \ddot{\theta}_1 \cos(\theta_1 - \theta_3) - m_3 l_1 \dot{\theta}_1^2 \sin(\theta_1 - \theta_3) \\
= F_3 \cos \theta_3
\end{aligned} \tag{4.19}$$

4.1.3 Modification for BEMT correction

For the wave-current model module, calculations of horizontal and vertical particle velocities are related to the horizontal and vertical coordinates of the turbine in different wave theories, these coordinates of the turbine hinge node and buoy hinge node are written as:

$$x_{\text{turbine}} = \frac{\partial \mathbf{X}_{\text{turbine}}}{\partial x} \tag{4.20}$$

$$z_{\text{turbine}} = \frac{\partial \mathbf{X}_{\text{turbine}}}{\partial z} \tag{4.21}$$

$$x_{\text{buoy}} = \frac{\partial \mathbf{X}_{\text{buoy}}}{\partial x} \tag{4.22}$$

$$z_{\text{buoy}} = \frac{\partial \mathbf{X}_{\text{buoy}}}{\partial z} \tag{4.23}$$

Moreover, the vertical particle velocities are varied along blades, so element coordinates are:

$$x_{\text{element}} = x_{\text{turbine}} + h_{\text{element}} \cos \theta_4 \quad (4.24)$$

$$z_{\text{element}} = z_{\text{turbine}} + h_{\text{element}} \sin \theta_4 \quad (4.25)$$

where h_{element} is the element position on the blade and θ_4 is the pitch angle of the turbine. If assuming that the turbine is kept horizontal during operation, the pitch angle is assume to be 0 degrees, so element coordinates will become:

$$x_{\text{element}} = x_{\text{turbine}} \quad (4.26)$$

$$z_{\text{element}} = z_{\text{turbine}} + h_{\text{element}} \quad (4.27)$$

Substituting these coordinates into the wave model, then this module has been modified to work for the mooring supported turbine.

The relative velocity modification of inflow velocity should be considered not only in the BEMT Equations but also in the Dynamic Wake Model and Morison Equation.

According to the methodology, the adapted dynamic inflow effects to the BEMT model [93, 29, 94]. On a blade element bounded by radii R_1 and R_2 the momentum thrust equation depends on the time derivative of the axial induction factor \dot{a} and is written as:

$$dF_A = 2\mathbf{u}a\dot{m} + \mathbf{u}m_A\dot{a} \quad (4.28)$$

where \dot{m} is the mass flow through the intersecting fluid annulus, a is the axial induction factor and m_A is the apparent mass of the blade section.

The mass flow through the annular element can be written as:

$$\dot{m} = \rho\mathbf{u}(1 - a)dA \quad (4.29)$$

where ρ is the water density and $dA = \pi(R_2^2 - R_1^2)$.

For a turbine of radius R , Tuckerman [95] suggests that the apparent mass acting on the rotor can be approximated by an enclosing fluid ellipsoid, which through the use of potential flow theory is expressed as:

$$m_A = 8/3\rho R^3 \quad (4.30)$$

Substituting Equation 4.29 and 4.30 into Equation 4.28 and each term divided by π , ρ , u^2 , dA and multiplied by 2, the final form of the unsteady thrust coefficient for an annulus can be obtained as:

$$C_{FA} = 4a(1 - a) + \frac{16}{3\pi u} \frac{(R_2^3 - R_1^3)}{(R_2^2 - R_1^2)} \dot{a} \quad (4.31)$$

Substituting the thrust coefficient $C_T = 4a(1 - a)$ into Equation 4.31 and replace the inflow velocity with the modified horizontal relative velocity, U_x gives:

$$C_{FA} = C_T + \frac{16}{3\pi U_x} \frac{(R_2^3 - R_1^3)}{(R_2^2 - R_1^2)} \dot{a} \quad (4.32)$$

The last term in right hand of Equation 4.32 can be used to calculate the additional force from the dynamic wake effects.

The inertial forces caused by fluid acceleration effects is expressed as a Morison equation, and as presented by Buckland [30] and Chapman [31]. The inertial force per unit length, dl , in the wave propagation direction on a submerged body can be written as:

$$dF_{\text{in}} = \rho C_m A \frac{\partial \mathbf{u}}{\partial t} dl \quad (4.33)$$

where A is the cross horizontal sectional area parallel to the flow and C_m is the inertia coefficient which is expressed as:

$$C_M = 1 + C_A = 1 + \frac{M_A}{\rho A dl} \quad (4.34)$$

where M_A is the added mass for a blade element.

For blade elements, the added mass in axial and tangential directions can be approximated with that of a fixed pitched plate as Theodorsen's theory [33]:

$$M_{A,\text{axial}} = \rho \pi \left(\frac{c \sin \beta}{2} \right)^2 dl \quad (4.35)$$

$$M_{A,\text{tan}} = \rho \pi \left(\frac{c \cos \beta}{2} \right)^2 dl \quad (4.36)$$

which is the mass of an enclosing fluid cylinder with radii r of half the vertical and horizontal chord components c of the respective blade sections with section angle β [19].

Substituting Equations 4.34, 4.35 and 4.36 into Equation 4.33 and plugging the relative velocity U into the Equation gives the equations for the inertia forces in the axial and tangential directions for a blade element as

$$dF_{\text{in,axial}} = \rho \left(1 + \frac{\pi((c \sin \beta)/2)^2}{A_\alpha} \right) A_\alpha \frac{\partial U_x}{\partial t} dr \quad (4.37)$$

$$dF_{\text{in,tan}} = \rho \left(1 + \frac{\pi((c \cos \beta)/2)^2}{A_\alpha} \right) A_\alpha \frac{\partial U_y}{\partial t} dr \quad (4.38)$$

where A_α is the cross sectional area of the airfoil at the blade section.

When the external forces based on the initial conditions for the first time step are calculated from the BEMT equations with a wave-current model, dynamic wake model and Morrison equations, the system Lagrange's equation solver will start to solve the differential equations of motion for the mooring supported turbine. Then the new values and the angular velocities of $\dot{\theta}_1, \dot{\theta}_2, \dot{\theta}_3$ are obtained to work as the new initial conditions for the next time step. This loop process will continue until the time step reaches the end time of the simulation.

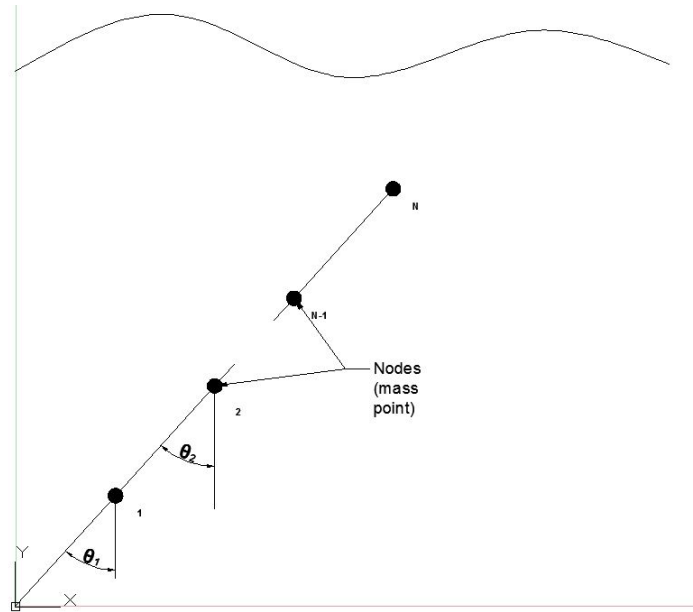


Figure 4.5: A multi-pendulum system with a finite number of rods and masses

4.2 Developed model with finite element method

The method shown previously is now extended to include the mooring line dynamics using as a basis finite element method. It is necessary to divide rods in pendulum system into a finite number of segments with lumped mass nodes. The segment is assumed to be fully flexible in bending directions, thus the whole system becomes a multi-pendulum system with a finite number of rods and masses as shown in Figure 4.5.

In \sum_1^n order to derive the governing equations of motion for a single tension mooring line system, the Euler-Lagrange differential equations of the system is written in global coordinates:

$$[\mathbf{M}] = \begin{bmatrix} \sum_{i=1}^n M_i & \sum_{i=2}^n M_i & \dots & \sum_{i=n}^n M_i \\ \sum_{i=2}^n M_i & \sum_{i=2}^n M_i & \dots & \sum_{i=n}^n M_i \\ \vdots & \vdots & \dots & \vdots \\ \sum_{i=n}^n M_i & \sum_{i=n}^n M_i & \dots & \sum_{i=n}^n M_i \end{bmatrix} \quad (4.40)$$

$$\boldsymbol{\psi} = \begin{bmatrix} 0 & \theta_1 - \theta_2 & \dots & \theta_1 - \theta_n \\ \theta_2 - \theta_1 & 0 & \dots & \theta_2 - \theta_n \\ \vdots & \vdots & \dots & \vdots \\ \theta_n - \theta_1 & \theta_n - \theta_2 & \dots & 0 \end{bmatrix} \quad (4.41)$$

$$\begin{aligned} & ([\mathbf{M}] + [\mathbf{ma}]) [\mathbf{l}] \cos(\boldsymbol{\psi}) \left[\ddot{\boldsymbol{\theta}} \right] \\ & + ([\mathbf{M}] + [\mathbf{ma}]) [\mathbf{l}] \sin(\boldsymbol{\psi}) \left[\dot{\boldsymbol{\theta}} \right]^2 \\ & - [\mathbf{M}] g \sin [\boldsymbol{\theta}] - [\mathbf{CV}] \left[\dot{\boldsymbol{\theta}} \right] = [\mathbf{F}] \end{aligned} \quad (4.39)$$

where:

$$[\mathbf{m}] = \begin{bmatrix} \sum_{i=1}^n ma_i & \sum_{i=2}^n ma_i & \dots & \sum_{i=n}^n ma_i \\ \sum_{i=2}^n ma_i & \sum_{i=2}^n ma_i & \dots & \sum_{i=n}^n ma_i \\ \vdots & \vdots & \dots & \vdots \\ \sum_{i=n}^n ma_i & \sum_{i=n}^n ma_i & \dots & \sum_{i=n}^n ma_i \end{bmatrix} \quad (4.42)$$

$$[\mathbf{l}] = \begin{bmatrix} l_1 & l_2 & \dots & l_n \\ l_2 & l_2 & \dots & l_n \\ \vdots & \vdots & \dots & \vdots \\ l_n & l_n & \dots & l_n \end{bmatrix} \quad (4.43)$$

$$[\boldsymbol{\theta}] = \begin{bmatrix} \theta_1 \\ \theta_2 \\ \vdots \\ \theta_n \end{bmatrix} \quad (4.44)$$

$$[\mathbf{CV}] = \begin{bmatrix} CV_1 \\ CV_2 \\ \vdots \\ CV_n \end{bmatrix} \quad (4.45)$$

$$[\mathbf{F}] = \begin{bmatrix} F_1 \\ F_2 \\ \vdots \\ F_n \end{bmatrix} \quad (4.46)$$

M_i is the lumped mass for each node, ma_i is the lumped added mass for each node, l_i is the length of each segment, g is the gravitational acceleration, CV_i is the viscous damping coefficient of each segment which is

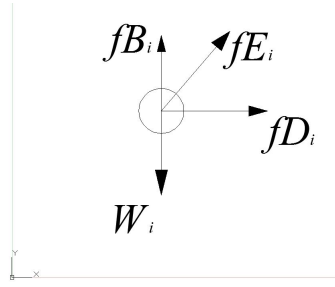


Figure 4.6: Forces on each mass node

calculated by the method presented by [9], θ_i is the angle shown in Figure 4.5.

The components of external force on each node is shown in Figure 4.6. The weight W_i is counted in Equation 4.39, so the external forces becomes:

$$F_i = fE_i + fD_i \cos \theta_i + fB_i \sin \theta_i \quad (4.47)$$

$$fE_i = Q_i / l_i \quad (4.48)$$

where

$fD_i =$ drag force on the segment

$fB_i =$ buoyancy force on the segment

$Q_i =$ the generalized force on the segment which can be calculated from Equation 4.13

In this method the inertia velocity of the turbine itself is calculated from the backward difference method for the position $\mathbf{X}_{\text{turbine}}$ at time t_{it} :

$$\mathbf{U}_T = \frac{\partial}{\partial \Delta t} (\mathbf{X}_{\text{turbine}}^{it} - \mathbf{X}_{\text{turbine}}^{it-1}) \quad (4.49)$$

similarly, the relative velocity of the buoy:

$$\mathbf{U}_B = \frac{\partial}{\partial \Delta t} (\mathbf{X}_{\text{buoy}}^{it} - \mathbf{X}_{\text{buoy}}^{it-1}) \quad (4.50)$$

In this system it has also been assumed that the turbine is naturally buoyant and buoy is positively buoyant, so the masses should not be included in the weight calculation. However, masses of the device should be considered in an inertia matrix.

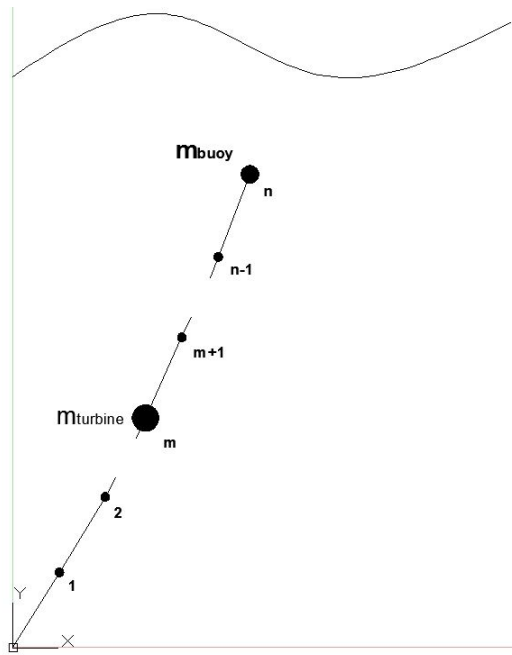


Figure 4.7: System with device masses

Figure 4.7 shows the buoy is attached to the n -th node which is the end of the mooring line and the turbine is attached to the m -th node. Thus the final inertia matrix becomes:

$$[\mathbf{MR}] = \begin{bmatrix} \sum_{i=1}^{m-1} M_i + (M_m + mt) + \sum_{i=m+1}^{n-1} M_i + (M_n + mb) & \sum_{i=2}^{m-1} M_k + (M_m + mt) + \sum_{i=m+1}^{n-1} M_i + (M_n + mb) & \dots & (M_n + mb) \\ \sum_{i=2}^{m-1} M_k + (M_m + mt) + \sum_{i=m+1}^{n-1} M_i + (M_n + mb) & \sum_{i=2}^{m-1} M_k + (M_m + mt) + \sum_{i=m+1}^{n-1} M_i + (M_n + mb) & \dots & (M_n + mb) \\ \vdots & \vdots & \ddots & \vdots \\ (M_n + mb) & (M_n + mb) & \dots & (M_n + mb) \end{bmatrix} \quad (4.51)$$

$$[\mathbf{mR}] = \begin{bmatrix} \sum_{i=1}^{m-1} ma_i + (ma_m + mat) + \sum_{i=m+1}^{n-1} ma_i + (ma_n + mab) & \sum_{i=2}^{m-1} ma_i + (ma_m + mat) + \sum_{i=m+1}^{n-1} ma_i + (ma_n + mab) & \dots & (ma_n + mab) \\ \sum_{i=2}^{m-1} ma_i + (ma_m + mat) + \sum_{i=m+1}^{n-1} ma_i + (ma_n + mab) & \sum_{i=2}^{m-1} ma_i + (ma_m + mat) + \sum_{i=m+1}^{n-1} ma_i + (ma_n + mab) & \dots & (ma_n + mab) \\ \vdots & \vdots & \ddots & \vdots \\ (ma_n + mab) & (ma_n + mab) & \dots & (ma_n + mab) \end{bmatrix} \quad (4.52)$$

where m_t and m_{at} are the mass and added mass of turbine, m_b and m_{ab} are the that of buoy.

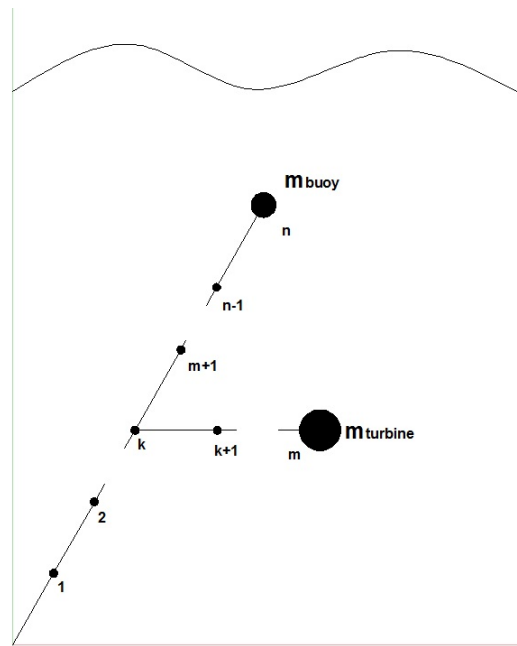


Figure 4.8: “Flail” system

The schematic of system shown in Figure 4.8 is now extended to incorporate the dynamics of the turbine and buoyant reaction forces when subjected to wave-current conditions. Figure 4.8 shows the final diagram of the system studied here, the final matrix is listed blow. In a “flail” mooring system, the inertia matrix and the weight matrix are different from the single mooring system. As Figure 4.8 shows, the buoy and turbine are attached at the n -th and m -th node and the three section pendulum is hinged at the k -th node, so the inertia matrix and weight matrix become:

$$\begin{aligned}
 & [\mathbf{M}_f] = \\
 & \left[\begin{array}{cccccccc}
 \sum_{i=1}^n M_i & \sum_{i=2}^n M_i & \dots & \sum_{i=k}^n M_i & \sum_{i=k+1}^m M_i & \dots & \sum_{i=m+1}^n M_i & M_n \\
 \sum_{i=2}^n M_i & \sum_{i=2}^n M_i & \dots & \sum_{i=k}^n M_i & \sum_{i=k+1}^m M_i & \dots & \sum_{i=m+1}^n M_i & M_n \\
 \vdots & \vdots \\
 \sum_{i=k}^n M_i & \sum_{i=k}^n M_i & \dots & \sum_{i=k}^n M_i & \sum_{i=k+1}^m M_i & \dots & \sum_{i=m+1}^n M_i & M_n \\
 \sum_{i=k+1}^m M_i & \sum_{i=k+1}^m M_i & \dots & \sum_{i=k+1}^m M_i & \sum_{i=k+1}^m M_i & \dots & \sum_{i=m+1}^n M_i & M_n \\
 \vdots & \vdots \\
 M_m & M_m & \dots & M_m & M_m & \dots & M_m & M_n \\
 \sum_{i=m+1}^n M_i & \sum_{i=m+1}^n M_i & \dots & \sum_{i=m+1}^n M_i & \sum_{i=m+1}^n M_i & \dots & \sum_{i=m+1}^n M_i & M_n \\
 \vdots & \vdots \\
 M_n & M_n & \dots & M_n & M_n & \dots & M_n & M_n
 \end{array} \right]
 \end{aligned}$$

(4.55)

Substituting Equations 4.53 4.54 and 4.55 into Equation 4.39, the governing equation for a “flail” system with finite number of segments can be obtained from:

$$\begin{aligned}
& ([\mathbf{MR}_f] + [\mathbf{mR}_f]) [\mathbf{1}] \cos([\psi]) \left[\ddot{\boldsymbol{\theta}} \right] \\
& + ([\mathbf{MR}_f] + [\mathbf{mR}_f]) [\mathbf{1}] \sin([\psi]) \left[\dot{\boldsymbol{\theta}} \right]^2 \\
& - [\mathbf{M}_f] g \sin([\theta]) - [\mathbf{CV}] \left[\dot{\boldsymbol{\theta}} \right] = [\mathbf{F}] \quad (4.56)
\end{aligned}$$

4.2.1 Wave excitation on buoy

The wave excitation is considered to be a factor to the system, the buoy will be excited by the wave at a different magnitude according to its shape. In this section the buoy is considered to be a sphere, the hydrodynamics of the buoy will be discussed in next chapter. The external forces including wave excitation on the system of the tension mooring turbine is shown in Figure 4.9.

The wave excitation in two directions can be defined as the exciting force and drift force, and is based on the work from Wu [96], the wave induced exciting and drift forces acting on a submerged sphere is given as:

$$f_j = -\rho\omega^2 A_{S_B} (\phi_1 + \phi_D) n_j ds \quad (4.57)$$

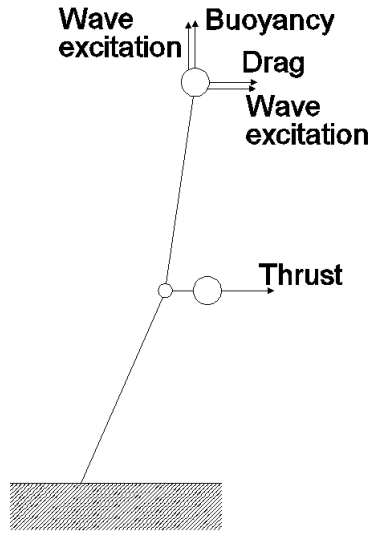


Figure 4.9: Forces on the system

and

$$\bar{f}_j = \frac{1}{4} \rho \omega^2 A_{S_B}^2 \nabla \phi_{ID} \cdot \nabla \phi_{ID}^* n_j ds \quad (4.58)$$

where ρ is the water density, ω is the wave frequency, A is the wave amplitude, S_B is the body surface, ϕ_1 is incident wave velocity potential, ϕ_D is the diffraction potential, n_j is the the body's normal vector pointing into the water, $\phi_{ID} = \phi_1 + \phi_D$ and the symbol * denotes the complex conjugate.

In this investigation an assumption has been made that the diffraction potential is not taken into account in order to simplify the calculation. Therefore the the exciting and drift forces can be simplified to:

$$f_j = -\rho\omega^2 A_{SB} \phi_1 n_j ds \quad (4.59)$$

and

$$\bar{f}_j = \frac{1}{4} \rho\omega^2 A_{SB}^2 \nabla\phi_1 \cdot \nabla\phi_1^* n_j ds \quad (4.60)$$

Moreover, the added mass effect should be considered, these added mass forces on the buoy in both horizontal and vertical directions are:

$$F_{ax} = \frac{2}{3} \rho\pi R^3 \frac{\partial^2 \phi_1}{\partial x \partial t} \quad (4.61)$$

and

$$F_{ay} = \frac{2}{3} \rho\pi R^3 \frac{\partial^2 \phi_1}{\partial y \partial t} \quad (4.62)$$

where R is the buoy radius.

4.3 Solving scheme

The original ESRU BEMT code is based on a rigid supported turbine, the position of the turbine will not change by time. However, the coordinates of the mooring supported turbine are variable by time and the relative velocity should be calculated by the relative motion between the turbine and wave-current inflow. Figure 4.10 shows the main process of the simulation. The process nodes with dark background are works based on this thesis, which are different from the original BEMT.

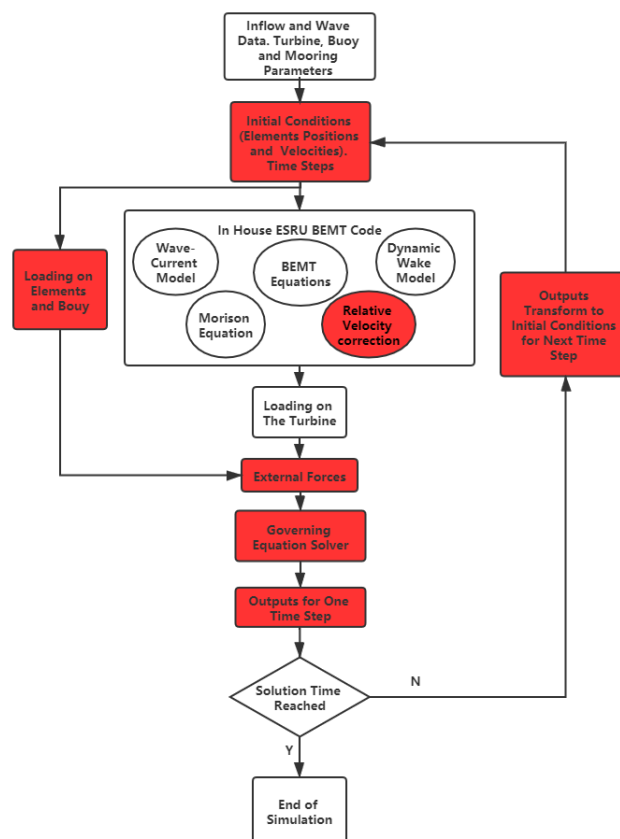


Figure 4.10: Solving process

There are some variables in input parameters which can be defined by

users for different mooring turbine devices. The state of motion for the system in the first time step is defined by the initial conditions. The loading on each mooring element and buoy is obtained as the external forces and the loading on the turbine is calculated by BEMT code with relative velocity modification. After the external forces are determined, the governing equation can be solved for the new state of motion of the system. The new values will be used as initial conditions for the next time step until the simulation reaches the end time.

4.4 Summary

This chapter has explained two fast simulation algorithms that is developed to model the neutrally buoyant turbine supported from a tension cable based mooring system based on the modified ESRU BEMT code. The methodology presented here is arguably the simplest form of representing the complicated interactions between the instationary marine environment, the rotating turbine blades and the tension mooring system, while still retaining the capability to resolve the most dominant hydrodynamic loading effects. In the next chapter investigations will be undertaken to inform the relationships between a turbine's inflow, operating, turbine and mooring parameters to the generated loads on the rotor.

Chapter 5

Investigation of the relationships between the rotor loads and input parameters

“As order exponentially increases, time exponentially speeds up.”

– *Ray Kurzweil.*

This section focuses on variables such as turbine dimensional parameters, buoyancy, wave-current coupled forces and mooring line parameters. Sea states with both regular and irregular waves are investigated, the wave data was collected by UK Offshore Operators Association and provided by the British Oceanographic Data Center [1]. The irregular waves are generated from JONSWAP spectrum [25].

5.1 Model verification

A method in predicting the line's profile for a typical taut mooring system has been presented by Lingzhi Xiong [90], The properties of the mooring line are tabulated in Table 5.1 and the water depth is 300m.

Table 5.1: Mooring line properties

Parameter	Length (m)	Diameter(mm)	Wet(kg/m)	EA (MN)
Ground chain	100	147	367	1220
Mid-section	218	208	7.8	348
Fairlead chain	50	147	367	1220

In order to verify the developed model, the mooring line's profile had been compared with Xiong's data. Moreover, the elasticity of the mooring line in developed model was considered here to give an accurate comparison. Note an assumption that the elasticity was ignored had been made in other simulations. Table 5.2 gives the line tension at the fairlead. The initial angles for the mooring line segments are all set to be $\pi/2$, which means the mooring line is lay on the seabed at first. Then the external forces are applied on the fairlead. Then a constraint is applied to the system, the constraint is that the projection of the mooring line on the z-coordinate cannot exceed 310m. The mooring line's profile is obtained at the end of the simulation.

Table 5.2: Line tension at the fairlead

Fairlead position	F_x (kN)	F_z (kN)	Total tension (kN)
X=190m	251.2	659.9	706.1
X=200m	885.7	1603.7	1832.0
X=210m	4824.1	7346.2	8788.5

The horizontal distance between the fairlead and the anchor point varies from 190m to 210m, with a step of 10m. Line's profile are compared with the results based on Xiong's work in Orcflex. As shown in Figure 5.1,

good agreement has been achieved in fairlead at 200m and 210m, but the developed model failed to work when the fairlead is at 190m. This means the developed model is applicable to the condition that the tension on the mooring lines is high enough to make the mooring to be approximately straight. The application of the system where has large buoyancy, thrust and mooring lines length shorter than water depth make the developed model reach the requirement.

5.2 Investigation of waves

Table 5.3 shows the sea states investigated in the simulations to obtain the thrust and torque on the turbine. Steep and swell waves are investigated to make comparison on how wave excitation on the buoy affect the loads on the turbine. The sea site is based on Nevalainen's studies[19], the assumed hypothetical site for the generic turbine was chosen off the north east coast of the Orkney islands, Scotland. This site provided a flow speed around 2.5m/s and a n average depth of 50m.

Table 5.3: sea states

sea states	1	2	3	4	5
H_s [m]	4.322	1.07	2.665	1.07	2.665
T_z [s]	6.135	11.07	6.135	11.07	6.135
water depth(m)	50	50	50	50	50
steepness(H/gT)	0.0719	0.0099	0.0443	0.0099	0.0443
wave model	three-step	linear	three-step	random	random
sea states	6	7	8	harsh winter	
H_s [m]	1.008	2.665	1.008	10.12	
T_z [s]	4.653	6.135	4.653	10.06	
water depth(m)	50	40	50	50	
steepness(H/gT)	0.0237	0.0443	0.0237	0.1027	
wave model	three-step	three-step	random	three-step	

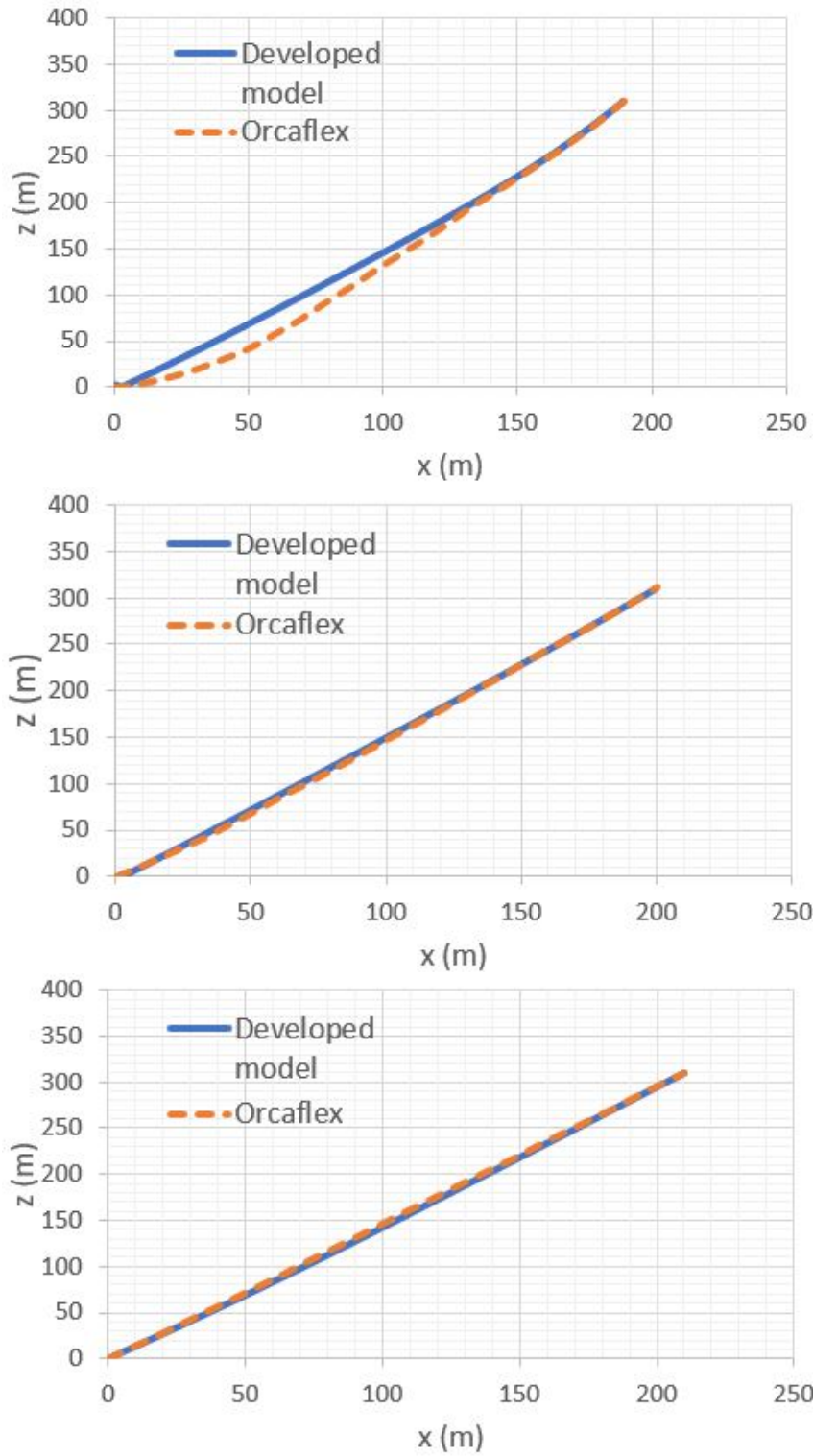


Figure 5.1: Comparison of the line's profile in water (Fairlead at $x=190\text{m}$, 200m and 210m , $z=310\text{m}$)

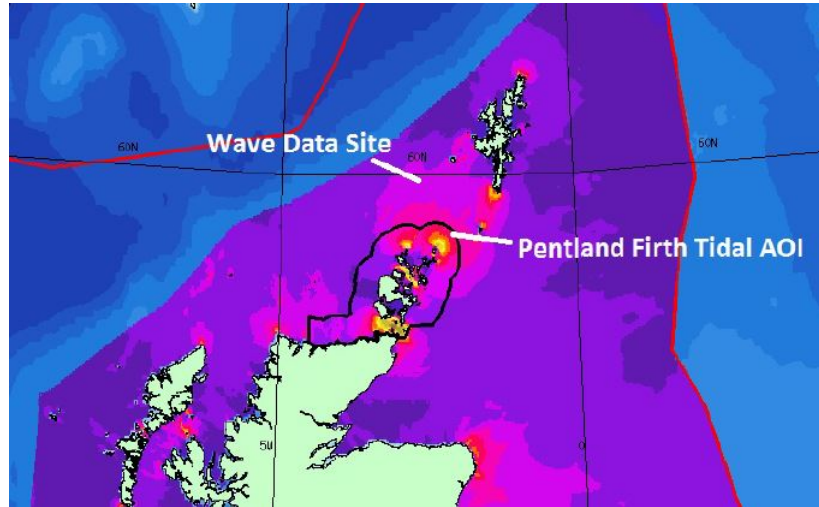


Figure 5.2: The sea site chosen by Nevalainen[19]

5.2.1 Initial conditions

The first step for solving the system is to confirm initial conditions. In this study, a set of initial conditions is considered, which is shown in Table 5.4

Table 5.4: Initial conditions for preliminary model

Initial conditions					
$\theta_1 = \frac{\pi}{4}$	$\dot{\theta}_1 = 0$	$\theta_2 = 0$	$\dot{\theta}_2 = 0$	$\theta_3 = \frac{\pi}{2}$	$\dot{\theta}_3 = 0$

Angles in Table 1 are all measured in radian. For analysis of pendulum dynamics, usually more initial conditions should be taken into consideration. However for the mooring supported tidal turbine, when the buoyancy and wave-current coupled force are applied on the system, the turbine will oscillate around the equilibrium position during operation, no matter what the initial conditions are set. The reduction of force and torque on the turbine resulted by the tension mooring system during op-

eration, is the main topic of this thesis to investigate. This is so that only one initial condition is considered in this study, it is that mooring lines l_1 and l_2 are at vertical position and l_3 is at horizontal position.

For a developed model, it is necessary to define the initial condition for all segments as Table 5.5 shows

Table 5.5: Initial conditions for developed model

Initial conditions		
$\theta_1 \sim \theta_{k=\frac{\pi}{4}}$	$\dot{\theta}_1 \sim \dot{\theta}_k=0$	$\theta_{m+1} \sim \theta_n=0$
$\dot{\theta}_{m+1} \sim \dot{\theta}_n=0$	$\theta_{k+1} \sim \theta_{m=\frac{\pi}{2}}$	$\dot{\theta}_{k+1} \sim \dot{\theta}_m=0$

The initial angles are set for every segment separately in order to represent an untensioned mooring line. Moreover, this method can be applied to a general mooring system as well. Parameters for the turbine, buoy and mooring line are given below

case 1:segment length = 0.5m $m_{\text{buoy}} = 5\text{t}$ $m_{\text{turbine}} = 80\text{t}$ $l_1 = 30\text{m}$ $l_2 = 15\text{m}$
 $l_3 = 3\text{m}$ turbine diameter = 20m buoy radius = 3m $\Omega_r = 1.25\text{rad/s}$ Blade profile: NRELs814 Mooring line material: Dyneema

case 2:segment length = 0.5m $m_{\text{buoy}} = 300\text{kg}$ $m_{\text{turbine}} = 1000\text{kg}$ $l_1 = 20\text{m}$
 $l_2 = 10\text{m}$ $l_3 = 3\text{m}$ turbine diameter = 4m buoy radius = 1.1m $\Omega_r = 1.25\text{rad/s}$
 Blade profile: NRELs814 Mooring line material: Steel

case 3:segment length = 0.5m $m_{\text{buoy}} = 300\text{kg}$ $m_{\text{turbine}} = 1000\text{kg}$ $l_1 = 20\text{m}$
 $l_2 = 10\text{m}$ $l_3 = 3\text{m}$ turbine diameter = 4m buoy radius = 1.1m $\Omega_r = 1.25\text{rad/s}$
 Blade profile: NRELs814 Mooring line material: Dyneema

For case 1, the turbine diameter is set to be same as AR2000 and the weight is half of the AR1500. For case 2 and 3, the turbine diameter and weight is same as SIT Instream Turbine[97].

5.2.2 Comparison of preliminary and developed models

In this part, the results for two models in three regular sea states are discussed under Case 1. The turbine is submerged in a swell wave in the first sea state and linear wave theory is applied, loading in the developed model is slightly higher than that in the preliminary model, this is because there are external force terms on every element in the developed model. The same trend is in the second sea state where three step wave theory is applied [37], but results from two models are closer when compared with the first sea state. In the harsh winter sea state, the developed model generates a higher loading value, it shows this to be a transition from the curve of preliminary model. Moreover, the torque value turns to negative in some time steps in harsh winter sea state as Figure 5.5, this will be discussed in detail in the next section.

In the system with smaller size of turbine and buoy as Case 2 shows a similar shape of curve, the system loading in the preliminary model is higher than the developed model as for Figure 5.6. In this case the mooring line weight is about 1/6 of the the buoyancy, the mooring line weight becomes an important factor, the system starts to vibrate in the developed model after running for 1 minute. However, the system will not vibrate

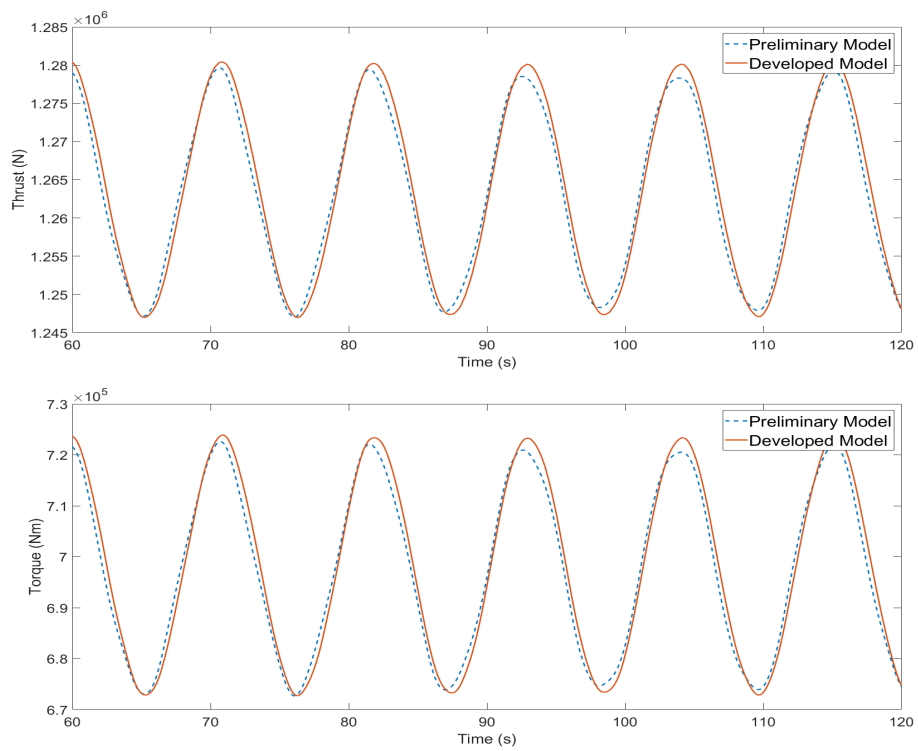


Figure 5.3: Case 1, regular waves generated from sea state 2, current speed is 2.5m/s

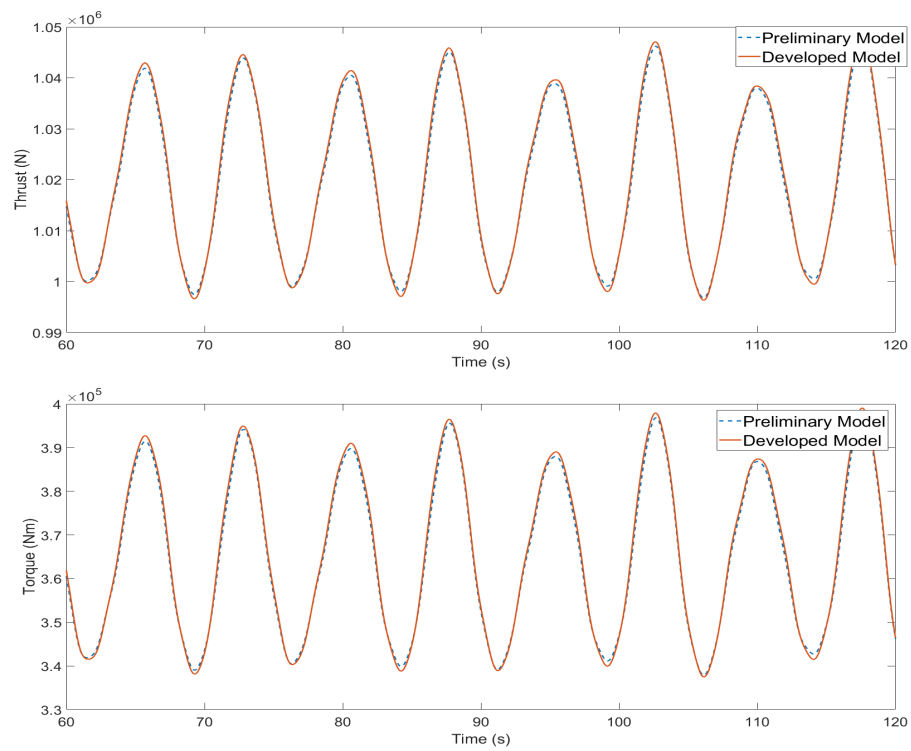


Figure 5.4: Case 1, regular waves generated from sea state 3, current speed is 2.5m/s

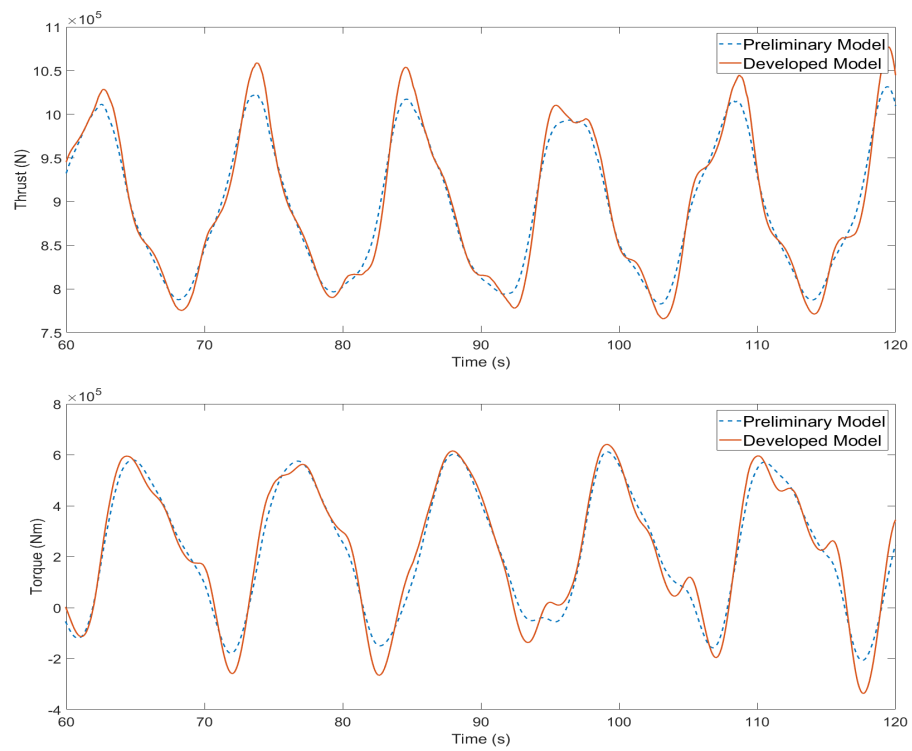


Figure 5.5: Case 1, regular waves generated from harsh winter, current speed is 2.5m/s

in the preliminary model because of the mooring line is being considered as three rigid rods and only three lumped masses in the system, which is not fully representative of a low tension system. Moreover, in a system where the mooring line is made of dyneema as Case 3, the density of this material is similar to water. The system loading in the developed model shows a significant improvement, as shown in Figure 5.7.

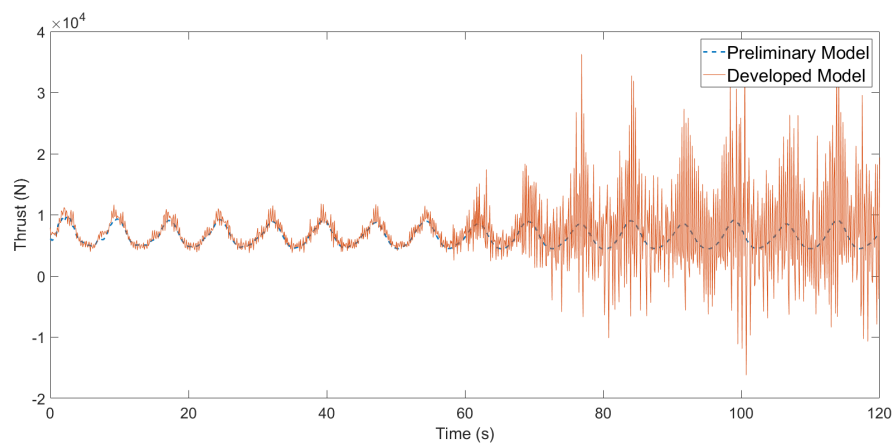


Figure 5.6: Case 2, regular waves generated from sea-state 7, current speed is 2.5m/s

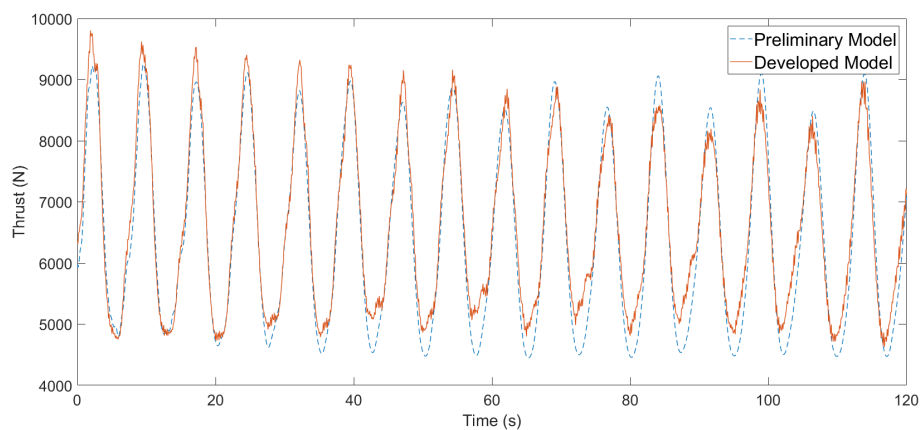


Figure 5.7: Case 3, regular waves generated from sea-state 7, current speed is 2.5m/s

In order to avoid the vibration of steel wire mooring systems in Case 2, a factor Alpha is introduced to Equation 4.56 as a multiplier to enlarge the viscous coefficient term CV so that the vibration can be damped effectively. Figure 5.8 and 5.9 shows the comparison of the turbine thrust loading in different Alpha. It indicates that the higher viscous damping coefficient will reduce the vibration of the system that mooring lines are made from steel, the coefficient term effects in the dyneema mooring line system is not as obvious as that of steel mooring. In addition, the large viscous damping will make the convergence of the solution procure quicker.

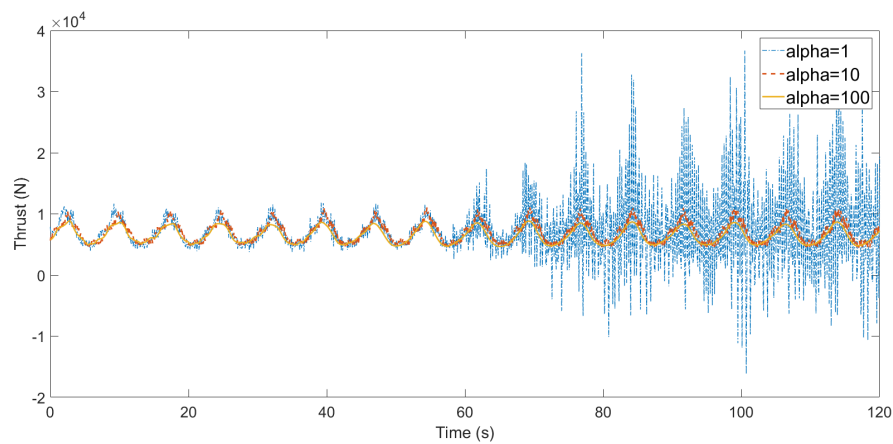


Figure 5.8: Case 2, turbine thrust loading in different Alpha

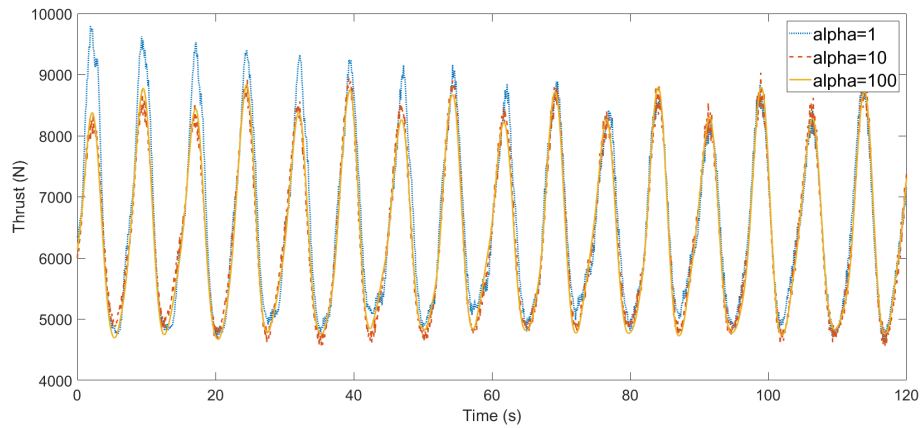


Figure 5.9: Case 3, turbine thrust loading in different Alpha

5.2.3 Regular waves

Firstly, the results with and without wave excitation on the buoy are compared in the same sea states. In sea state 3, a three-step approximate wave-current interaction model was applied in this simulation since its steepness is larger than 0.02 [62]. However, the hub height will drop to around 22.5m in operation compared to the original height which was set at 30m from the seabed, so for the rigid supported turbine the hub height is modified to the same as a mooring one. Figure 5.10 shows the result for Case 1 in sea state 3, it showed that the mooring supported turbine has a favorable performance in reduction of peak thrust on the turbine when compared to the rigid supported turbine and the result that considered wave excitation on the buoy shows a different waveform as that without wave excitation. The mean values of the three curves are close which are 1.019MN for rigid supported, 1.019MN for that without wave excitation on buoy and 1.016MN for that with wave excitation on buoy. However, the

standard deviation of the thrust on a mooring supported turbine considered wave excitation on the buoy is 28.23kN and without wave excitation is 16.90kN which are 69.69% and 41.73% of that on rigid structure's value 40.50kN.

The results for torque shows a different trend compared with thrust, torques on the mooring supported turbine with and without wave excitation on buoy both have more fluctuation than that of rigid supported. Although the mean values are similar which are 364.91kN·m, 364.66kN·m and 361.98kN·m for rigid, without and with wave excitation on buoy separately, the standard deviation are $18.19 \times \text{kN} \cdot \text{m}$, $87.14 \text{kN} \cdot \text{m}$ and $83.41 \text{kN} \cdot \text{m}$. This is because of the influence of the relative velocity modification in the vertical direction which will be expressed later in this section.

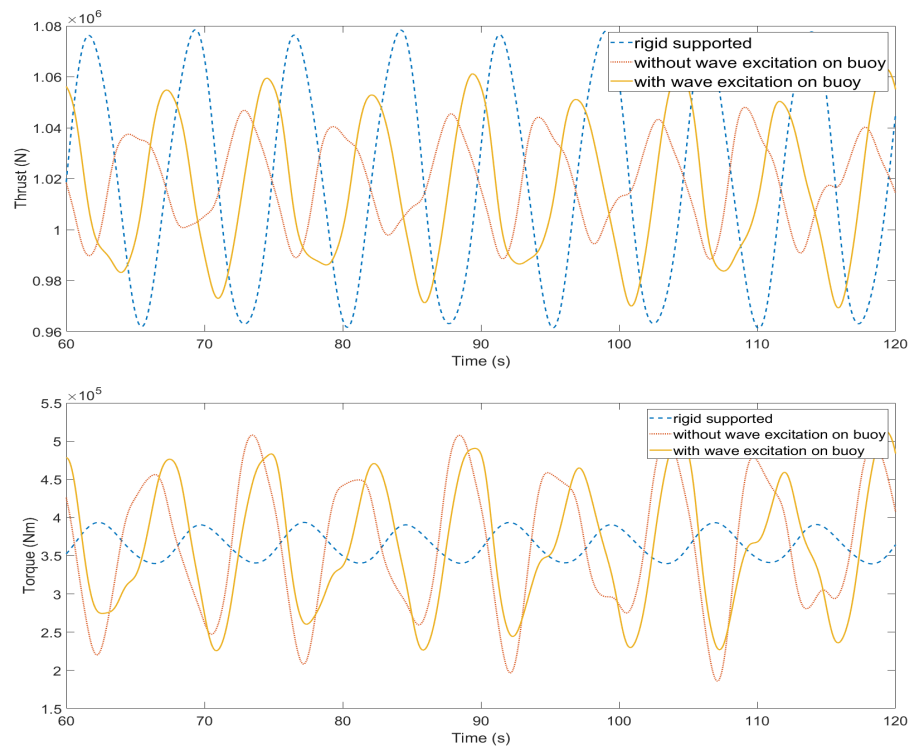


Figure 5.10: Thrust and torque for Case 1 in sea state 3

Figure 5.11 shows the result for the turbines in case 1 operating in sea state 1. The wave height is higher than that of sea state 3 but the hub height is around 22m, so the mean values are slightly lower than those of sea state 3 which are 962.41kN, 963.75kN and 962.53kN for rigid supported, mooring turbine without and with wave excitation on buoy. The standard deviations are 65.04kN, 27.66kN (42.54%) and 47.52kN (73.07%) separately. The mean values of torque are 301.53kN·m, 302.10kN·m and 302.85kN·m and the standard deviations are 23.72kN·m, 141.84kN·m and 137.15kNm.

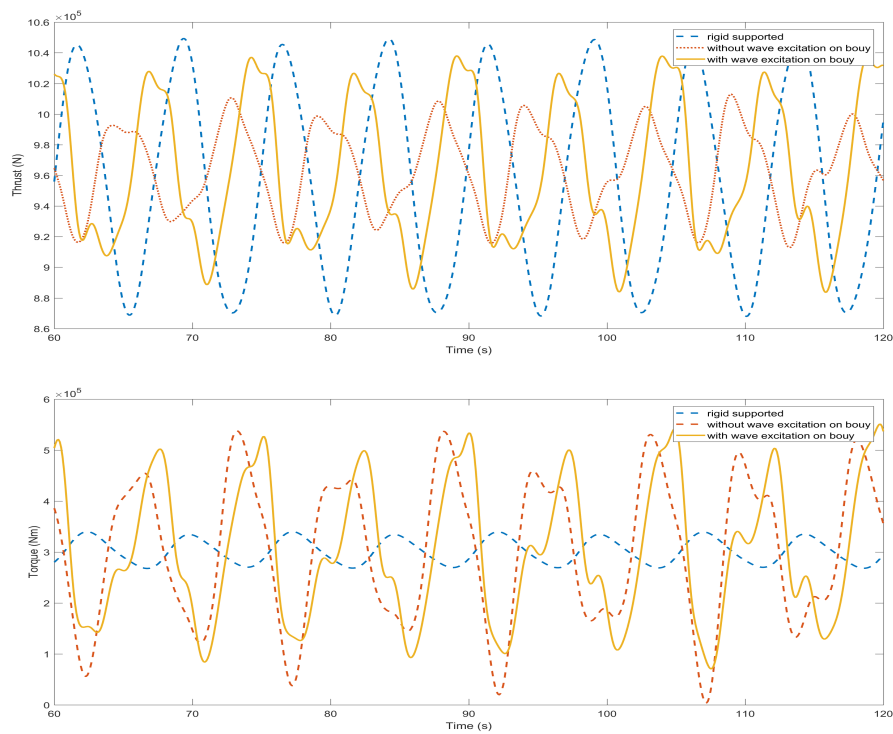


Figure 5.11: Thrust and torque for Case 1 in sea state 1

Figure 5.12 gives results for the system operating in sea state 4. It shows a favorable performance in the reduction of peak loading both in thrust

and torque and the wave excitation on buoy gives a positive effect in load reduction. The reason is that the buoy will oscillate more regularly in the wave with long wave periods, as Figure 5.15 shows. In this sea state, the mean values of thrust are 1.260MN, 1.265MN and 1.265MN for rigid supported turbine, mooring turbine without and with wave excitation on buoy respectively. The standard deviations are 47.35kN, 11.59kN (24.5%) and 6.56kN (13.9%) separately. The average torque values are 694.47kN·m, 699.92kN·m and 699.06kN·m and the standard deviations are 58.19kN·m, 24.98kN·m and 20.86kN·m.

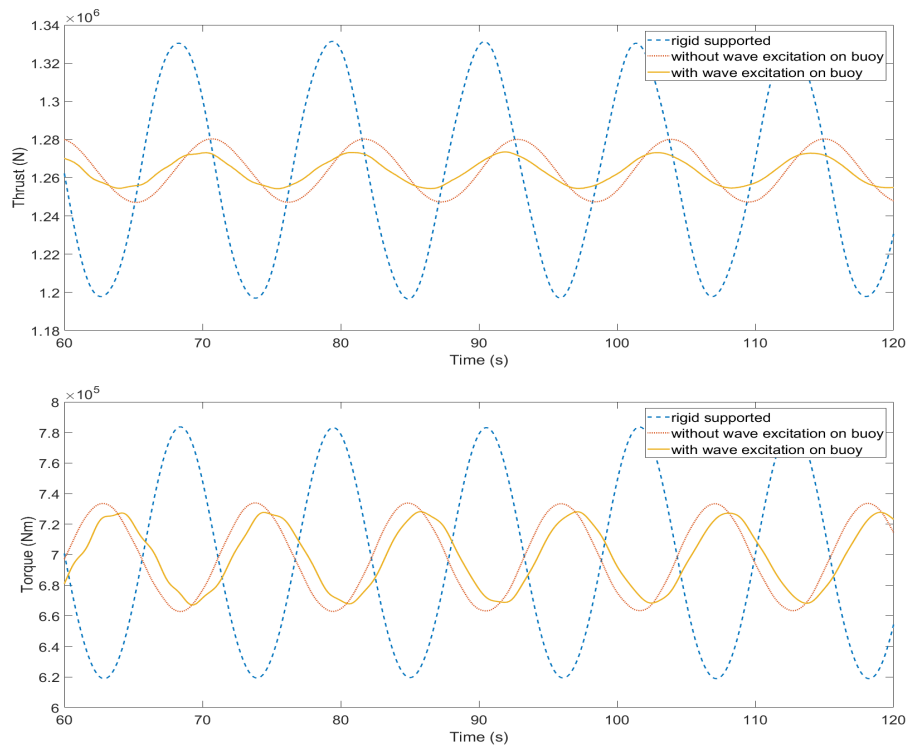


Figure 5.12: Thrust and torque for Case 1 in sea state 2

The result for harsh winter conditions, extreme storm condition, is shown in Figure 5.13, the peak loading reduction in thrust is performed simi-

larly as sea state 4. The mean values are 930.03kN, 8.97MN and 8.94MN separately, the standard deviations are 390.80kN, 86.67kN (22.2%) and 37.57kN (9.6%). However the torque shows negative values which indicates that the directions of torque have reversed, in reality this means the turbine will be stalled due to displacement being so large, as Figure 5.15 shows, that the velocities on blade elements changed. This phenomenon will be discussed in detail in Section 5.15.

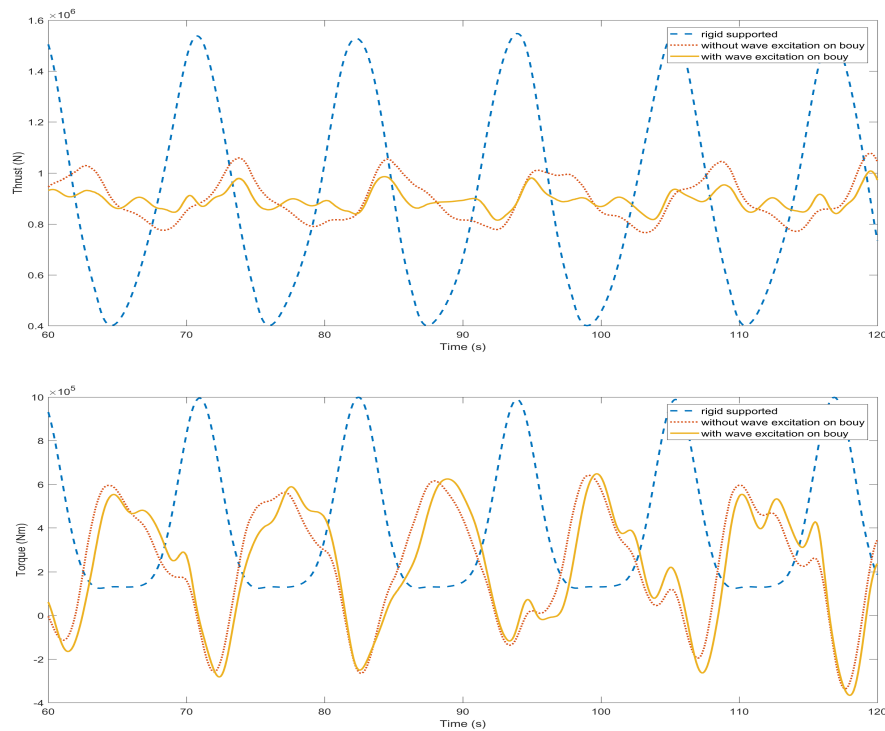


Figure 5.13: Thrust and torque for Case 1 in harsh winter

In sea state 6, the performance of the system is different from all the sea states above, the peak loading of thrust as a result of wave excitation on buoy becomes larger than the rigid supported turbine. The mean values of thrust are 1.045MN, 1.044MN and 1.040MN for rigid supported

turbine, mooring turbine without and with wave excitation on buoy. The standard deviations are 5.82kN, 6.28kN and 13.43kN separately. The average torque values are 396.44kN·m, 394.84kN·m and 390.25kN·m and the standard deviations are 169.08kN·m, 20.73kN·m and 35.48kN·m. More investigations has been undertaken for the system in this sea state, the result will be given in Section 5.2

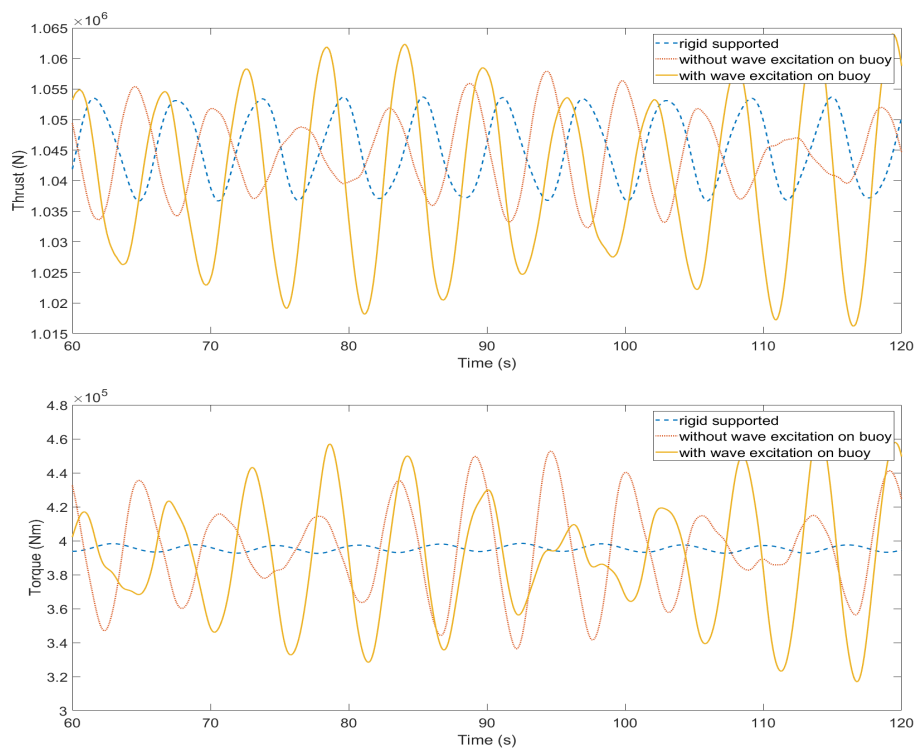


Figure 5.14: Thrust and torque for Case 1 in sea state 6

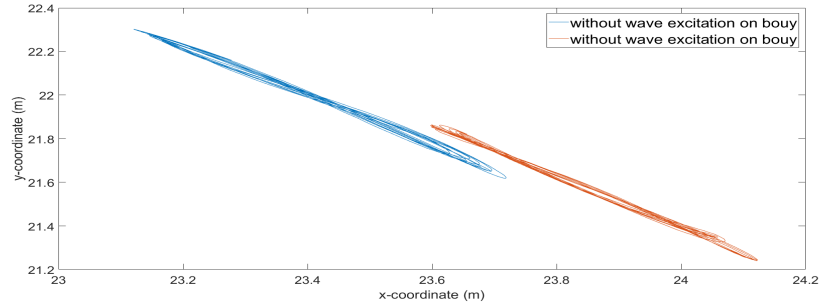
Figure 5.15 gives trajectories for buoys and turbines in some sea states. The system is dragged to a deeper position due to the forces in the horizontal direction increasing under wave excitation. As mentioned above, the motions of buoy and turbine are smooth in sea state 4 which makes the peak loading reduction remarkable. However, the system shows large

displacements in harsh winter and generates high values of inertia velocities .

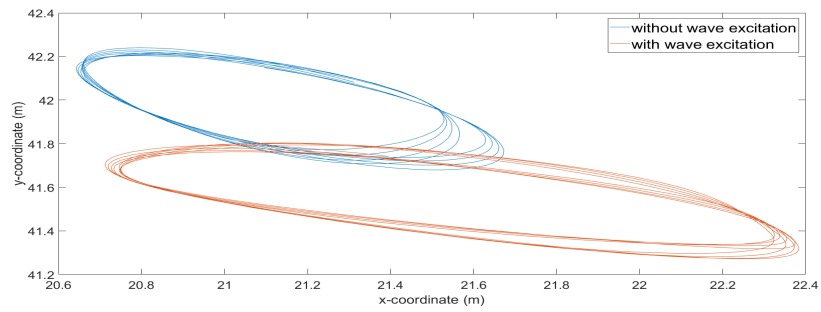
5.2.4 Random waves

Results from sea state 4, 5 and 8 are given in Figure 5.16, Figure 5.17 and Figure 5.18, a 1 minutes simulation windows of comparisons between the total thrust and torque on mooring supported turbine (blue solid line) with that on rigid supported turbine (red dot line) under irregular waves during operation are shown in the result. It is obvious that the mooring supported turbine shows a favorable performance in the reduction of peak thrust on the turbine.

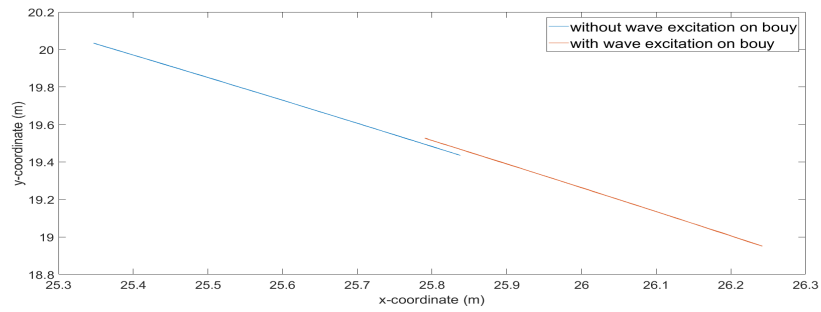
In sea state 4, the standard deviation of the thrust on mooring supported turbine are 13.26kN and 11.87kN for without and with wave excitation on buoy which are 33.52% and 30.01% of that on a rigid one's value of 39.57kN. The peak torque on the turbine reduced as commendable in this sea state, the standard deviation are 13.22kN·m and 9.80kN·m for the mooring without and with wave excitation on the buoy, the standard deviation for a rigid one is 54.98kN·m.



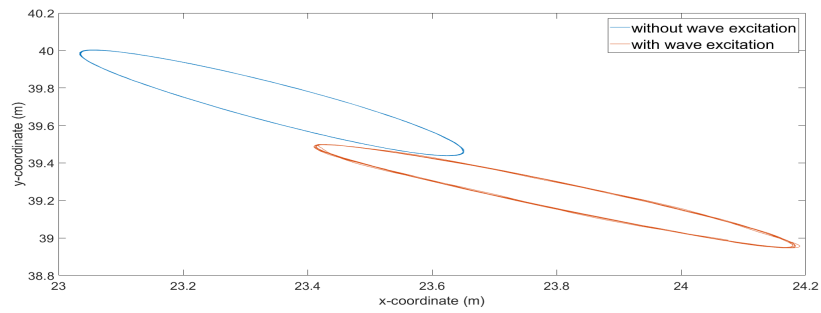
(a) turbine



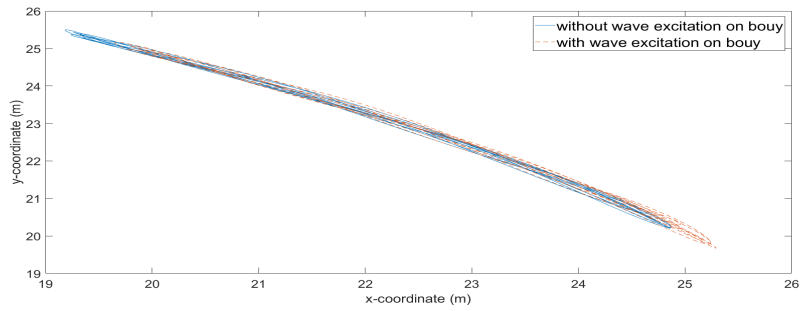
(b) buoy



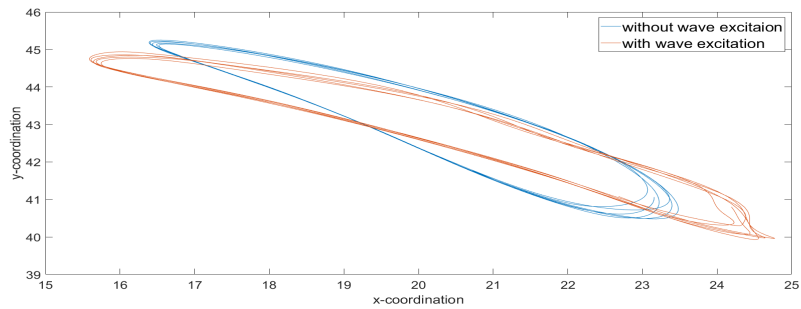
(c) turbine



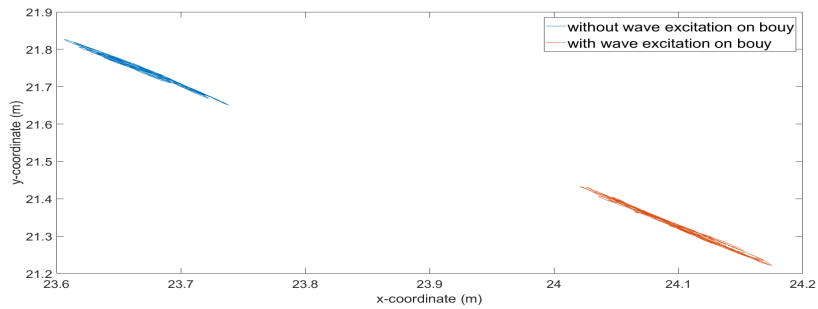
(d) buoy



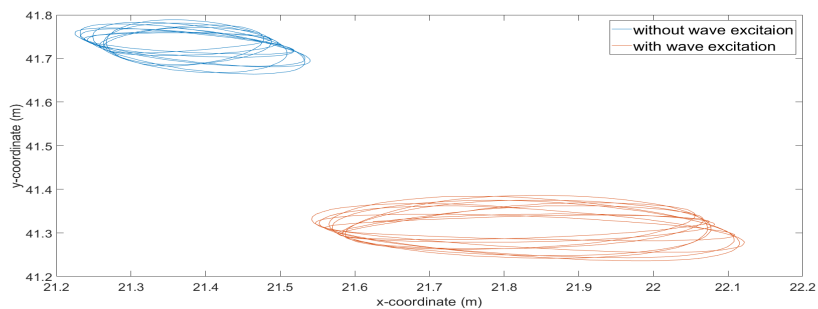
(e) turbine



(f) buoy



(g) turbine



(h) buoy

Figure 5.15: Trajectories for different sea states. (a)(b) are the turbine and buoy trajectories in sea state 3, (c)(d) are the turbine and buoy trajectories in sea state 4, (e)(f) are the turbine and buoy trajectories in harsh winter, (g)(h) are the turbine and bouy trajectories in sea state 6

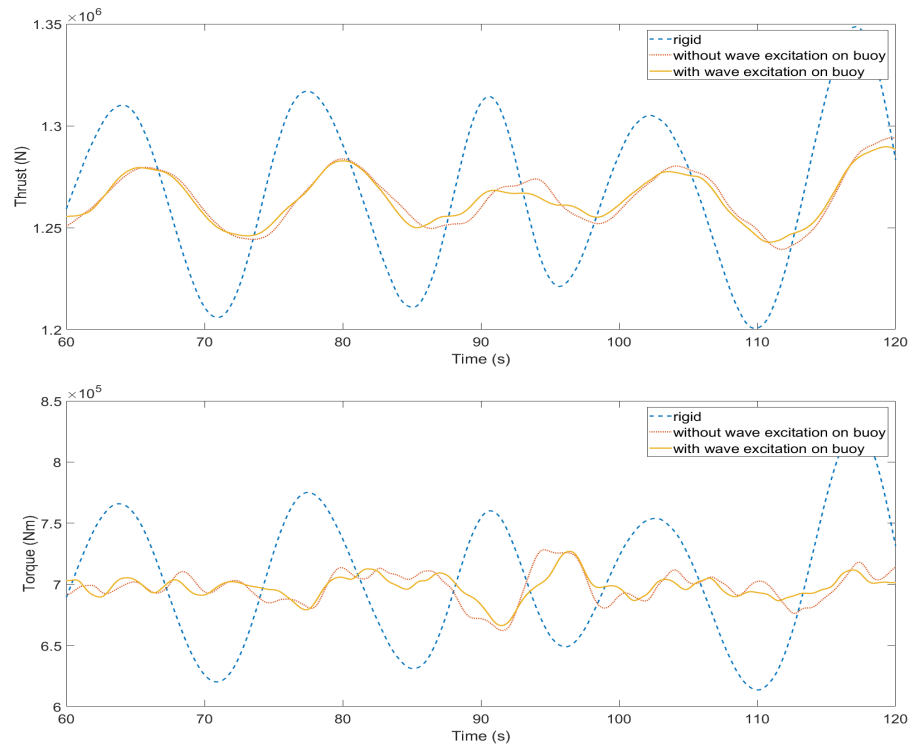


Figure 5.16: Random waves generated from significant wave height 1.07m and mean wave period 11.07s, current speed is 2.5m/s

In sea state 5, the standard deviation of the thrust on mooring supported turbines are 7.60kN and 9.87kN for without and with wave excitation on the buoy, which are 18.56% and 24.11% of that on a rigid one's value of 40.92kN. However, the peak torque on the turbine is not reduced as commendable as thrust but is better than the regular waves, the standard deviations are 50.16kN·m and 42.12kN·m for the mooring one without and with wave excitation on buoy, while standard deviation for a rigid one is 40.97kN·m

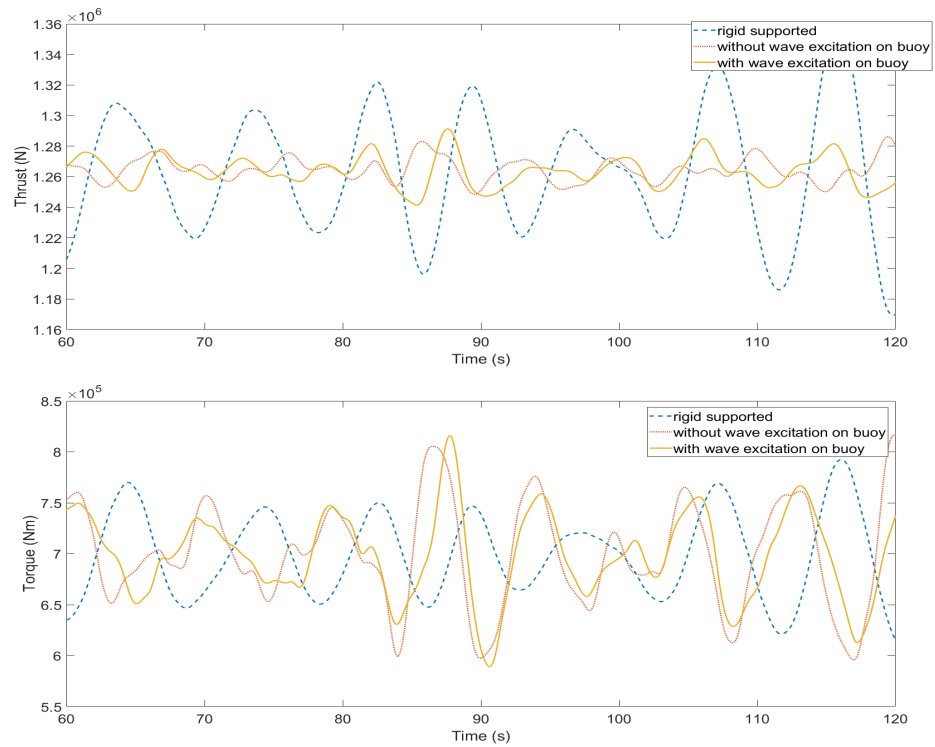


Figure 5.17: Random waves generated from significant wave height 2.665m and mean wave period 6.135s, current speed is 2.5m/s

In sea state 8, the standard deviation of the thrust on a mooring supported turbine is 3.27kN and 4.88kN for without and with wave excitation on buoy which is 38.70% and 57.79% of that of a rigid one's value 8.46kN. The peak torque on the turbine is not reduced as well as the regular waves in this sea state, while the standard deviation is 18.04kN·m and 15.33kN·m for the mooring one without and with wave excitation on the buoy, standard deviation for a rigid one is 6.88kN·m

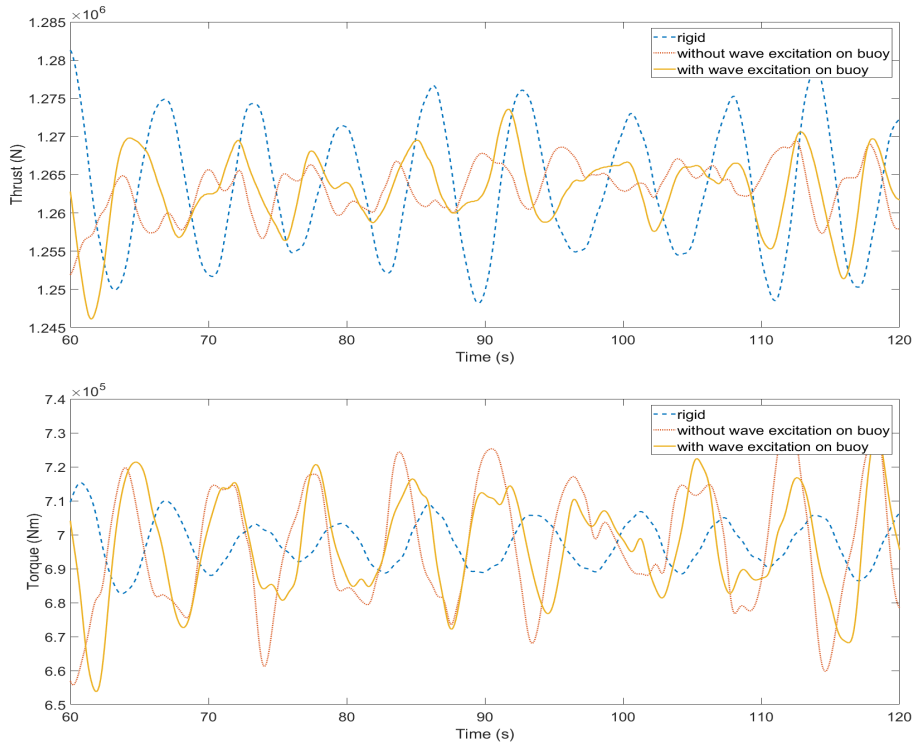


Figure 5.18: Random waves generated from significant wave height 1.008m and mean wave period 4.653s, current speed is 2.5m/s

5.2.5 Blade section velocities

A case that the turbine generate negative torque in harsh winter was described in the previous section, the reason is that the large displacement of turbine in harsh winter makes the inflow velocity vectors on the blade sections change in direction, as Figure 5.19 shows.

The turbine moves along the wave in the wave trough, the inertial velocity of turbine U_T is coupled with the wave-current velocity field and transferred to the local rotating blade coordinate system [32], the two velocities, $U1$ and $U1y$, are obtained to modify the horizontal inflow and the

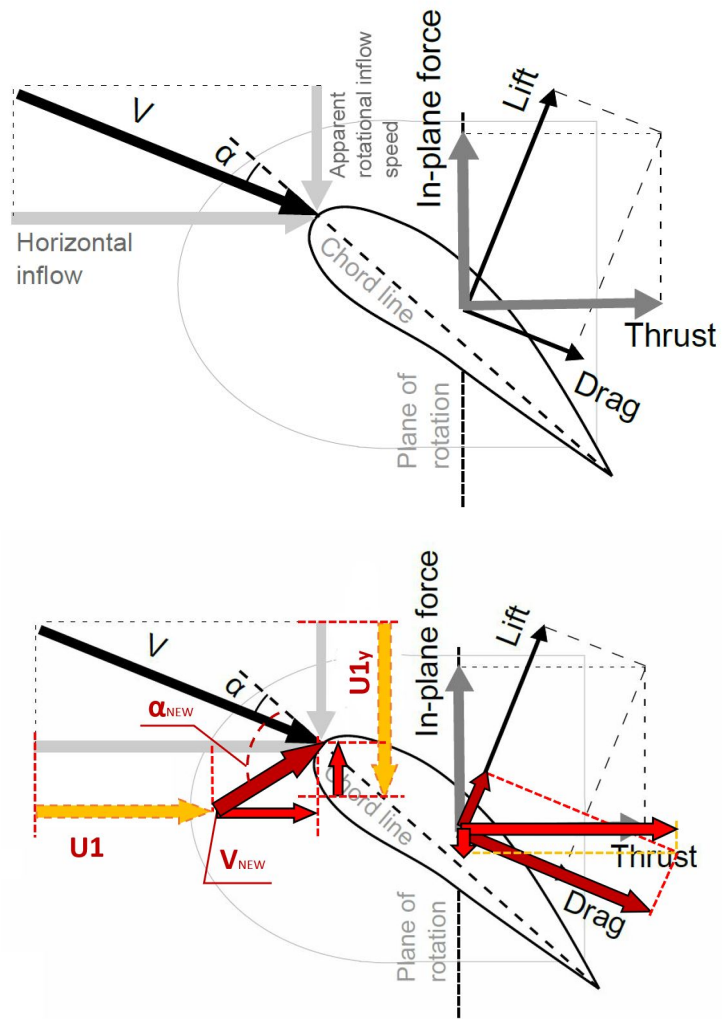
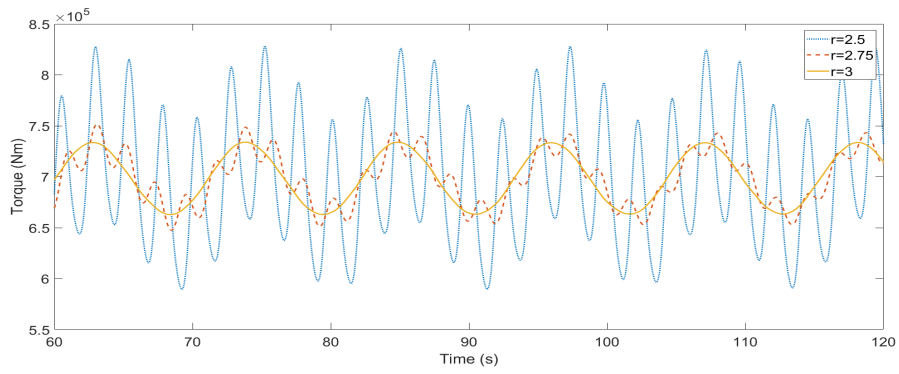
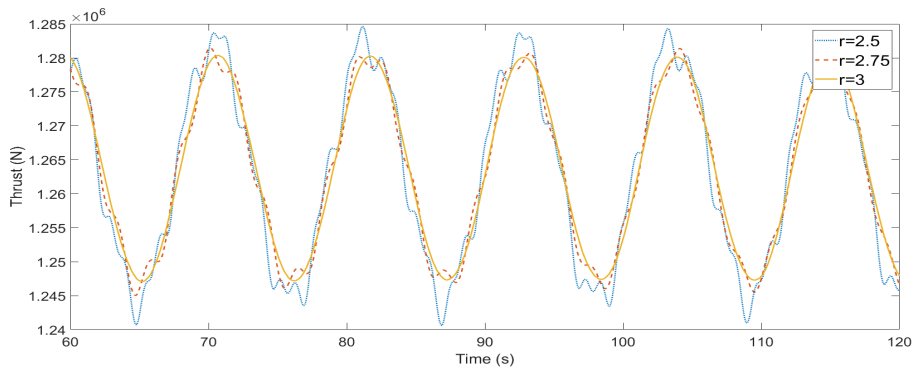


Figure 5.19: The inflow velocity vectors on blade sections in harsh winter

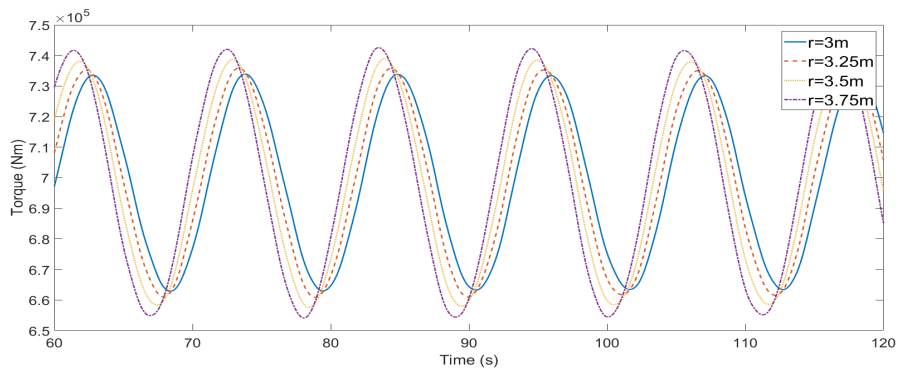
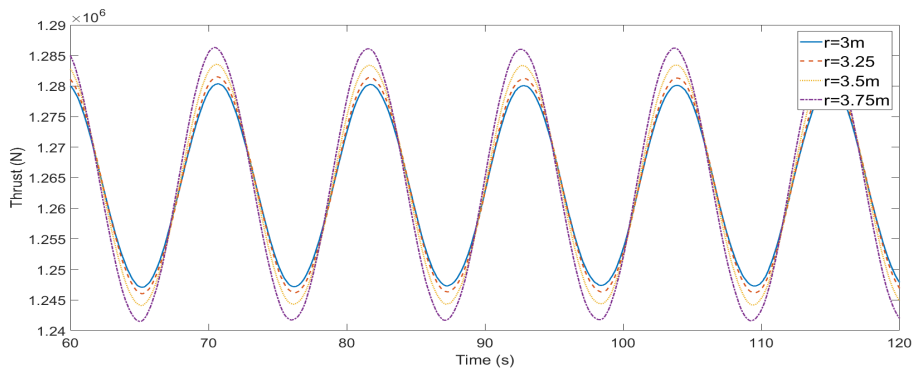
apparent rotational inflow speed in order to calculate the relative velocity for the blade section. The new relative velocity will result in a larger angle of attack which generates a smaller lift force but a larger drag force on the blade section. Therefore the in-plane force is change to another direction, which means the torque on the rotor is turned into negative values and the blade stalled. The blade profile that performs better than a NRELs814 in larger angles of attack or setting a pitch angle to the be applied to avoid this phenomenon , but this remains to be investigated in the future.

5.2.6 Buoy Effect

The other external forces are the buoyancy and drag force which are depend on the volume and shape of the buoy, in this report the shape is a sphere. Figure 5.20 shows the comparison of thrust and torque on the turbine with 6 different buoy radius in sea state 2. The result indicates that high buoyancy may not mean a satisfactory performance in load reduction especially the torque on the turbine may increase at high buoyancy condition, because the system will become over tension and approach a rigid supported turbine, the loading on the turbine tends to increase.



(a)



(b)

Figure 5.20: Case 1, regular waves generated from sea-state 3, (a) gives the buoy radius smaller than 3m, (b) gives the buoy radius larger than 3m

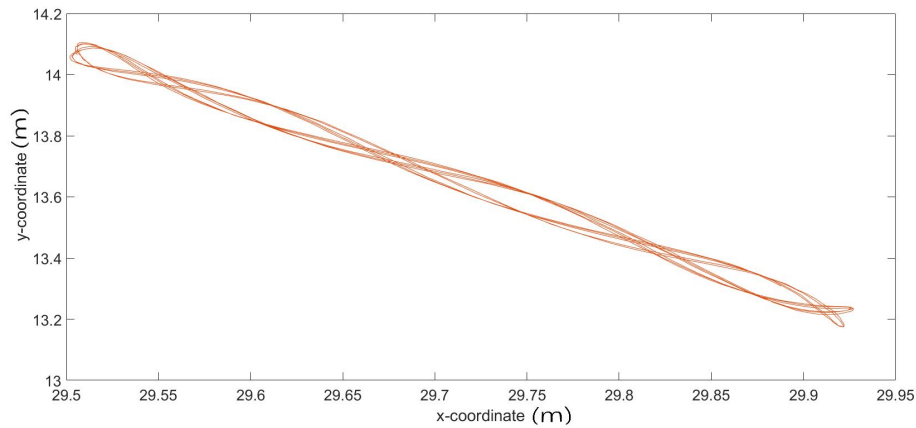


Figure 5.21: Trajectories of turbine hinge node for buoy radius 2.5m

In addition, the low buoyancy can be accepted in the reduction of peak loads for thrust, because lower buoyancy will make θ_1 increase which means the turbine will move closer to seabed and the wave effect is abating. But the low buoyancy makes the torque start to oscillate, which is unacceptable. Figure 5.21 shows the trajectory for the turbine with a 2.5m radius buoy, the motion is not as stable as that in 5.15(c) and it reveals a periodicity in the curve which may generate the oscillates in torque. Moreover, the lowest vertical coordinate of the hinge node is less than 13.2m and the radius of turbine is 10m, the distance from seabed to the blade is less than 3.2m, this case should be considered during designing the system to avoid the blade hitting the seabed. Overall, the buoy design is a important stage for the tension mooring supported turbine, buoyancy close to the total thrust on the turbine is the best choice.

5.2.7 Morrison effects

According to the results above, the variation of torque values on tension mooring supported turbine is larger than that of rigid supported ones in similar sea states. The reason is added mass effects on blade sections, the inertia force which added into the in-plane force to calculate the torque is as Equation 4.38, the relative velocity term for a rigid supported turbine is the wave particle velocity in the vertical direction transferred to the local rotating blade coordinate system. However the inertia velocity of the turbine itself is considered to be coupled with the wave particle velocity to obtain the final relative velocity of the inertia force for the mooring supported turbine, this results in an increase of inertia forces on blade sections in the mooring supported turbine, then the total torques increases as the in-plane forces rise. Moreover the way calculated the inertia force on blade section for rigid supported turbine is not applicable for a turbine which can move in the water as a tension mooring supported turbine does, therefore further investigation should be done in the added mass effects to the mooring supported turbine blade.

Figure 5.22 gives the torque on the mooring supported turbine without Morrison effects in sea state 3, the torque reduces as expect. This indicates that the Morrison effect which is the added mass on the blade plays a significant role in torque on a turbine which can move in a vertical direction. Moreover, the Morrison effect module in BEMT could be improved in future.

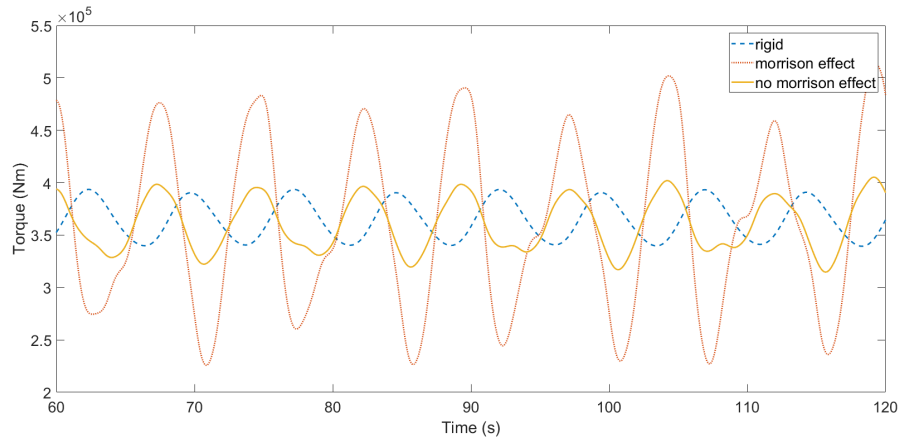


Figure 5.22: Morrison effects in torque

5.3 Discussions in the System Parameters

In the last section, the buoyancy force is set to be approximately to equal the thrust load on the rotor in order to give a best performance in load reduction. However, when the turbine has a large diameter as Case 1, the size of buoy will be large as well. This sometimes makes the installation of the system difficult due to a huge force required to submerge the buoy down into its location in the water column.

The conditions that loads on the turbine increases in sea state 6 show wave packets both with and without wave excitation on the buoy. The velocity of turbine can be considered as the phase velocity moving in same propagation direction with the phase velocity of the wave-current at troughs but in opposite direction at peaks (defined as relative velocity modification for blade inflow velocity calculation), then the oscillation of the turbine and the oscillation of buoy envelopes and results in a pattern in the loading result.

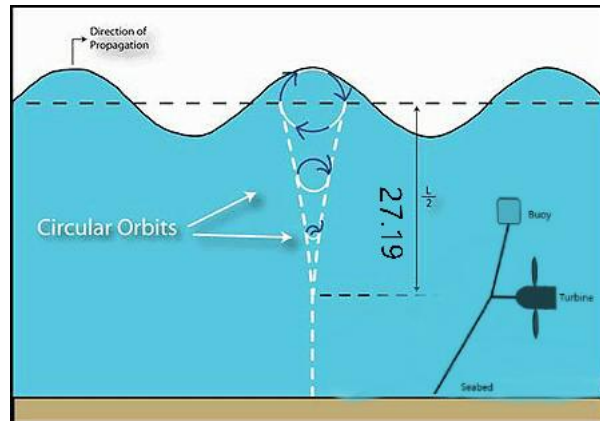


Figure 5.23: Water particle paths under waves in deep water and the turbine position

For sea state 6, the wave length is 54.38m, the water particle path reaches 27.19m from the water surface and the turbine hub is at the height of around 21m from seabed, as shown in Figure 5.23. It revealed that the wave only affected half of the rotor but excited the buoy significantly as shown in Figure 5.15(h) so that the beat pattern in the result with wave excitation on buoy is more obvious in Figure 5.14. Furthermore, the loading reduction for mooring supported turbine does not show advantages in competition of rigid supported because of the wave only reaching half of the turbine and the oscillation envelopes.

In order to improve the permanence of mooring supported turbines in conditions as sea state 6, a variable length of the mooring line, buoy diameter and turbine diameter are investigated in this section to indicate a sensitive analysis for the system. This work will establish relationships of different devices based on the same concepts.

5.3.1 Mooring line length

The wave effects on a buoy has a remarkable increase on system loading due to the short wave period. In this part the length of mooring line for L2 is reduced in order to move the buoy away from the water surface and deeper in the water column since the wave excitation will decrease

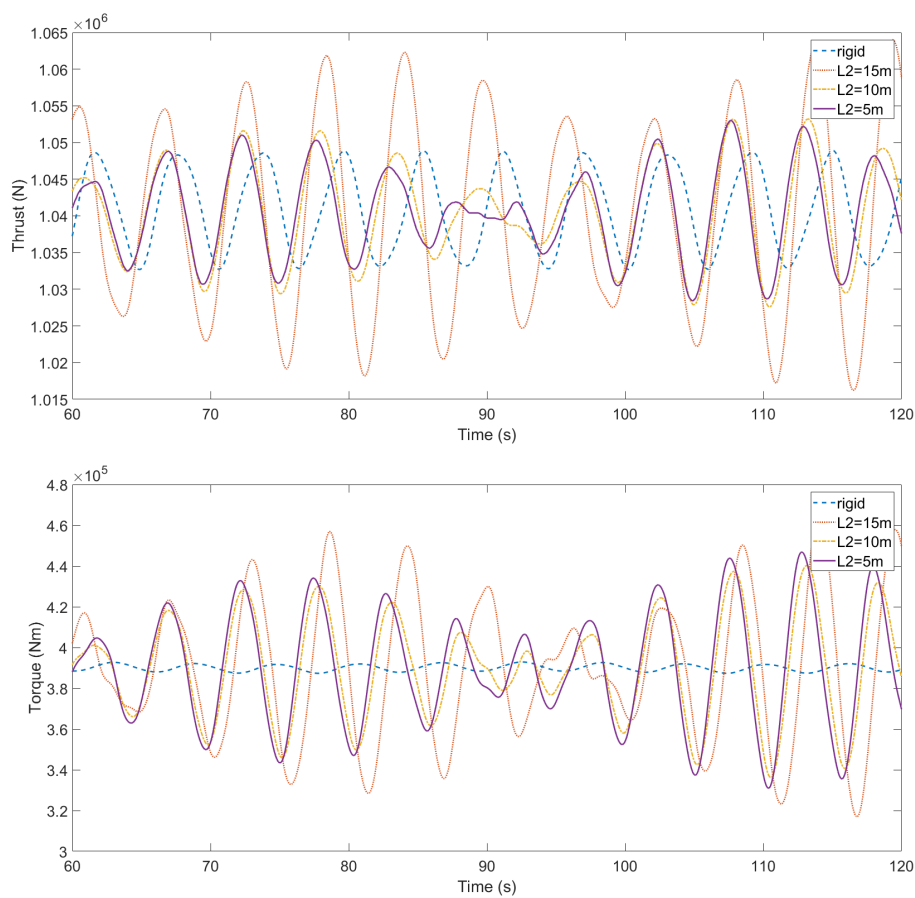


Figure 5.24: Thrust and torque on turbines for different second mooring line length in sea state 6

Figure 5.25 shows that the decrease of the L2 length gives a positive effect to the reduction of thrust on the turbine, the thrust becomes smaller than

the rigid supported turbine when L2 reduces to 5m, but the reduction for the torque on the turbine does not show a favorable performance.

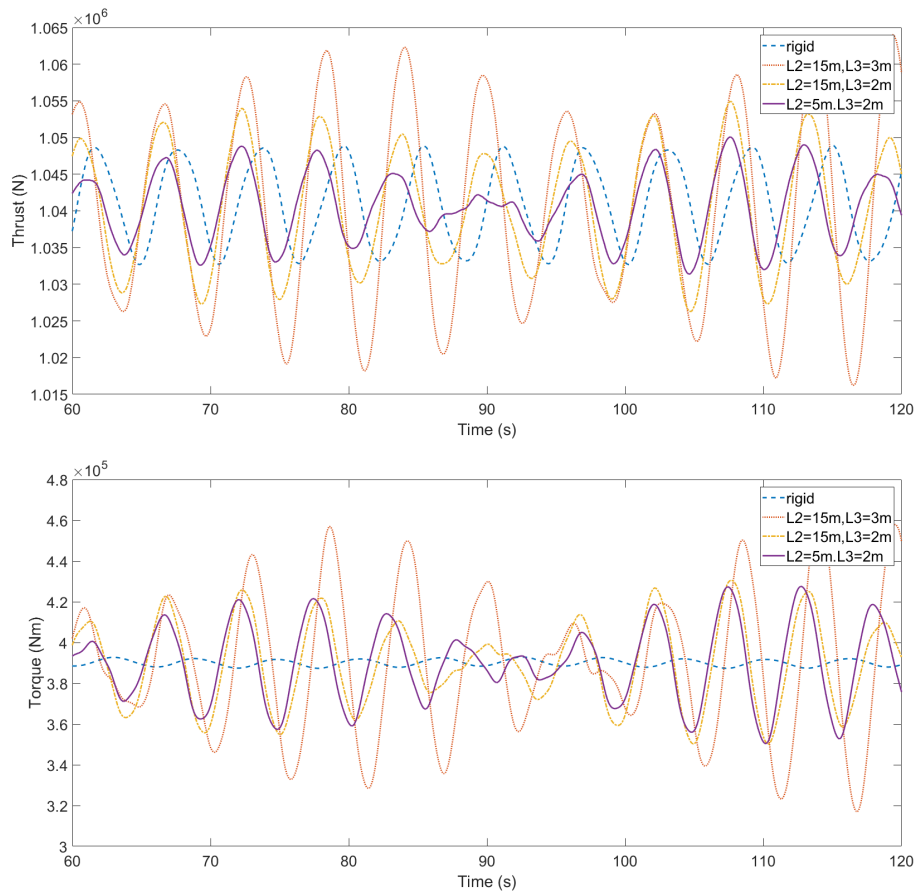


Figure 5.25: Thrust and torque on turbines for different third mooring line length in sea state 6

The decrease from 3m to 2m of the mooring line for L3 length shows a satisfactory performance in thrust reduction on turbine in sea state 6, it is showed that in a sea state with a low wave period (high frequency) in deep water, it is supposed to compact the system so that the oscillations of the system can be reduced. However, it should keep a safe distance between the turbine, buoy and mooring line L2 to avoid any risk of collision

between them. Besides, the inflow velocity will be effected by the buoy in front of the turbine and there may be an interaction between the buoy and turbine. Therefore the BEMT code could be modified to recalculate these inflow parameters, which is not considered in this report. In order to avoid the complicated interaction, it is supposed to make the buoy is sufficiently located above the turbine.

5.3.2 Smaller turbines

In this part, smaller turbines are applied to the system to reduce the thrust on the turbine and make the mooring line L1 longer, therefore the turbine will rise to a higher position where the wave affects the whole turbine. The second turbine is a Voith's 1MW horizontal axis turbine HyTide 1000 which diameter is 13 meters [?], the rotor is set to be the same TSR as Case 1 which is 5. At this case, the height of the turbine hub is around 27.6m from the seabed where the wave effect approximately reaches the whole turbine.

case 4: segment length = 0.5m $m_{\text{buoy}} = 3.5\text{t}$ $m_{\text{turbine}} = 200\text{t}$ $l_1 = 36\text{m}$ $l_2 = 10\text{m}$ $l_3 = 2\text{m}$ turbine diameter = 13m buoy radius = 2.4m $\Omega_r = 1.92\text{rad/s}$
NRELS814 Dyneema

The result shows that in sea state 3 the thrust loading increases compared with the rigid supported turbine as Figure 5.26, this is in contrast with the other cases. The reason is that the kinetic energy of the system increases when calculating the Lagrangian of the stem since the mass of the turbine is 2.5 times of the previous turbine in Case 1. In fact it

is not practical to set a turbine weighed 200t to be self buoyant, hence the turbine is modified to be 80t as the one in Case 1, the other parameters are kept the same. It is showed that the peak thrust loading on the turbine reduces as expected at 80t turbine, the standard deviation is slightly reduced from $5.1819 \times 10^3\text{N}$ of rigid to $4.8245 \times 10^3\text{N}$ of mooring, however standard deviation for the 200t turbine is $5.3285 \times 10^3\text{N}$. On the other hand the torque on the turbine is still larger than the rigid one as a result of Morrison effect descried in 5.1.6. This reveals that the self buoyant turbine attached to this tension mooring system should not have a large mass in order to make the turbine self buoyant accessibly, which requires a redesign of the gear box and shaft to reduce the weight as well as the power output.

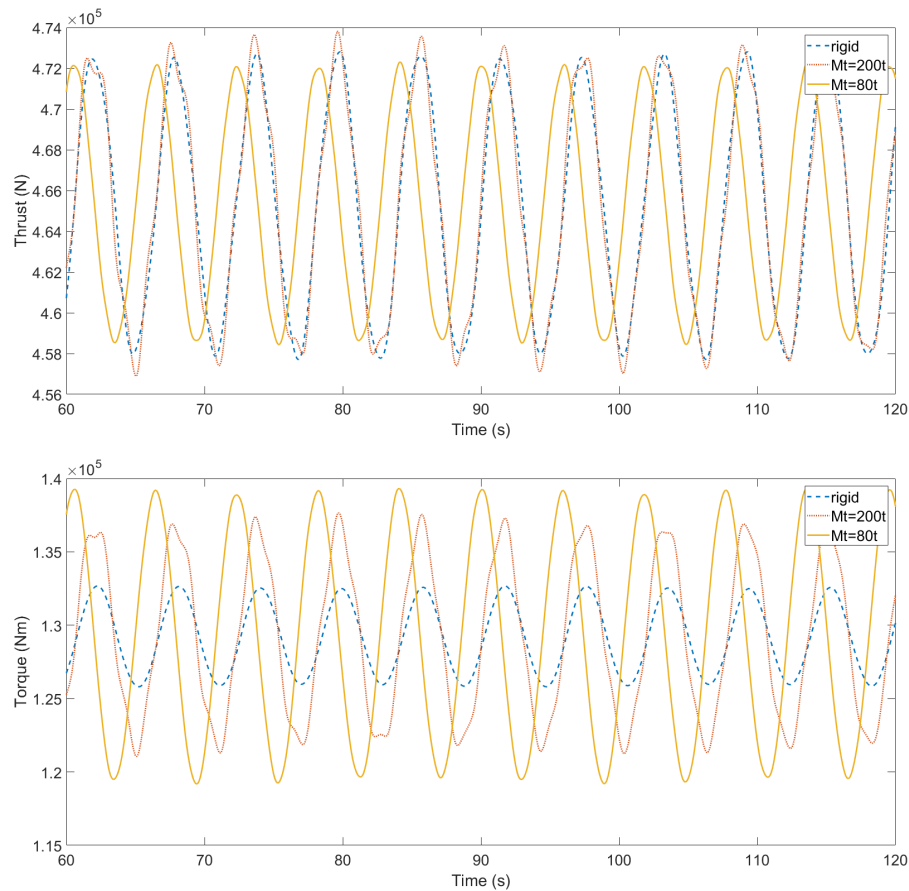


Figure 5.26: Loading on HyTide 1000 in sea state 3 at TSR 5 for different turbine weights

5.4 Summary

Within this chapter, the thrust loading reduction in most sea states are favorable especially in swell waves, but the reduction of torque on the rotor is not as satisfactory as the thrust due to the turbine vertical velocities. System parameters such as buoy radius, mooring line materials and mooring line length are investigated to obtain better understanding of the system. It is shown that the buoyancy forces should be approxi-

mately equal to the thrust to give a most satisfactory loading reduction and the mooring line parameters have a significant influence in the system stability. Moreover, two phenomenon are found, one is the negative torque caused by the blade stalling in extreme sea states, the other is that the system is not well suited to sea states the the wave particle paths can not approach the seabed.

Chapter 6

Summary and conclusion

Although there exists an increasingly substantial literature on the topic of TST hydrodynamic loading, there is limited information on a floating turbines operating in various inflow and geometrical parameters in regards to the loading in a general sense. It is hard to relate the different findings from different sources as the investigations of the parameters' influencing on the loads tend to be highly case-specific. Therefore the aim of this thesis is to establish a method to model the tensioned mooring TSTs and develop an understanding of it, where the parameter's influences were evaluated over the whole input domain, making the interpretation of the results valid for a large range of cases. Relating to the importance of understanding the relationships between a floating turbine's operating conditions and the experienced peak loads and fatigue life, the accuracy and applicability of the numerical models used to simulate these phenomena becomes key to insuring that the devices are suitably designed to withstand the expected load conditions.

This chapter presents a synthesis of the various results presented in the individual chapter, an overview of the findings from the numerical models are given in the first section. The second section gives the implications of the research findings which can improve the tension mooring supported turbine performance. The last section gives the limitation of this research and suggestions for the future studies.

6.1 Research findings and original contributions

The original contributions of the rigid supported turbine are summarized as:

- A fast simulation code combined with BEMT has been developed to model the monopile support structures for TST applications and analyses their dynamics including the added mass and hydrodynamic damping effects.
- A passive structure control technique was employed in rigid supported turbine, which used a TMD on the structure to do a fully coupled dynamic analysis in time domain. Variations in mass of the TMD in fore-aft direction was undertaken in order to compare the effects on the structure, when a TMD_x was implemented in the system, it had significant effects on the resonance reduction and fore-aft fatigue load-reduction under instant load fluctuations. How-

ever, TMD had an insignificant effect when modest unsteady wave-current coupled forces were applied on the structure for a long operating period. But changing the shape of tower-monopile supporting structure will improve the performance in a fatigue analysis.

- Unlike most large offshore wind turbines, the tidal turbine tower-monopile systems investigated in this project showed higher first natural frequencies due to the shorter length. Furthermore, the added mass correction will make natural frequencies of the structure slightly reduced.

The original contributions of the tension mooring supported turbine are summarized as:

- A methodology has been developed to model a full submerged tension mooring support system with a self buoyant turbine, the dynamics of the system and the loading on the turbine in various sea states can be simulated rapidly.
- Based on the results, the thrust comparison reveals that forces on mooring supported turbine blades are smaller and smoother than those on the rigid supported one in most sea states, especially for the swell waves and random waves. This means the fatigue performance of mooring supported turbine will be better for the blade loading. However torque on the turbine increases due to the Morrison effect under Stokes waves, which requires an improvement in the Morrison effect module.

- The tension mooring supported turbine under the influence from stokes wave with short wave length does not perform as good as that in longer wave length whose wave particle path can reach the seabed. Because the wave particle paths of long wave-length waves can reaches a deeper depth and affects the turbine efficiently. But the wave particle paths of some short wave-length waves can not reach the depth where the turbine is and only excite the buoy.
- In stokes waves, the wave excitation on a buoy will increase the loading in the system. Motions of the buoy and turbine will interact thus the waveform of the thrust and torque is different form that of a rigid mooring.
- The large displacements of the turbine due to the extreme waves in harsh winter results in negative torques, which may be harmful to the drive train and generators and must be avoided.
- The turbine will slightly move along a short section of an arc during operation if the buoyancy is suitable, which is an ideal operation environment. The buoy is a very important factor, when the buoyancy force which is reflected as the buoy radius is higher than a specific proportion of thrust, the ratio of which can be researched in the further research, and the motion of turbine will not be stable and will oscillate around an equilibrium position. Moreover, the mooring line length and the mooring material plays a significant role in system stability, where the system is suppose to be compact.

6.2 Theoretical implications of the research finding

The dynamic marine climate causes large load fluctuations on TSTs, this thesis found that the tension mooring supported system has a positive effect to the thrust load reduction in most sea states. Although the torque fluctuations can be a problem requiring further investigations, the system performance is satisfactory in swell waves which have a long wave length, both thrust and torque fluctuations decrease in favorable values. The tension mooring supported TSTs are applicable to the swell environment or stokes waves with long wave length, thus installing this system will improve fatigue performance, compared with rigid supported TSTs.

In extreme condition such as harsh winter storm, the tension mooring supported TSTs also reduces the thrust loading significantly but the turbine should be shut down and protected from potential blade in order to avoid negative torque actions. Furthermore, this stall phenomenon can also be investigated by improving the blade design and adding a high angle of attack pitch angle to the blade so that the turbine is able to work in the extreme condition with a favorable loading reduction.

In stokes waves that have short wave lengths such as sea state 6 in the previous sections, the tension mooring supported TST should operate at the position where the wave particle paths can reach the whole turbine. This requires the diameter of turbine not to be too large and the buoy is required need to supply a larger buoyancy when compared with the

thrust loading on the turbine, thus the turbine can operate in an appropriate location in water column. However, the load reduction in this condition is still not as satisfactory as the other sea states, it verges on the performance of a rigid supported turbine. Therefore, the tension mooring supported system should be designed for application in the environment where half of the most common wave length is larger than the water depth to give a satisfactory loading reduction in thrust.

The rotor speed is fixed in this research, which is not reliable for a turbine moving in waves. The rotor speed should be reduced when the turbine moves against the wave and increased when the turbine moves with the wave in order to give a constant TSR to the rotor during operation in wave-current interaction. The variable TSR will enlarge torques on the shaft, this may be the underlying reason why results of torques in some sea states shows different trend to thrust in this thesis.

The code itself is a very efficient providing a fast simulation process, a 3 minutes simulation of 0.1s time step for 20 elements per blade and 0.5m mooring line element length on a personal computer with 4 i7 cores takes around 1 hour. The outputs contain various data such as blade elements inflow conditions, forces on each element and so on, the status of turbine can be checked for every time step and a simple animation can be generated for motions of turbine. This is an efficient methodology for a highly dynamic system like a tension mooring supported turbine and other taut mooring systems to check its performance in different environmental conditions.

Chapter 7

Future works

The vertical velocity component of the wave motion had a large influence on the rotor out-of-plane bending moment of a turbine [32]. Furthermore, the tension mooring supported turbine itself has a vertical velocity because it can move in vertical direction, thus the out-of-plane bending moment may be greater than a rigid supported turbine. Furthermore, the torque on the rotor is also affected by the vertical velocity of turbine itself due to the Morrison effect. It is obvious that the vertical motion of turbine is a significant impact to the design of TST's drive train or internal components, therefore investigations of the turbine's vertical velocity influence on the rotor out-of-plane bending moment should be further investigated in the future. On the other hand, future modifications to the original Morrison effects may not be applicable to the blade elements on a turbine which can move in vertical direction, therefore Morrison effects modification should be improved in the future. In extreme sea state such as harsh winter storm, greater blade profiles and pitch angles should be

investigated in order to avoid the negative torque. Adjustable rotor speed will be a main research target in the future and should be applied to the model in order to give a reliable torque result.

During turbine operations, the movement of the turbine may cause rotational motions as pitch, this will have an influence on the inflow condition of each blade element. However the pitch effect is not taken into consideration in this thesis. In order to calculate the pitch angle of the turbine, the model should be extended to four pendulums and no finite elements on the fourth pendulum which represented the turbine. The mass of the turbine is considered as a lumped mass at the two nodes of the fourth pendulum and the thrust and torque is applied on the first node, the matrix of the system is required to modify this to be suitable for a new system. Furthermore, the added mass effects of the turbine could be applied to both nodes instead of one node as the recent model, the added mass effect of turbine may have a large influence on pitch. When the pitch angle of the turbine at this time step is obtained, it can be set to the blades as description in Section 4.1.3 as a initial condition for the next time step.

The damping of the system is a difficult factor to define especially for the water viscous damping, the method descried in Section 3.4 in this thesis works well for rigid supported turbine and the tension mooring supported turbine without consideration to excessive wave excitation on the buoy. However, in some conditions the calculation was not converged as Figure 5.4 and 5.6 when the wave excitation on the buoy is considered, the damping coefficient of the system had to be investigated and enlarged to make the system stop vibrating. It indicates that the wave excitation

may have an influence on the system natural frequency related to the damping calculation. The damping of the system is a factor remained for further research in future.

Appendix A

TURBINE MOTION ANIMATION

This appendix shows the pictures from the simulation animations in some sea states as supplementary of Figure 5.15. The turbine and the buoy are represent as nodes in the animation in order to simplify the complicate turbine sketches.

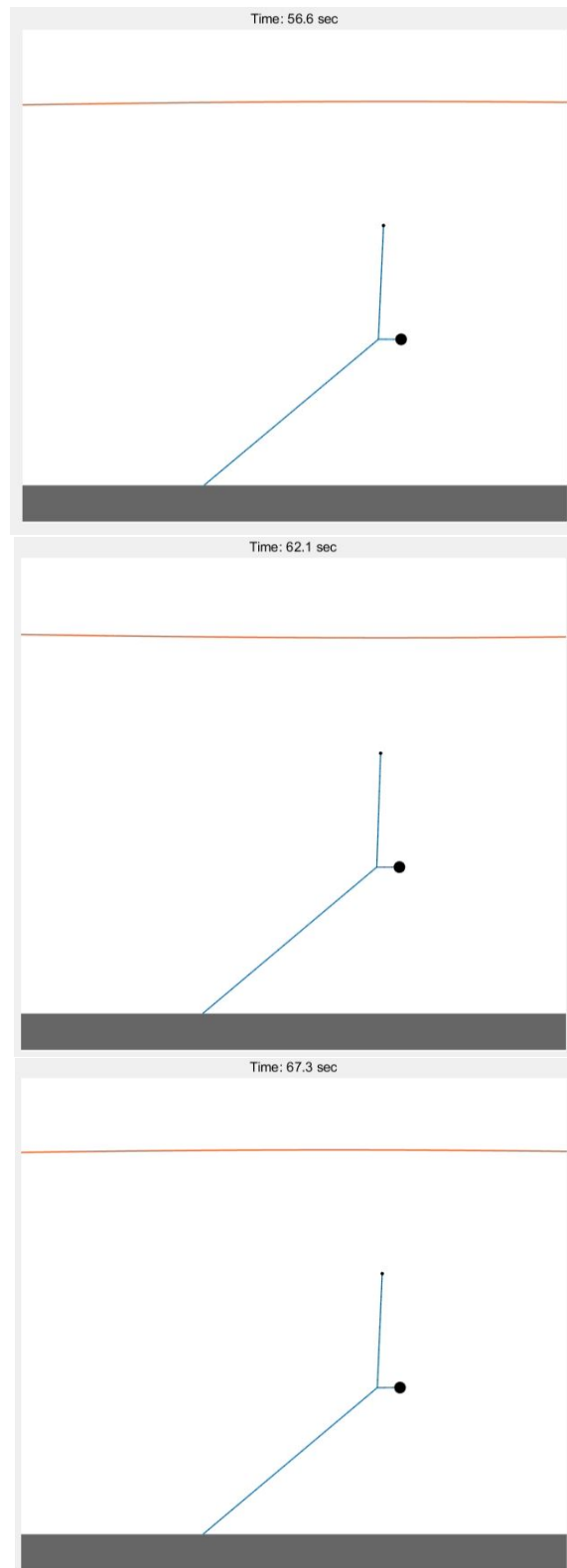


Figure A.1: The animation of simulation for swell waves ($H_s=1.07\text{m}$
 $T_s=11.07\text{s}$)

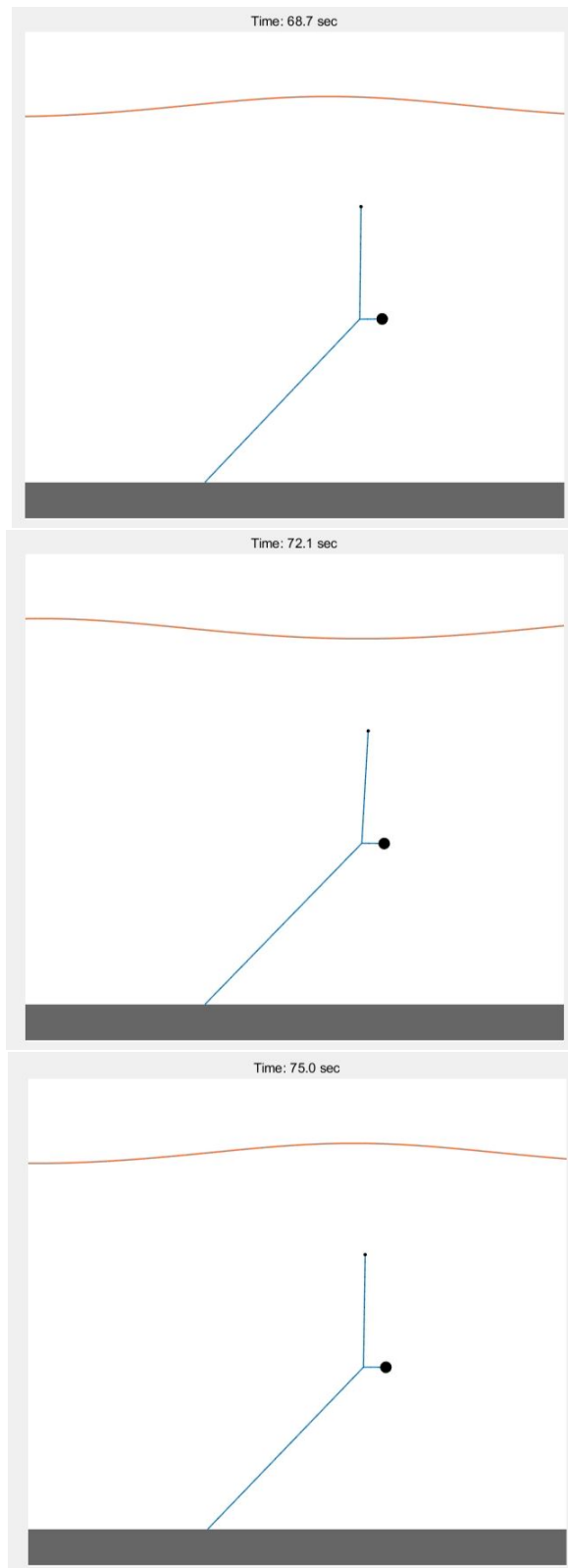


Figure A.2: The animation of simulation for seastate 3 ($H_s=2.665\text{m}$
 $T_s=6.135\text{s}$)

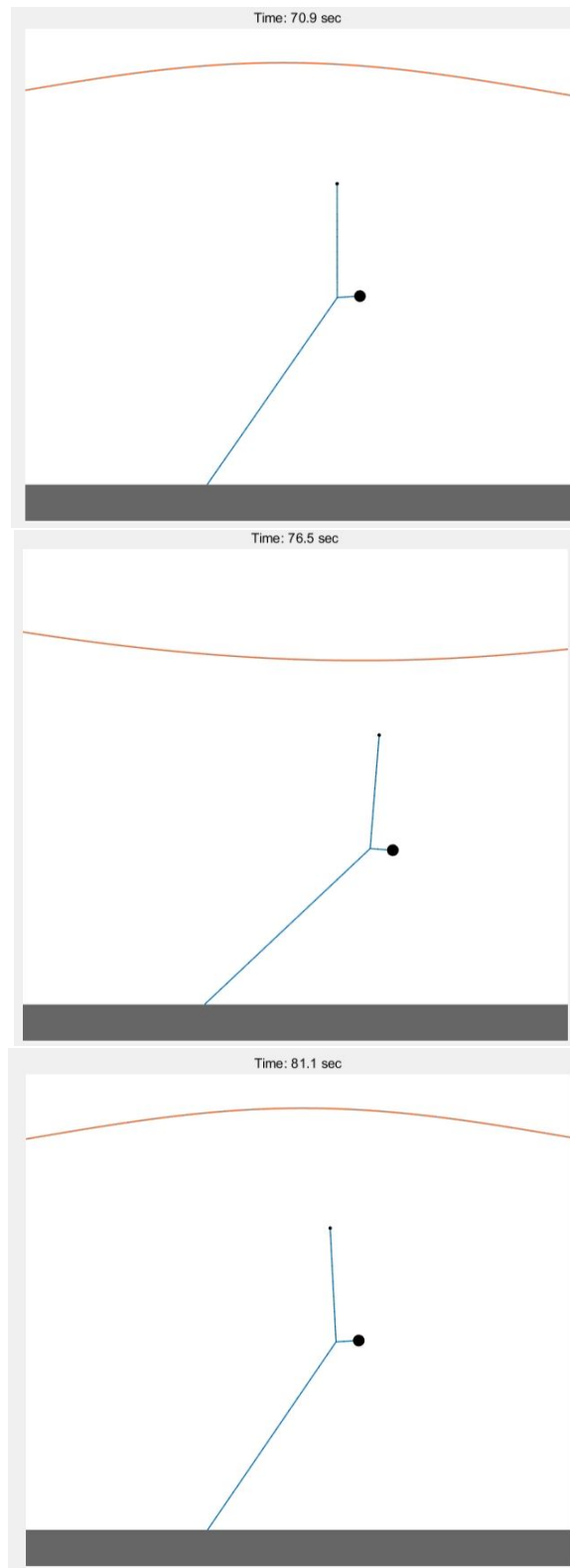


Figure A.3: The animation of simulation for harsh winter seastate ($H_s=10.12\text{m}$ $T_s=10.06\text{s}$)

Appendix B

DESIGN STANDARDS FOR USE IN TIDAL ENERGY SYSTEM

In the study presented, two standards have been consulted in order to calculate TST hydrodynamic loading. Brief descriptions of the standards used are as follows:

DNV-RP-C205[60]: This new Recommended Practice (RP) from Det Norske Veritas (DNV) provides guidance for modeling, analysis and prediction of environmental conditions. It also gives guidance for calculating environmental loads acting on structures generated by waves, currents and winds. The RP is based on state of the art within modeling and analysis of environmental conditions and loads, as well as technical development of recent R&D projects and the design experience from recent and ongoing projects. The basic principles applied in this RP are in agreement with the most recognized rules and reflect industry practice and latest

research.

IEC 62600-2[42]: This technical specification provides the essential design requirements to ensure the engineering integrity of wave, tidal and other water current energy converters, referred to as marine energy converters (MECs), for a specified design life. Provides an appropriate level of protection against damage from all hazards that may lead to failure of the primary structure, defined as the collective system comprising the structural elements, foundation, mooring and anchors, piles, and device buoyancy designed to resist global loads. This document applies to wave, tidal and other water current converters and to structures that are either floating or fixed to the seafloor or shore. This document addresses site-specific conditions, safety factors for critical structures and structural interfaces, external load cases, failure probability and failure consequences for critical structures and structural interfaces, and failsafe design practices.

References

- [1] Natural Environment Research Council. British oceanographic data centre web page. Accessed: 2017-09-15.
- [2] EMEC. Tidal devices. Accessed: 2016-09-30.
- [3] B. Spencer and S. Nagarajaian. State of the art of structural control. *Journal of Structure Engineering*, 129:845–856, 2003.
- [4] T. Soong and B. Spencer. Supplemental energy dissipation: state-of-the-art and state-of-the practice. *Engineering Structures*, 24:243–259, 2002.
- [5] A. Wilmink and J. Hengeveld. Application of tuned liquid column dampers in wind turbines. Technical report, Mecal Applied Mechanics: the Netherlands, 2006.
- [6] Matthew A. Lackner and Mario A. Rotea. Passive structural control of offshore wind turbines. *Wind Energy*, 14:373–388, 2011.
- [7] Xodus Group. Torr head tidal energy array eia. Environment impact assessment, Tidal Ventures, 2015.
- [8] J. V. der Temple. "Turbines Dynamics and Fatigue," in *Offshore Wind Power*, chapter 8. Multi-Science Publishing Company, 2009.
- [9] M. W. Wambsganss, S.S Chen, and J.A. Jendrzejczyk. Added mass and damping of a vibrating rod in confined viscous fluids. *Journal of Applied Mechanics*, 43(2):325–329, 1976.

- [10] T.M. Nevalainen, C.M. Johnstone, and A.D. Grant. An unsteady blade element momentum theory for tidal stream turbines. In *Proceedings of the 11th European Wave and Tidal Energy Conference*, Nantes, 2015.
- [11] Onur Can Yilmaz. The optimization of offshore wind turbine. Master's thesis, University of Massachusetts, Amherst, 2014.
- [12] Don W. Lobitz. A nastran-based computer program for structural dynamic analysis of horizontal axis wind turbines. In *Proceedings of the Horizontal Axis Wind Turbine Technology Workshop*, Cleveland, 1984. Department of Energy and NASA-Lewis.
- [13] K. Subbaraj and M. A. Dokainish. A survey of direct time-integration methods in computational structural dynamic—ii. implicit method. *Computers & Structures*, 32(6):1387–1401, 1989.
- [14] E. L. Van der Hooft, P. Schaak, and T. G. Van Engelen. Wind turbine control algorithms. Task-3 report, DOWEC project-DOWEC-F1W1-EH-03-094/0, 2003.
- [15] Mate Jelavić, Nedjeljko Perić, Petrović, Ivan, Stjepan Car, and Miroslav Mađerčić. Design of a wind turbine pitch controller for loads and fatigue reduction. In *European Wind Energy Conference & Exhibition, EWEC 2007*, 2007.
- [16] Gordon M. Stewart. Load reduction of floating wind turbines using tuned mass dampers. Master's thesis, University of Massachusetts - Amherst, 2012.

- [17] Fahim Sadek, Bifan Mohraz, Andrew W. Taylor, and Riley M. Chung. A method of estimating the parameters of tuned mass dampers for seismic applications. *Earthquake Engineering and Structural Dynamics*, 26:617–635, 1997.
- [18] C Amzallag, JP Gerey, JL Robert, and J Bahuaud. Standardization of the rainflow counting method for fatigue analysis. *International journal of fatigue*, 16(4):287–193, 1994.
- [19] T.M. Nevalainen. *The Effect of Unsteady Sea Conditions on Tidal Stream Turbine loads and durability*. Unpublished phd thesis, University of Strathclyde, 2016.
- [20] TM Nevalainen, CM Johnstone, and AD Grant. A sensitivity analysis on tidal stream turbine loads caused by operational, geometric design and inflow parameters. *International Journal of Marine Energy*, 2016.
- [21] Ralph I Stephens, Ali Fatemi, Robert R Stephens, and Henry O Fuchs. *Metal fatigue in engineering*. John Wiley & Sons, 2000.
- [22] ALSTOM. Alstom’s tidal turbine reaches 1mw in offshore conditions. Accessed: 2016-08-15, 2013.
- [23] British Oceanographic Data Centre. Wave data. Accessed: 2016-09-30.
- [24] Ibrahim Ozkol Elmas Anli. Classical and fractional-order analysis of the free and forced double pendulum. *Engineering*, 2:935–949, 2010.

- [25] *Environmental conditions and environmental loads (DNV-RP-C205). Recommended practice.* Det Norske Veritas, 2007.
- [26] Wojciech Szuminski Maria Przybylska. Non-integrability of flail triple pendulum. *Chaos, Solitons & Fractals*, 53:60–74, 2013.
- [27] P.H. Richter A. Ohlhoff. Forces in the double pendulum. *ZAMM - Journal of Applied Mathematics and Mechanics / Zeitschrift für Angewandte Mathematik und Mechanik*, 80(8):517–534, 2000.
- [28] A Grant D Clelland N Barltrop, K S Varyani and Xuan Pham. Wave-current interactions in marine current turbines. *Journal of Engineering for the Maritime Environment*, 220(4):195–203, 2006.
- [29] G. Gaonkar and D. Peters. Review of dynamic inflow modeling for rotorcraft flight dynamics. In *27th Structures, Structural Dynamics and Materials Conference, Structures, Structural Dynamics, and Materials and Co-located Conferences*, San Antonio, TX, U.S.A, 1986.
- [30] Hannah Buckland. *Combined current, wave and turbulent flows and their effects on tidal energy devices.* PhD thesis, Swansea University, 2014.
- [31] John Christopher Chapman. *Tidal Energy Device Hydrodynamics in Non-uniform Transient Flows.* PhD thesis, Swansea University, 2008.
- [32] Thomas Nevalainen. *The effect of unsteady sea conditions on tidal stream turbine loads and durability.* PhD thesis, University of Strathclyde, 2016.

- [33] J. Peiro J.I. Whelan, J.M.R. Graham. Inertia effects on horizontal axis tidal-stream turbines. In *9th European Wave and Tidal Energy Conference*, 2009.
- [34] Audrey E.D. Bowie. Flexible moorings for tidal current turbines. Master's thesis, University of Strathelde, 2012.
- [35] Ocean energy systems implementing agreement: an international collaborative programme. Technical report, IEA-OES, 2008.
- [36] Pratt D. Clarke J. & Grant A. Johnstone, C. A techno-economic analysis of tidal energy technology. *Renewable Energy*, 49:101–106, January 2013.
- [37] RA Dalrymple and JC Heideman. Nonlinear water waves on a vertically-sheared current. 1989.
- [38] simecatlantis. projects. Accessed:2019-06-13.
- [39] John Andrews and Nick Jelley. *Energy science: principles, technologies, and impacts*. Oxford University Press, 2017.
- [40] S. Harding D. R. Sutherland, B. G. Sellar and L. Bryden. Initial flow characterisation utilising turbine and seabed installed acoustic sensor arrays. In *In: Proceedings of the 10th European Wave and Tidal Energy Conference Series*, pages 2–5, Aalborg, Denmark, 2013.
- [41] J. P. Hardwick A. M. Colucci, A. Bouferrouk and L. Johanning. Characterising wave-current fields and their interaction from in situ measurements. In *Proceedings from the 10th European Wave and Tidal Energy Conference*, Aalborg, Denmark, 2011.

- [42] Design requirements for marine energy systems (iec 62600-2), 2016.
- [43] Energy Systems Research Unit. Website. Accessed:2018-09-30.
- [44] Michael Starling and Alex Scott. Foundations and moorings for tidal stream systems. Technical report, The Carbon Trust, 2009.
- [45] Madjid Karimirad, Kourosh Koushan, Sam Weller, Jon Hardwick, and Lars Johanning. Applicability of offshore mooring and foundation technologies for marine renewable energy (mre) device arrays. 2015.
- [46] SJ Banfield, NF Casey, Reza Nataraja, et al. Durability of polyester deepwater mooring rope. In *Offshore technology conference*. Offshore Technology Conference, 2005.
- [47] TJ Stallard, SD Weller, and PK Stansby. Limiting heave response of a wave energy device by draft adjustment with upper surface immersion. *Applied Ocean Research*, 31(4):282–289, 2009.
- [48] C Guedes Soares. *Renewable Energies Offshore*. CRC Press, 2015.
- [49] SD Weller, P Davies, AW Vickers, and Lars Johanning. Synthetic rope responses in the context of load history: Operational performance. *Ocean Engineering*, 83:111–124, 2014.
- [50] IML Ridge, SJ Banfield, and J Mackay. Nylon fibre rope moorings for wave energy converters. In *OCEANS 2010 MTS/IEEE SEATTLE*, pages 1–10. IEEE, 2010.
- [51] simecatlantis. ar1000-launching-at-emec. Accessed:2019-6-13.

- [52] Benoît Gaurier, Peter Davies, Albert Deuff, and Grégory Germain. Flume tank characterization of marine current turbine blade behaviour under current and wave loading. *Renewable Energy*, 59:1–12, 2013.
- [53] Pascal W Galloway, Luke E Myers, and AbuBakr S Bahaj. Quantifying wave and yaw effects on a scale tidal stream turbine. *Renewable energy*, 63:297–307, 2014.
- [54] N Barltrop, KS Varyani, A Grant, D Clelland, and Xuan Pham. Wave-current interactions in marine current turbines. *Proceedings of the Institution of Mechanical Engineers, Part M: Journal of Engineering for the Maritime Environment*, 220(4):195–203, 2006.
- [55] WMJ Batten, AS Bahaj, AF Molland, JR Chaplin, Sustainable Energy Research Group, et al. Experimentally validated numerical method for the hydrodynamic design of horizontal axis tidal turbines. *Ocean engineering*, 34(7):1013–1020, 2007.
- [56] IA Milne, AH Day, RN Sharma, and RGJ Flay. Blade loads on tidal turbines in planar oscillatory flow. *Ocean Engineering*, 60:163–174, 2013.
- [57] IA Milne, AH Day, RN Sharma, and RGJ Flay. Blade loading on tidal turbines for uniform unsteady flow. *Renewable Energy*, 77:338–350, 2015.
- [58] JI Whelan, JMR Graham, and J Peiro. Inertia effects on horizontal axis tidal-stream turbines. In *the 8th European Wave and Tidal Energy Conference*, 2009.

- [59] H. Buckland. *Combined current, wave and turbulent flows on tidal energy. Volume 1*. PhD thesis, Swansea University, 2013.
- [60] Environmental conditions and environmental loads (dnv-rp-c205), 2010.
- [61] Tao Wang and Jiachun Li. Effect of nonlinear wave-current interaction on flow fields and hydrodynamic forces. *Science in China Series A: Mathematics*, 40(6):622–632, 1997.
- [62] John D Fenton. A fifth-order stokes theory for steady waves. *Journal of waterway, port, coastal, and ocean engineering*, 111(2):216–234, 1985.
- [63] C Swan, IP Cummins, and RL James. An experimental study of two-dimensional surface water waves propagating on depth-varying currents. part 1. regular waves. *Journal of Fluid Mechanics*, 428:273–304, 2001.
- [64] James F Manwell, Jon G McGowan, and Anthony L Rogers. *Wind energy explained: theory, design and application*. John Wiley & Sons, 2010.
- [65] Martin OL Hansen. *Aerodynamics of wind turbines*. Routledge, 2015.
- [66] Tony Burton, David Sharpe, and Nick Jenkins. *Handbook of wind energy*. John Wiley & Sons, 2001.
- [67] Ian Masters, JC Chapman, MR Willis, and JAC Orme. A robust blade element momentum theory model for tidal stream turbines in-

- cluding tip and hub loss corrections. *Journal of Marine Engineering & Technology*, 10(1):25–35, 2011.
- [68] Hermann Glauert. Aerodynamic theory. *The Aeronautical Journal*, 34(233):409–414, 1930.
- [69] Robert Elliott Wilson and Peter Lissaman. Applied aerodynamics of wind power machines. 1974.
- [70] Wen Zhong Shen, Robert Mikkelsen, Jens Nørkær Sørensen, and Christian Bak. Tip loss corrections for wind turbine computations. *Wind Energy: An International Journal for Progress and Applications in Wind Power Conversion Technology*, 8(4):457–475, 2005.
- [71] Patrick J Moriarty and A Craig Hansen. Aerodyn theory manual. Technical report, National Renewable Energy Lab., Golden, CO (US), 2005.
- [72] Marshall L Buhl Jr. New empirical relationship between thrust coefficient and induction factor for the turbulent windmill state. Technical report, National Renewable Energy Lab.(NREL), Golden, CO (United States), 2005.
- [73] David A Spera et al. *Wind turbine technology: fundamental concepts of wind turbine engineering*, volume 3. ASME press New York, 1994.
- [74] Hermann Frahm. Device for damping vibrations of bodies., April 18 1911. US Patent 989,958.
- [75] J. Ormondroyd and Den Hartog J, P. The theory of dynamic vibration absorber. *Journal of Applied Mechanics Trans*, 50(7):9–22, 1928.

- [76] Jacob Pieter Den Hartog. *Mechanical vibrations*. Courier Corporation, 1985.
- [77] Pradipta Banerji, Mohan Murudi, Arvind H Shah, and Neil Poplewell. Tuned liquid dampers for controlling earthquake response of structures. *Earthquake engineering & structural dynamics*, 29(5):587–602, 2000.
- [78] Yukio Tamura, Kunio Fujii, Tamio Ohtsuki, Toshihiro Wakahara, and Ryuichi Kohsaka. Effectiveness of tuned liquid dampers under wind excitation. *Engineering structures*, 17(9):609–621, 1995.
- [79] Alex DD Craik. The origins of water wave theory. *Annual review of fluid mechanics*, 36, 2004.
- [80] Robert G Dean and Robert A Dalrymple. *Water wave mechanics for engineers and scientists*, volume 2. World Scientific Publishing Company, 1991.
- [81] Norifumi Kishida and Rodney J Sobey. Stokes theory for waves on linear shear current. *Journal of engineering mechanics*, 114(8):1317–1334, 1988.
- [82] RA Dalrymple and JC Heideman. Nonlinear water waves on a vertically-sheared current. 1989.
- [83] Klaus Hasselmann, TP Barnett, E Bouws, H Carlson, DE Cartwright, K Enke, JA Ewing, H Gienapp, DE Hasselmann, P Kruseman, et al. Measurements of wind-wave growth

and swell decay during the joint north sea wave project (jonswap).
Ergänzungsheft 8-12, 1973.

- [84] Willard J Pierson Jr and Lionel Moskowitz. A proposed spectral form for fully developed wind seas based on the similarity theory of sa kitaigorodskii. *Journal of geophysical research*, 69(24):5181–5190, 1964.
- [85] Odd Faltinsen. *Sea loads on ships and offshore structures*, volume 1. Cambridge university press, 1993.
- [86] Carl Runge. Über die numerische auflösung von differentialgleichungen. *Mathematische Annalen*, 46(2):167–178, 1895.
- [87] Wilhelm Kutta. Beitrag zur näherungsweise integration totaler differentialgleichungen. *Z. Math. Phys.*, 46:435–453, 1901.
- [88] Nigel DP Barltrop and Adrian J Adams. *Dynamics of fixed marine structures*, volume 91. Butterworth-Heinemann, 2013.
- [89] Matthew A Lackner and Mario A Rotea. Passive structural control of offshore wind turbines. *Wind energy*, 14(3):373–388, 2011.
- [90] Lingzhi Xiong, Jianmin Yang, and Wenhua Zhao. Dynamics of a taut mooring line accounting for the embedded anchor chains. *Ocean Engineering*, 121:403–413, 2016.
- [91] Peter L Fraenkel. Power from marine currents. *Proceedings of the Institution of Mechanical Engineers, Part A: Journal of Power and Energy*, 216(1):1–14, 2002.

- [92] Walter Schütz. A history of fatigue. *Engineering Fracture Mechanics*, 54:263–300, 1996.
- [93] E.Bossanyi. *BLADED for windows theory manual*. Garrad Hassan and Partners Limited, Bristol, England, 1997.
- [94] J. Schepers and H. Snel. Final results of the eu joule project "dynamic inflow". Technical report, ECN-RX. Netherland Energy Research Foundation ECN, 1995.
- [95] L. B. Tuckerman. Inertia factors of ellipsoids for use in airship design. Technical report, United States, 1926.
- [96] GX Wu, JA Witz, Q Ma, and DT Brown. Analysis of wave induced drift forces acting on a submerged sphere in finite water depth. *Applied ocean research*, 16(6):353–361, 1994.
- [97] MARTIME JOURNAL. Schottel instream turbine. Accessed: 2018-07-23.
- [98] The Mathworks, Inc., Natick, Massachusetts. *MATLAB version 9.3.0.713579 (R2017b)*, 2017.
- [99] MJ Hochrainer. Tuned liquid column damper for structural control. *Acta Mechanica*, 175(1-4):57–76, 2005.